PROPAGATION OF PERIODIC DISTURBANCES IN THE NEIGHBOURHOOD OF THE LAMINAR BOUNDARY LAYER.

Thesis
submitted by

JOHN MORGAN, A.R.C.S.T.

for the degree of
Doctor of Philosophy

University of Edinburgh,
October, 1963.

Graduated July 1964

CONTENTS

SYMBOLS.

The following symbols are used to describe the quantities indicated in this list unless otherwise stated in the text.

x = distance from leading edge of the flat plate.

y = distance from the surface of the flat plate.

z = distance from the centre line of the plate.
perpendicular to x and y.

U_o = free stream velocity.

U = mean velocity at a point in the boundary layer.

u = x component of fluctuation velocity.

v = y component of fluctuation velocity.

w = z component of fluctuation velocity.

u', v', w' = root mean square values of u, v, and w.

c = wave velocity.

β_r = $2\pi f$, where f = oscillation frequency.

α = $\frac{2\pi}{\lambda}$ = wave number.

λ = wave length of oscillation.

ν = kinematic viscosity of air.

δ = boundary layer thickness.

δ^* = boundary layer displacement thickness.

$\delta^* = 1.72\sqrt{\frac{\nu x}{U_o}}$ for Blasius distribution.

$\delta^* = 0.341\delta$ relation used by Tollmien and Schlichting.

$R = \frac{U_o \delta^*}{\nu}$ = Reynolds number.

$Rx = \frac{U_o x}{\nu}$ = x - Reynolds number.

a = ribbon amplitude.

CHAPTER I

Introduction and Historical Survey of Boundary Layer Research

I. 1. Introduction

When a fluid flows past a solid surface there is a region of retarded flow between the surface and the main flow. This region is known as the boundary layer and it can be either laminar or turbulent. The forward, laminar, part of the boundary layer is fairly well understood; it consists of steady streamline flow with the velocity decreasing to zero at the surface. It also creates a moderate drag on the surface. On the other hand the turbulent part of the boundary layer is not so well understood. It is known that the motion is of a random nature and that it creates a greater drag on the surface than the laminar flow. The transition from laminar to turbulent flow depends on the velocity of the flow, the smoothness of the surface, the temperature etc., but it is not known what fundamental fluid processes produce turbulence.

The object of the present work is to discover what

happens in the transition from laminar to turbulent flow. The experimental work is confined to the case of the flow of air over a smooth flat plate with zero pressure gradient along the direction of flow.

I. 2. Historical Survey

The dynamical equations of motion for an inviscid fluid were first derived by Euler some two hundred years ago. Almost a century later the complete equations of motion for a viscous fluid were derived by several workers- notably Navier, Poisson, Saint Venant and Stokes and these equations are usually referred to as the Navier-Stokes equations.

Theoretical hydrodynamics based on Euler's equation had achieved a high degree of completeness but there were contradictions between this theory and the experimental results obtained with real fluids. In the case of a body moving at constant speed through a fluid, the theory led to the rather startling result that the force in the direction of motion was always zero, i.e. there could be no drag on the body. This gross disagreement with observed effects is known as d' Alembert's paradox.

During this period experimentalists were forming their own empirical science which was necessary to solve the many important problems arising at this time. In 1883, Osborne Reynolds (1) while investigating the flow of water through pipes, demonstrated that there were two types of flow, namely, laminar and turbulent and that the transition from laminar to turbulent flow was characterised by a dimensionless parameter R, which is defined as $R = \frac{Vd}{\nu}$, where

V = velocity

d = a characteristic length

ν = kinematic viscosity

The formulation of the Navier-Stokes equations did not help to bring theory closer to experiment, because of the great mathematical difficulties involved in their solution.

In 1904 however, Prandtl (2) succeeded in combining theory with experiment when he introduced the concept of the boundary layer. He postulated that in a fluid of small viscosity the effect of the viscosity could be neglected everywhere except in regions of large velocity gradient. He showed that it was then possible to consider the flow past a solid body to be of two regions; (1) a thin layer, in the

neighbourhood of the body, where the velocity rises from zero to the free stream value, and where, therefore the effect of viscosity could not be neglected and (2) the remaining fluid, outside this layer, where the effect of viscosity could be neglected.

If x is the distance along a surface and y is the distance normal to it, and if u and v are the corresponding velocity components, then the viscous stresses in the boundary layer will be shear stresses acting parallel to the surface and proportional to the dominant velocity gradient $\partial u/\partial y$; elsewhere the viscous stresses are small. From this the essential approximations of the boundary layer theory follow, namely, that the viscosity of the fluid need only be considered in the boundary layer and only the shear stresses arising from the gradient $\partial u/\partial y$ are of importance. These approximations lead to a simplification of the Navier-Stokes equations and the resulting equations, known as the boundary layer equations, have been found readily amenable to analysis.

For the case of a flat plate at zero incidence the boundary layer equations were first solved by Blasius (3)

in 1908. Using a substitution method, Blasius transformed the equation into a non-linear third order differential equation which could not be solved analytically, but which he solved numerically. In 1938 Howarth (4) solved the Blasius equation with a high degree of accuracy and the velocity distribution across the boundary layer shown in figure 1 was obtained from his solution.

Experimental evidence to test this theory has been obtained by several workers, and in 1942 Nikuradse (5) carried out some very careful measurements which agreed well with the theory.

In 1914 Prandtl had shown, by his classical experiments with spheres, that the flow in the boundary layer could be laminar or turbulent. From the measurements taken by early workers it was found that the transition from laminar to turbulent flow on a flat plate occurred at a critical Reynolds number (Rx crit.) of between 3×10^5 and 5×10^5 but recently, Schubauer and Skramstad (6), working with a particularly low free stream turbulence, succeeded in reaching a critical Reynolds number of $Rx = 3 \times 10^6$.*

G.I. Taylor (7) suggested that transition followed

* Higher values of Rx have been observed, particularly in flight.

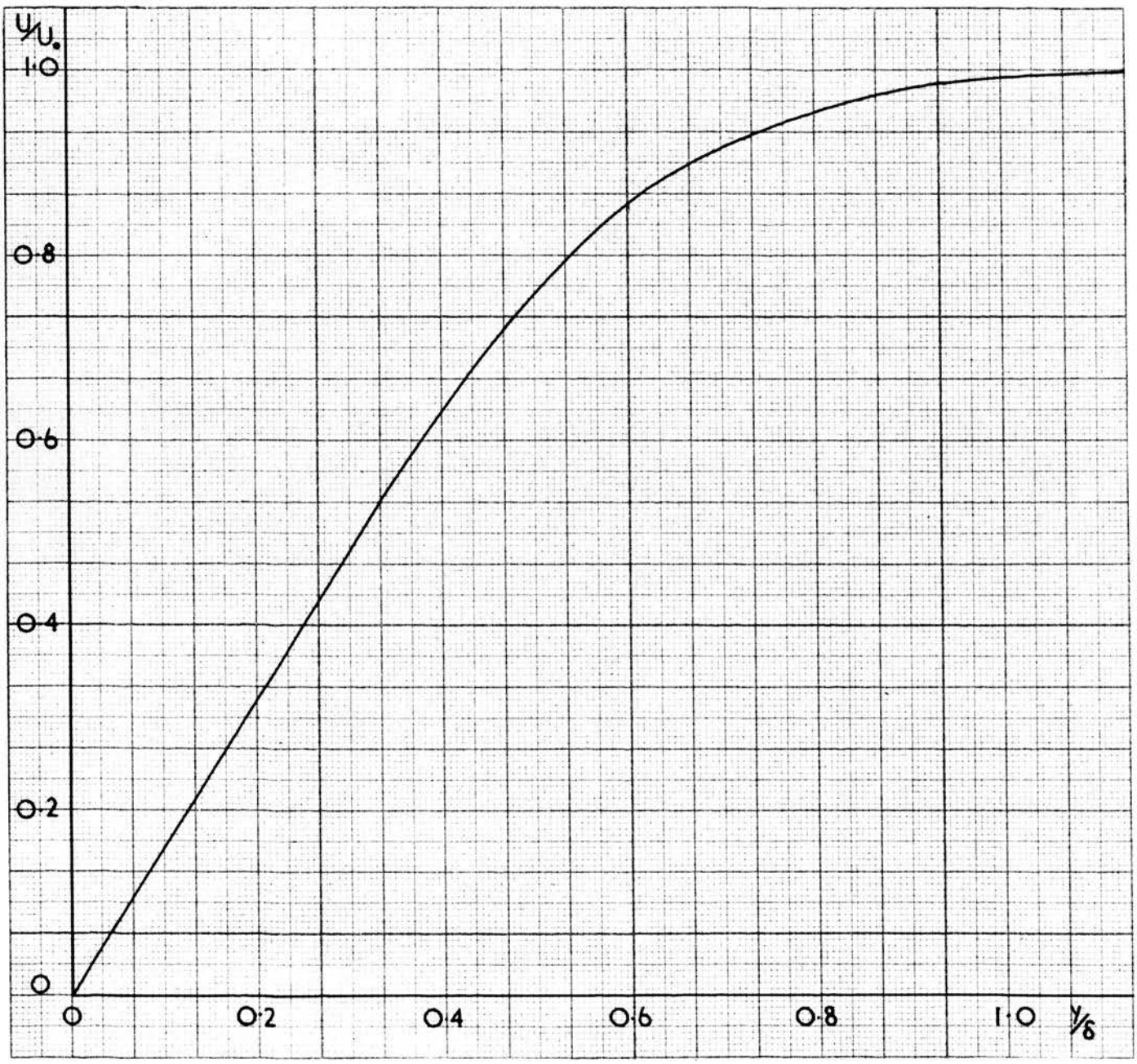

Figure 1

Velocity distribution across a laminar boundary layer.

from local transient separation of the flow, caused by pressure gradients associated with disturbances in the flow. On the basis of this hypothesis, he obtained good agreement with the results of experiments on a sphere in a wind tunnel with a high degree of free stream turbulence. This theory, however, requires that separation should occur immediately before transition, and more recent experimental work has shown that transition can occur without flow separation.

The most successful theoretical method of treating the problem of boundary layer stability has been to consider a small disturbance superimposed on the primary flow. If all such disturbances are damped, the primary flow is inherently stable; otherwise it is inherently unstable.

The small disturbance method was first applied to the problem of stability by Lord Rayleigh (8) who outlined a general mathematical theory. Tietjens (9) applied Rayleigh's theory using profiles intended to reproduce flow along a wall, but his solution was seriously limited because his profile was approximated to a set of straight lines. The work of Tollmien (10) and (11), and Schlichting (12) and

(13) produced a more rigourous solution by approximating the Blasius distribution to a straight line and a parabola and this solution was further improved by Lin (14). In brief, the theory considered a two dimensional flow in which the mean velocity U is a function of y only, and V = 0. From the equation of continuity

$$\frac{\partial (U + u)}{\partial x} + \frac{\partial v}{\partial y} = 0$$

where u and v are the velocity components of the disturbance. It follows that:-

$$\frac{\partial u}{\partial x} + \frac{\partial v}{\partial y} = 0$$

and a stream function ψ can be introduced such that

$$u = -\frac{\partial \psi}{\partial y}, v = \frac{\partial \psi}{\partial x}.$$

The function ψ is expressed in the form

$$\psi = F(y) e^{i\alpha(x - ct)}$$

$$= F(y) e^{i(\alpha x - \beta t)}$$

where $\alpha = 2\pi/\lambda$, and λ is the wavelength of the disturbance and c is in general complex $c = c_r + c_i$.

The quantity β_i can be regarded as a coefficient of amplification.

Expressing lengths and velocities non-dimensionally in terms of δ^* and U_o and putting

$$F(y) = U_o \delta^* \phi(\eta), \text{ where } \eta = y/\delta^*,$$

an equation of the following form is obtained from the equation of motion when linearised in the disturbance components:-

$$(U - c)(\phi'' - \alpha^2\phi) - U''\phi = \frac{1}{i\alpha R_{\delta^*}}(\phi'''' - 2\alpha^2\phi'' + \alpha^4\phi)$$

with the boundary conditions,

$$\eta = 0, \quad \phi = 0, \quad \phi' = 0$$

$$\eta = \infty, \quad \phi = 0, \quad \phi' = 0$$

The mathematical details of the solution of this equation are adequately discussed by Schlichting (15).

The equation with its boundary conditions can be shown to constitute a boundary value problem and this implies that for any given profile, U (y), there exists a functional relation between the parameters α, R_{δ^*} and c which the solution must satisfy. c_r and c_i are therefore functions of α and R_{δ^*}.

Since neutral stability is obtained when $c_i = 0$, α can be determined as a function of R_{δ^*} and can be

represented graphically. To keep the parameters dimensionless the neutral curve is usually plotted as $\alpha\delta^*$ against R_{δ^*} or $\beta_r\nu/U_o^2$ against R_{δ^*}. Any disturbance inside these curves will be amplified while all other disturbances will be damped.

The neutral stability curve calculated by Schlichting and the improved calculations due to Lin are shown in figure 2.

Calculations of curves for values of c_i other than zero have been made by Schlichting (16) and Shen (17) and the curves calculated by Shen are shown in figure 3. From Shen's curves calculations were made of the growth of the amplitude of a disturbance, relative to its amplitude at the neutral curve, as it crosses the amplifying region at constant $\beta_r\nu/U_o^2$. The result of these calculations is shown in figure 4.

The Tollmien-Schlichting theory for small disturbances was treated with some reserve until in 1947 Schubauer and Skramstad (6) produced conclusive evidence that the theory was substantially correct. Using the boundary layer on a flat plate in a wind tunnel with extremely low free stream

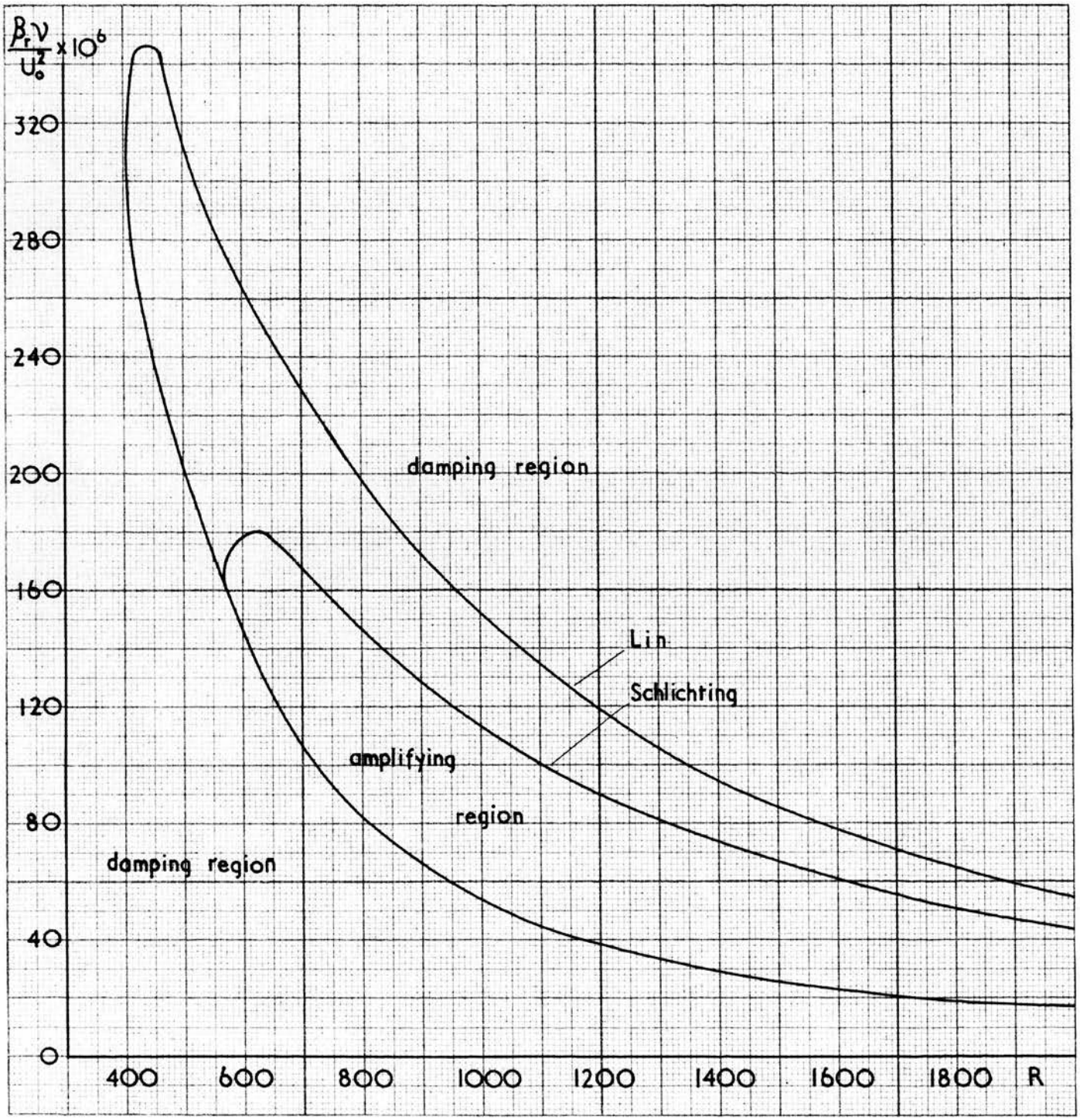

Figure 2

Neutral stability curves calculated by Schlichting and Lin.

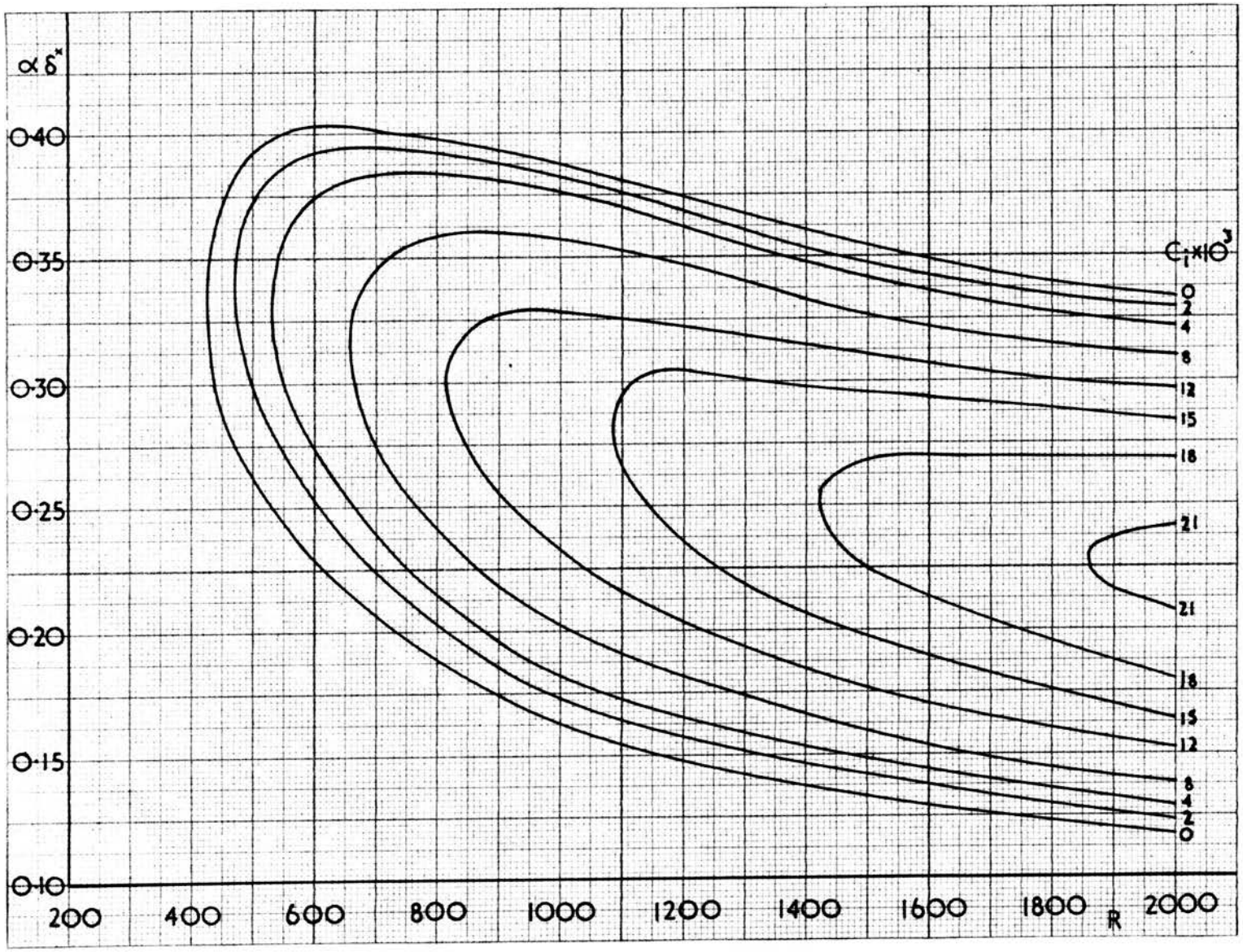

Figure 3

Curves of constant c_i calculated by Shen.

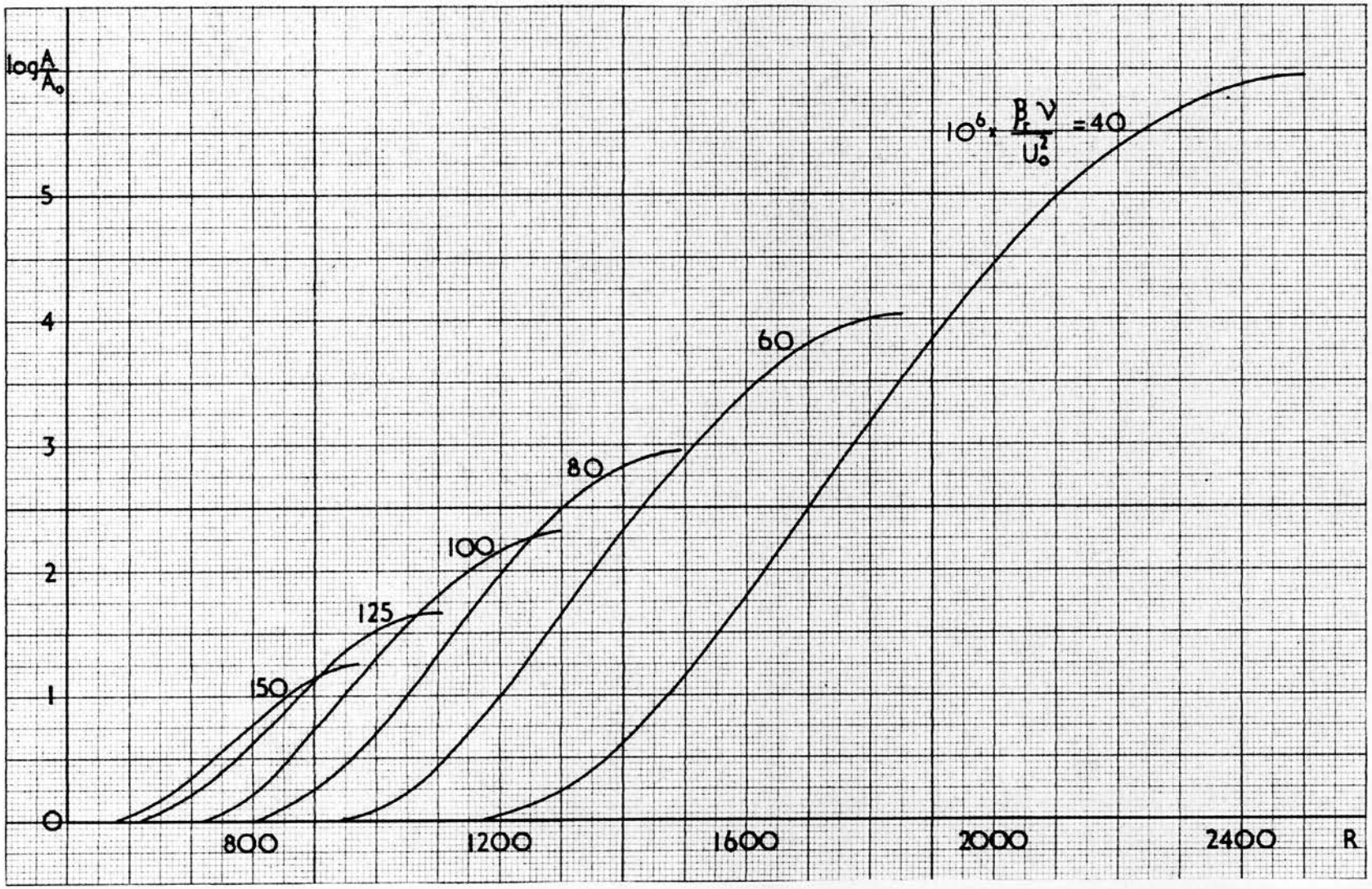

Figure 4

Curves showing growth of disturbance as it crosses the amplifying region at constant $\beta_r \nu / U_0^2$

turbulence, they demonstrated that sinusoidal oscillations, of the kind considered by the theory, appeared naturally in the boundary layer. They also showed the existence of a neutral curve by injecting artificial oscillations into the boundary layer and observing whether they were amplified or damped. The experimental neutral curve obtained by them is shown in figure 5.

A promising development to the understanding of the origin of turbulence was the work of Emmons (18). Emmons suggested, from the result of experiments with a water table, that turbulence develops initially, not along a continuous front, but at isolated spots and each spot, as it passes down-stream grows into an expanding region of turbulent flow. The spots occur with a random distribution in space and time. As the fluid flows down-stream from the beginning of the transition region, the number of spots increases and eventually the resulting expanding regions of turbulent flow coalesce to form continuous and fully developed turbulent flow in the boundary layer. Experimental investigations of disturbance patterns in a laminar boundary layer on a flat plate, by Schubauer and Klebanoff (19),

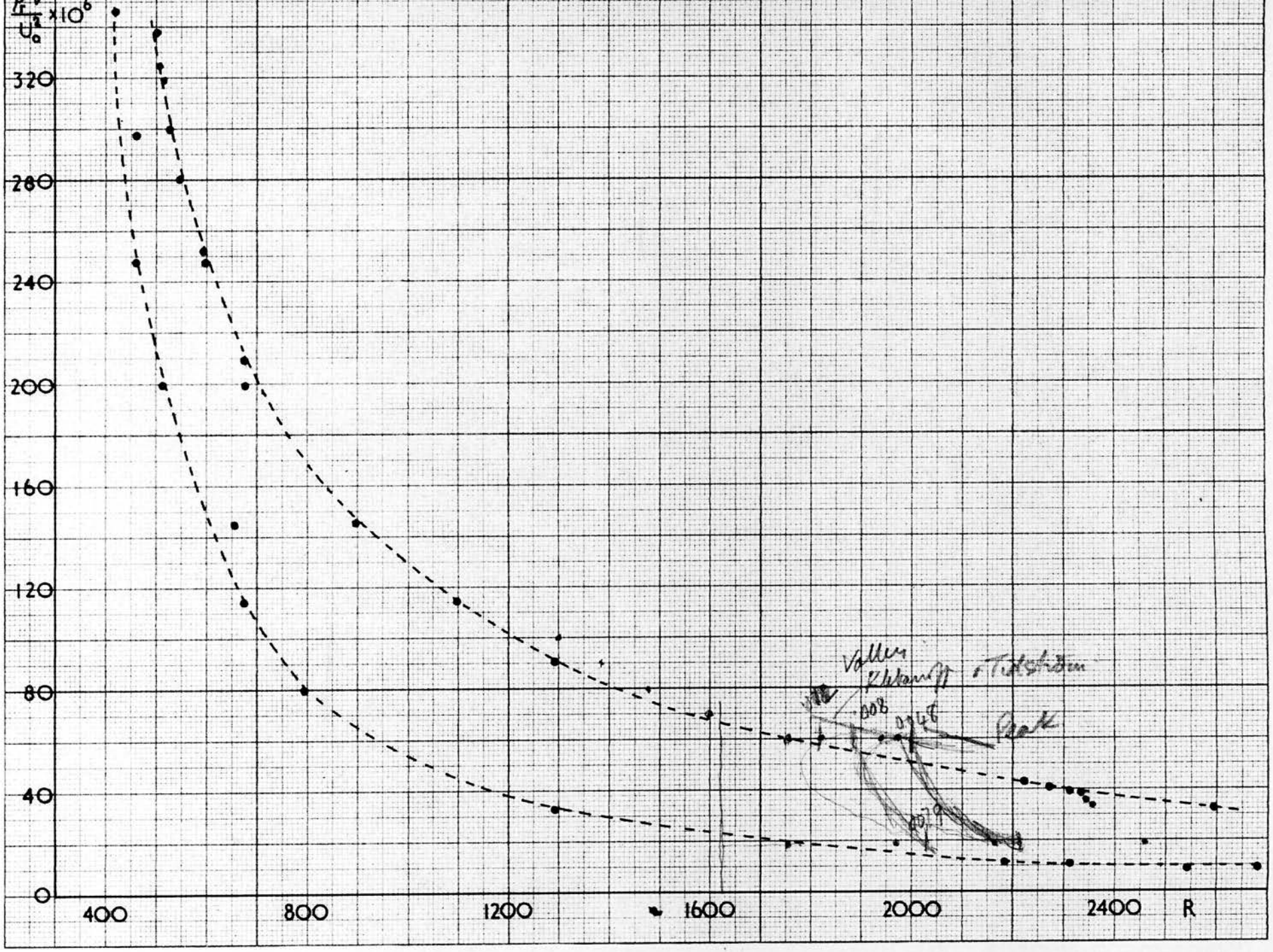

Figure 5

Neutral stability curve obtained experimentally by Schubauer and Skramstad.

confirmed Emmons' theory and provided further details of the shape and speed of the individual turbulent regions as they grew from the initial spots.

It is now recognised that the Tollmien-Schlichting theory is essentially correct and that if a small disturbance is introduced into the boundary layer its growth can be predicted. At some stage, however, this disturbance will not be infinitesimal and the theory will no longer apply. The problem of dealing with finite disturbances in the boundary layer is extremely complex, since approximations making the initial equations linear, cannot be made.

Various theoretical approaches have been made to the problem of the non-linear behaviour of disturbances in the boundary layer and these will be outlined briefly.

The non-linear effect has been examined theoretically by Meksyn and Stuart (20) in 1951 and again by Stuart (21) in 1958. Their treatment was based on a two-dimensional oscillation and they concluded that the non-linear effect would produce distortion of the mean flow.

In 1957 Lin (22) predicted that the non-linear behaviour would manifest itself, with increasing wave amplitude, in

the generation of higher harmonics in the vicinity of the critical layer before any distortion of the flow is observed.

It was shown by Gortler (23) and Liepmann (24) that concave curvature of the wall had a destabilising effect on the boundary layer flow and in 1957 Gortler and Witting (25) proposed the concept that the concave streamline curvature associated with the wave motion, may generate longitudinal vortices in a manner similar to that prescribed for a concave surface.

A theoretical analysis has been carried out by Benney and Lin (26) for the case of parallel flow. They considered the non-linear behaviour of a primary oscillation which consisted of two components, a two-dimensional Tollmien-Schlichting wave and a superposed three-dimensional wave which had a periodic spanwise variation in wave amplitude. The non-linear interaction of these two modes, when the two-dimensional component predominated, gave rise to a longitudinal-eddy system in the nature of a secondary flow, with the same spanwise wavelength as the primary oscillation. This vortical motion was found to be strongest at points where the primary oscillations gave a convex streamline,

which is contrary to the predictions of the Gortler-Witting theory. A more detailed analysis using the above method has been given by Benney (27).

Recently, experimental work has been concentrated largely on the three-dimensional nature of the boundary layer before transition occurs.

In 1957 Hama, Long and Hegarty (28) investigated the flow phenomena as disclosed by dye patterns on a flat plate which was towed in a water tank. Two-dimensional vortices shed by a trip wire were found to deform into three-dimensional vortex loops with a marked transverse wavelength. The vortex loop stretched and intensified as it travelled down-stream and eventually a turbulent spot was created near the tip of the vortex loop. In 1960 Hamma (29) observed exactly the same phenomenon when the disturbance was introduced by a vibrating ribbon and concluded that the formation of vortex loops must be a guiding physical principle of the transition from laminar to turbulent flow.

The three-dimensional nature of the boundary layer, before transition was also observed by Klebanoff and Tidstrom (30) in 1959. They concluded, that the three-

dimensional nature of the boundary layer was an inherent consequence of the wave amplification and played an important role in the transition process.

In 1962, Klebanoff, Tidstrom and Sargent (31) decided to control the spanwise variation in wave amplitude in order that the structure and significance of the three-dimensionality could be reliably studied in detail. Sufficient data were obtained by Klebanoff et. al. to evaluate the existing theoretical approaches.

Klebanoff et. al. measured the harmonic content of the wave in the vicinity of the critical layer and found that it was not what would be expected from Lin's theory (1957). They found no real evidence of any strong harmonic content occurring before distortion of the mean flow.

Their observations indicated the existence of longitudinal vortical motion very similar to that described in the Gortler-Witting theory, but the location of the vortex relative to the primary oscillations was found to be exactly opposite in phase to the theoretical prediction. They concluded that although the Gortler-Witting mechanism may have been present it did not play a dominant role in the transition process.

An attempt was made to resolve the question as to whether the longitudinal vortices observed could be accounted for by the occurrence of vortex loops such as had been observed by Hama. From their observations they came to the conclusion that the longitudinal eddy system was not a manifestation of the vortex loop. However they postulated that the dye technique marked the fluid particle and would show the behaviour of the mean flow but not necessarily that of the disturbance.

Although the Lin-Benney theory has been applied to parallel flow only, Klebanoff et. al. assumed that the gross features could apply to Blasius flow. They found that the theoretical conclusions of Benney and Lin were remarkably consistent with the experimental results obtained by themselves and conclude that most of the experimentally observed phenomena could be accounted for, if the Lin-Benney theory was extended to the case of the Blasius distribution.

It would appear that initially in the process of transition from a laminar to a turbulent boundary layer, a small two-dimensional disturbance travels down the boundary layer and is amplified according to the Tollmien-

Schlichting theory. Eventually the non-linear effects become no longer negligible and this seems to produce a three- dimensional effect in the wave. Once this stage has been reached it is possible that other mechanisms may come into operation before breakdown to turbulence finally occurs.

CHAPTER II

Description of Apparatus

II. 1. Description of Wind Tunnel

The wind tunnel used was a modification of N.P.L. design No. A 155. This is an open circuit tunnel with an 18 inch octagonal working section and a contraction ratio of 3.16:1. The modification of the N.P.L. design was the addition of extra settling lengths before and after the contraction; this ensured that the flow in the working section was as streamlined as possible. A plan view of the tunnel is shown in figure 6.

The working section of the tunnel, by which is meant the section in which the bulk of the measurements were made and which is the second section after the contraction, was made of $\frac{1}{4}$ inch Perspex sheet; the remainder of the tunnel being constructed of $\frac{1}{8}$ inch hardboard formed on wooden stringers and the whole supported on steel girders embedded in concrete blocks. To reduce the transmission of vibrations to the tunnel through the floor, the concrete blocks were insulated from the floor by felt pads and held in place by rubber covered steel pins.

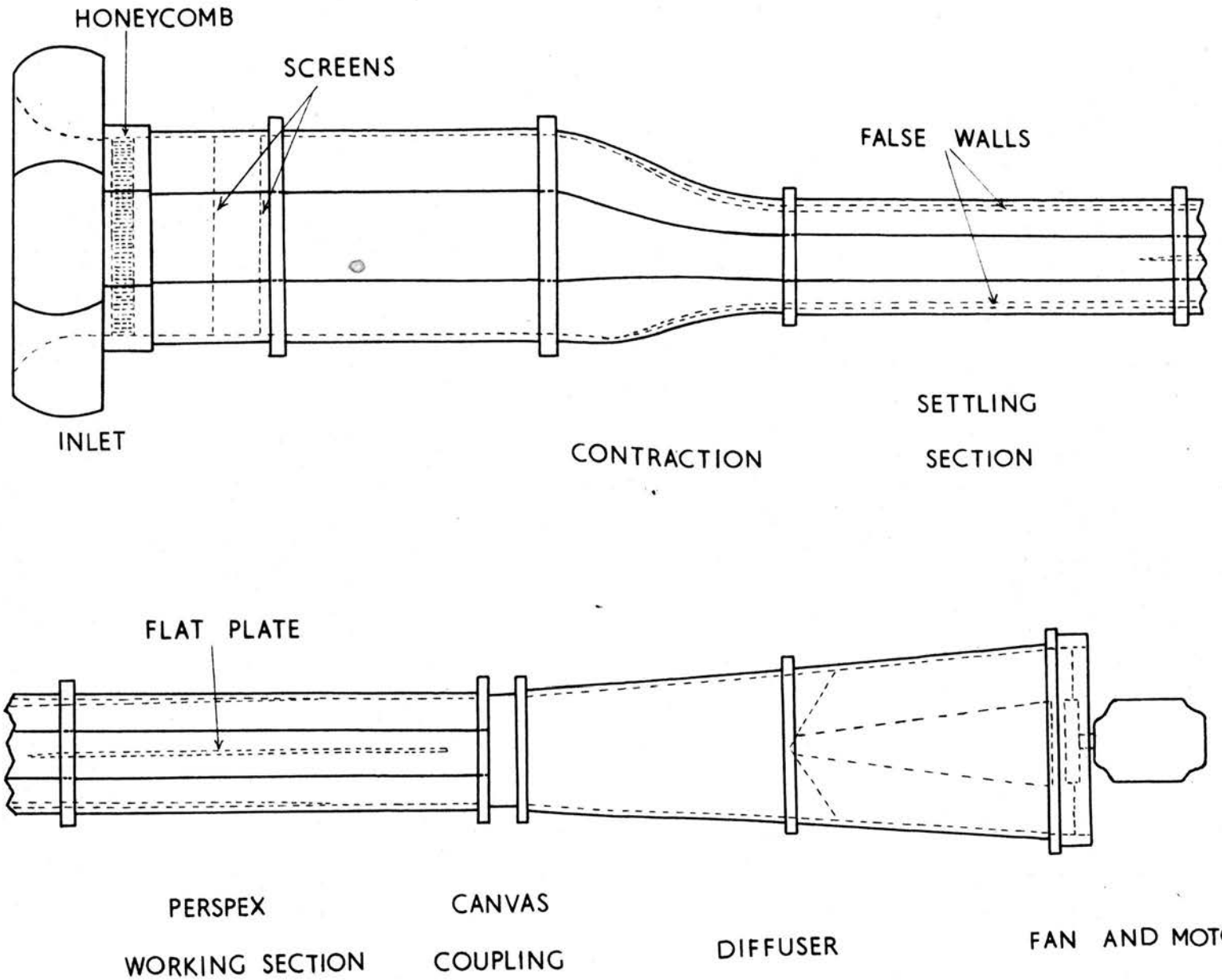

SCALE 1 inch represents 2 feet

Figure 6

Plan view of wind tunnel

The inlet section was fitted with a honeycomb straightener made of hexagonal brass tubes 4 inches long and $\frac{3}{8}$ of an inch from face to face. Positioned 15 inches and 27 inches down-stream from the honeycomb were two mesh screens of 32 S.W.G. wire with 30 wires to the inch. With these screens in place the free stream turbulence in the working section was 0.3%.

A flat plate made of a Perspex sheet 6 feet long, 18 inches high and $\frac{1}{4}$ of an inch thick was fitted in the working section of the tunnel, spanning it from floor to ceiling and positioned so that its leading edge was 4 feet down-stream from the end of the contraction. The leading edge was tapered to a knife edge over a distance of 4 inches. The plate was bolted to the floor and ceiling of the tunnel in such a way that it was under a slight tension, thus ensuring that the plate did not bend or warp.

To counteract the pressure drop along the tunnel, false walls of 1/16 inch Perspex were fitted to the vertical sides of the tunnel. These false walls began at the contraction and were parallel to the tunnel walls until the leading edge of the flat plate; they then diverged until they met the tunnel wall near the end of the working section. A certain

amount of fine control of the pressure gradient was obtained with small adjusting screws at various positions along the wall.

The air flow through the tunnel was produced by a four bladed suction fan driven by a 7.5 H.P. D.C. motor. The current to the field coils was obtained from a 240 Volt D.C. supply and the current in the armature was supplied by a D.C. generator driven by an A.C. motor, the field coils of this generator being supplied from a stepped potential divider across a 240 Volt D.C. supply. By incorporating a small rheostat for fine control a continuous speed control of the fan was possible. A diagram of the arrangement is shown in figure 7.

II. 2. Automatic Control of the Wind Speed

In order to ensure that the wind speed remained constant an automatic control was incorporated.

A pitot-static tube was placed in the tunnel opposite the working side of the flat plate. The tappings from the tube were connected to the two inverted cups of a pressure balance which could be set in equilibrium for any particular wind speed. When the wind speed in the tunnel altered, the

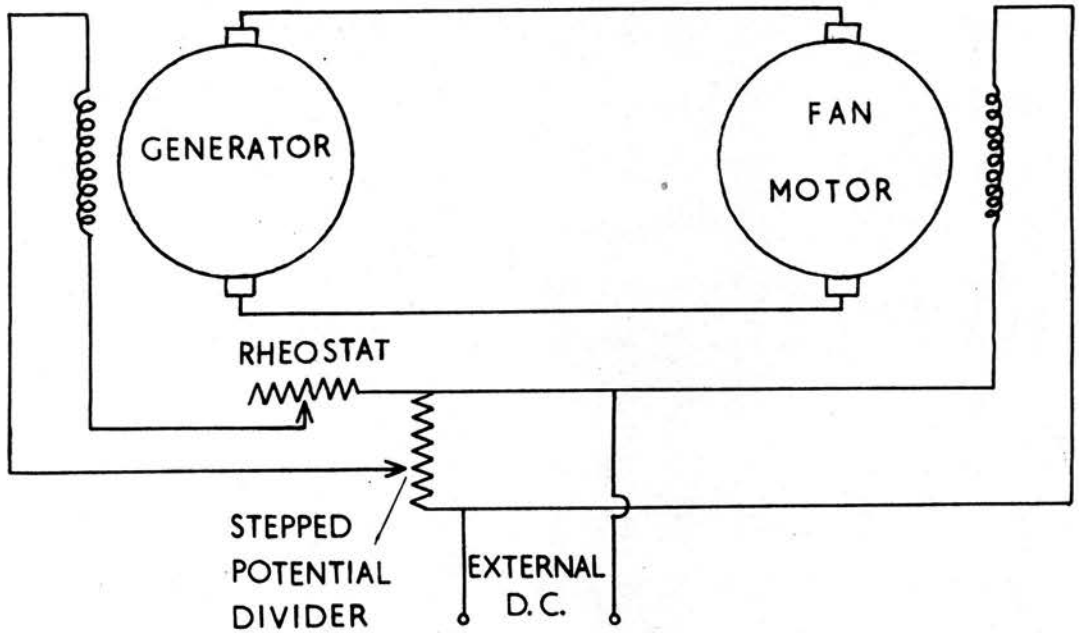

Figure 7

Speed control circuit

equilibrium of the pressure balance was destroyed and this was arranged to activate the coil of a relay. A small D.C. motor was then connected to its supply voltage and drove the contact of the small rheostat controlling the wind speed.

Diagrams of the pressure balance and relay system are shown in figures 8 and 9 . Two relays were required so that compensation could be made for either increase or decrease of wind speed. The variable resistance R_3 was required to adjust the speed of the motor. This was necessary since, if the motor drove the rheostat contact too quickly then, owing to the time delay of the system the contact, and therefore the windspeed, would oscillate. In practice the speed of the motor was adjusted so that the contact just ceased to oscillate. Switches S_1 and S_2 were safety switches so that the motor could not drive the contact beyond the end of the rheostat and switch S_3 was to enable switches S_1 and S_2 to be bypassed.

II. 3. Traversing Mechanisms

Two traversing mechanisms were used at different stages of the work.

The first was attached to a framework of 2 inch angle iron girders built round the working section of the tunnel.

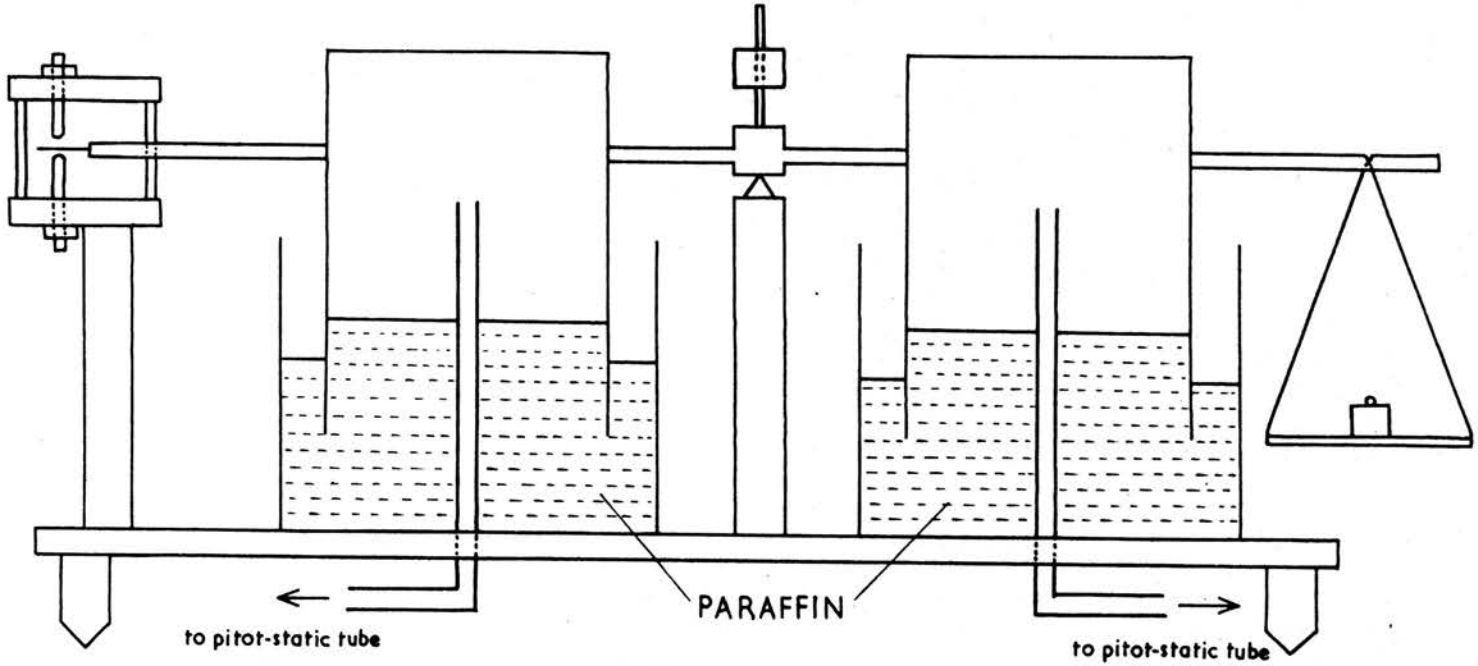

Figure 8

Diagram of pressure balance

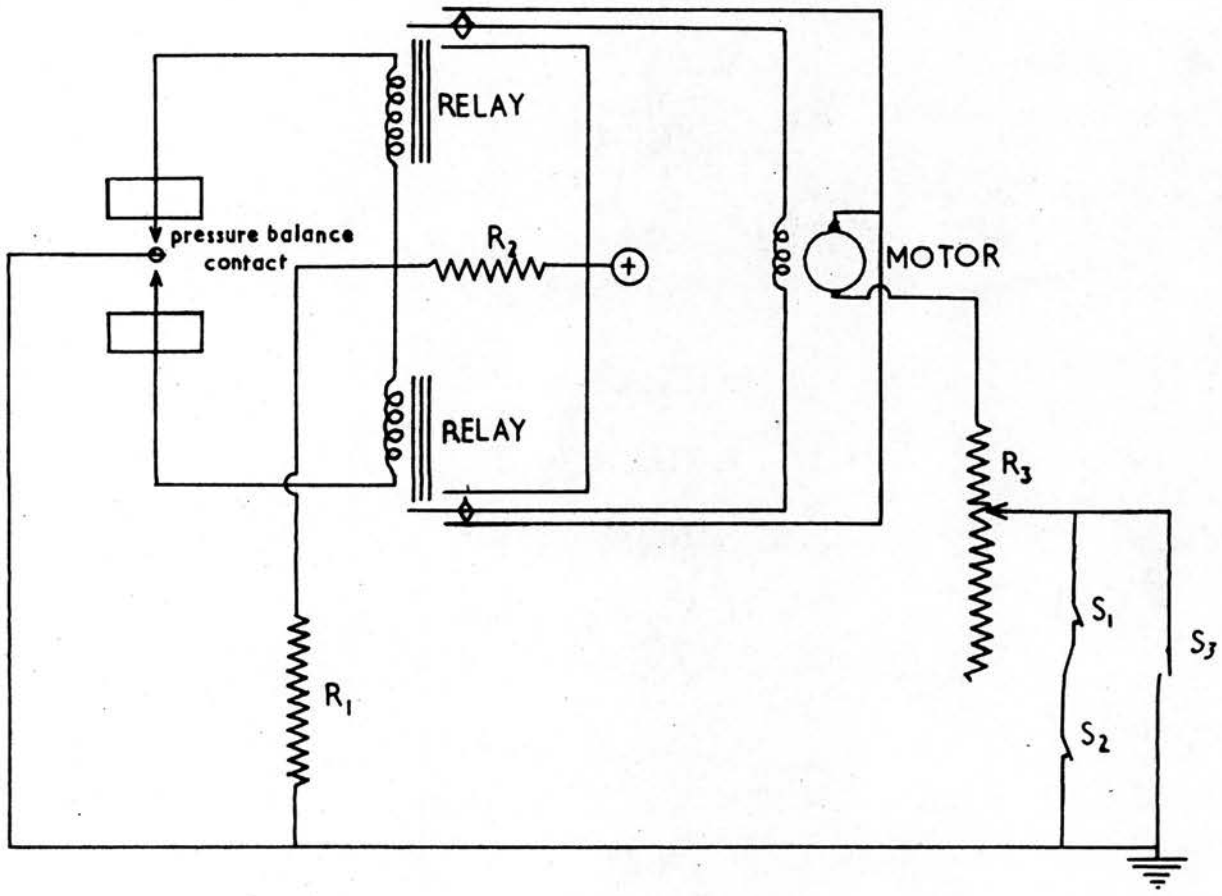

Figure 9

Automatic speed control circuit

It consisted of two brass bars, one inside and one outside the tunnel, connected at each end by a ¼ inch diameter steel rod. These rods moved freely through two brass collars screwed to the angle iron. Fixed to the outer brass bar and bearing on the angle iron were two micrometers, thus allowing accurate movement, perpendicular to the flat plate, of the inner brass bar. Fitted over the inner bar was a 2 inch long brass sleeve which could move freely along the bar. The sleeve was moved up or down stream by a screwed rod which passed through a nut attached to the sleeve. The rod was turned from outside the tunnel by means of a small gear box fitted to the end of the inner bar. Fixed to the sleeve were two streamlined rods which supported a light hollow tube, and instruments, used to investigate the flow, were mounted in this tube. A diagram of this traversing mechanism is shown in figure 10 .

The second traversing mechanism ran on two brass rails running parallel to the flat plate and fixed to the floor and ceiling of the tunnel. It consisted of a rectangular brass plate with four ball races fitted to the top and bottom so that they ran on the brass rails. Fixed to a pivot on the brass plate was a brass boom whose extreme

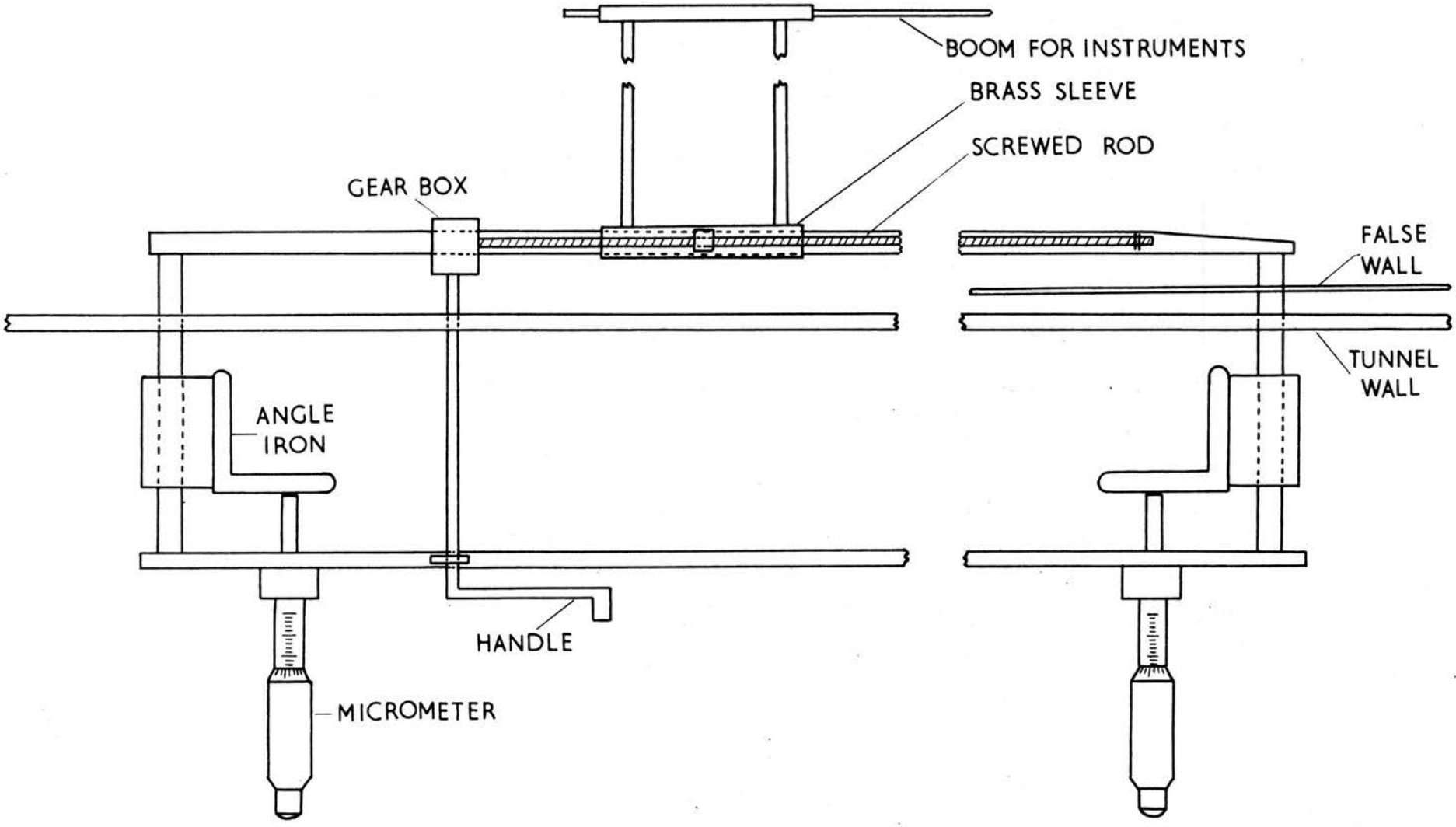

Figure 10

Diagram of first traversing mechanism

upstream end bore against the flat plate, and this contact was maintained by a spring fixed between the brass plate and the other end of the boom. The boom also carried, at its upstream end, a further pivoted arm which was driven from outside the tunnel by means of a flexible cable and a micrometer. An instrument carried on the end of this arm could thus be moved in a direction perpendicular to the flat plate. The actual measurement was made with a clock gauge mounted on the arm and bearing on the flat plate. Diagrams of this mechanism are shown in figures 11 and 12.

The first traversing mechanism was designed so that there was no contact between it and the tunnel walls, and so, it was hoped, cutting down the amount of vibration transmitted to any instrument. Owing to the resonant nature of the mechanism, however, it was found when using hot-wires (described in Chapter IV) that vibrations produced by the traversing mechanism masked any signal picked up from the flow. The second traversing mechanism, although it was attached to the tunnel, was a more massive construction and the vibrations produced in any instrument it carried were small compared with the signals being picked up from the flow. The second traversing mechanism was therefore used for all hot wire measurements.

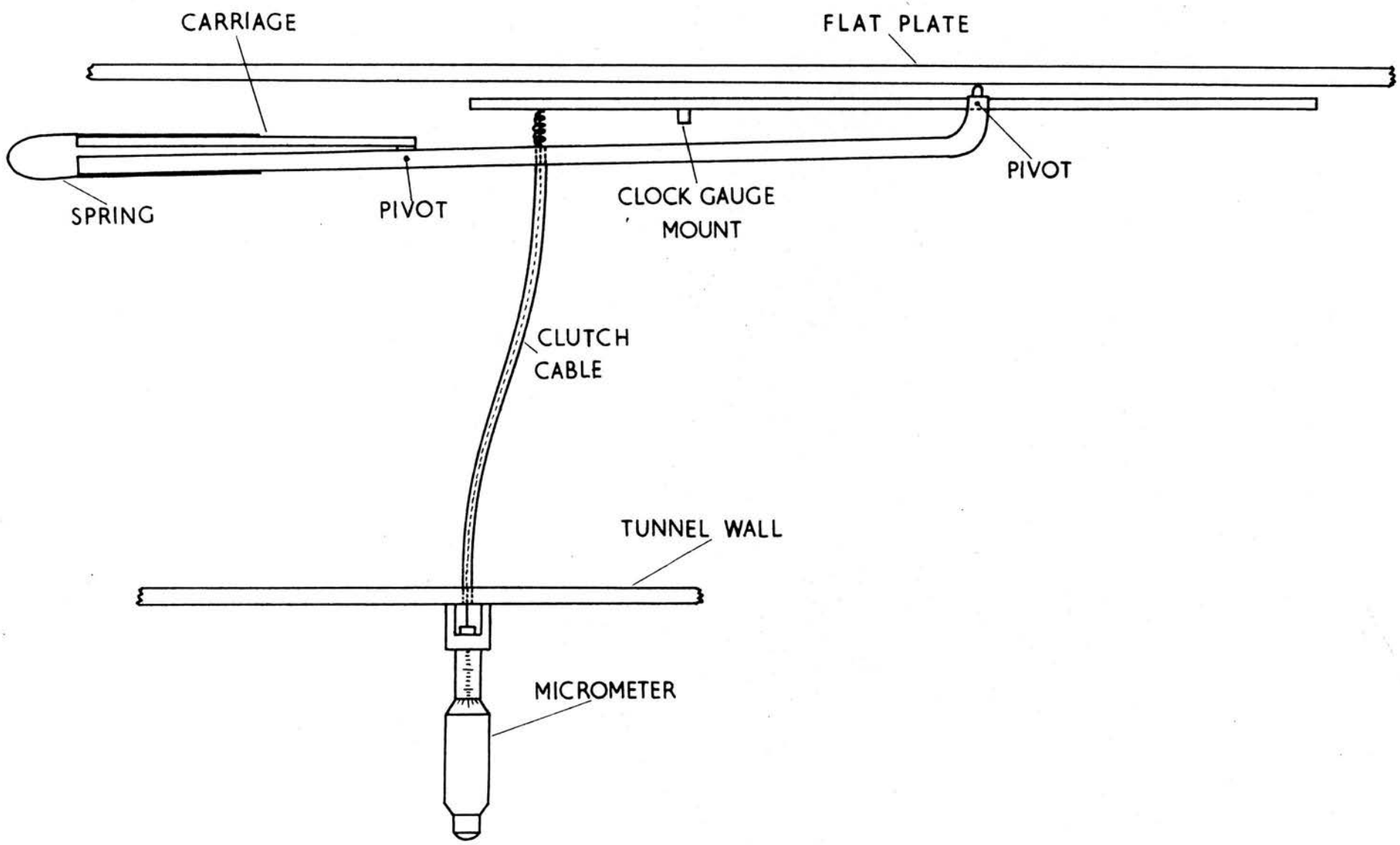

Figure 11

Plan view of second traversing mechanism

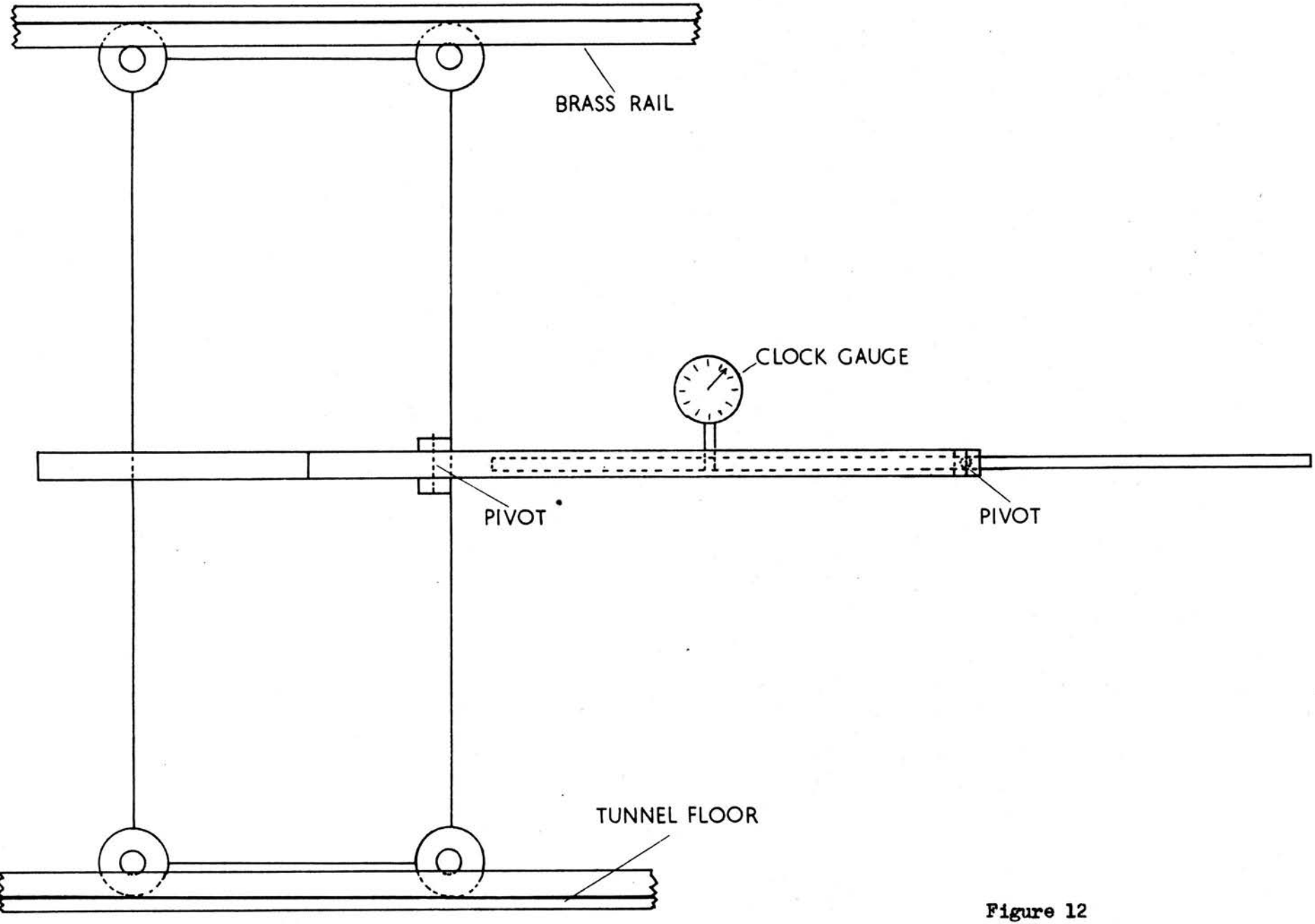

Figure 12

Front elevation of second traversing mechanism

CHAPTER III

Preliminary Measurements and Introductions of Artificial Disturbances into the Boundary Layer

III. 1. Calibration of Wind Speed

The automatic control system kept the wind speed constant, but the value of the wind speed depended on the amount of weights on the scale pan of the pressure balance. In order to obtain any particular value of wind speed, the pressure balance was calibrated by determining the relationship between the wind speed and the weight on the scale pan.

To do this, a standard pitot-static tube, of N.P.L. design, was placed in the working section of the tunnel, at a position 2 feet down-stream from the leading edge. The difference between the total head pressure and the static pressure was measured by a sloping tube manometer. Various weights were placed on the scale pan of the pressure balance and the system allowed to come to equilibrium. The reading on the sloping tube manometer was taken and from the calibration of the manometer the corresponding velocity was

obtained. The calibration of the pressure balance was thus obtained and the result is shown in figure 13.

The sloping tube manometer used contained paraffin and the surface area of the paraffin in the reservoir was approximately 1,500 times the cross section area of the sloping tube. This meant that any error due to the fall of the paraffin level in the reservoir was negligible. The slope of the tube was measured directly using a travelling microscope and it was found to be at an angle of $\sin^{-1} 0.1579$ to the horizontal to an accuracy of 0.13%.

The calibration of the sloping tube manometer was checked using a calibrated Chattock gauge and found to be satisfactory.

III. 2. Measurement and Adjustment of the Pressure Gradient along the Flat Plate

The position of the neutral stability curve for small disturbances and the shape of the boundary layer profile, vary quite considerably with change of pressure gradient along the flat plate. Calculations on this have been made by Schlichting and Ulrich (32) and the results are shown in figures 14 and 15. Figure 14 shows the position of the neutral stability curve, drawn on the $\alpha\delta^*$, R plane, for

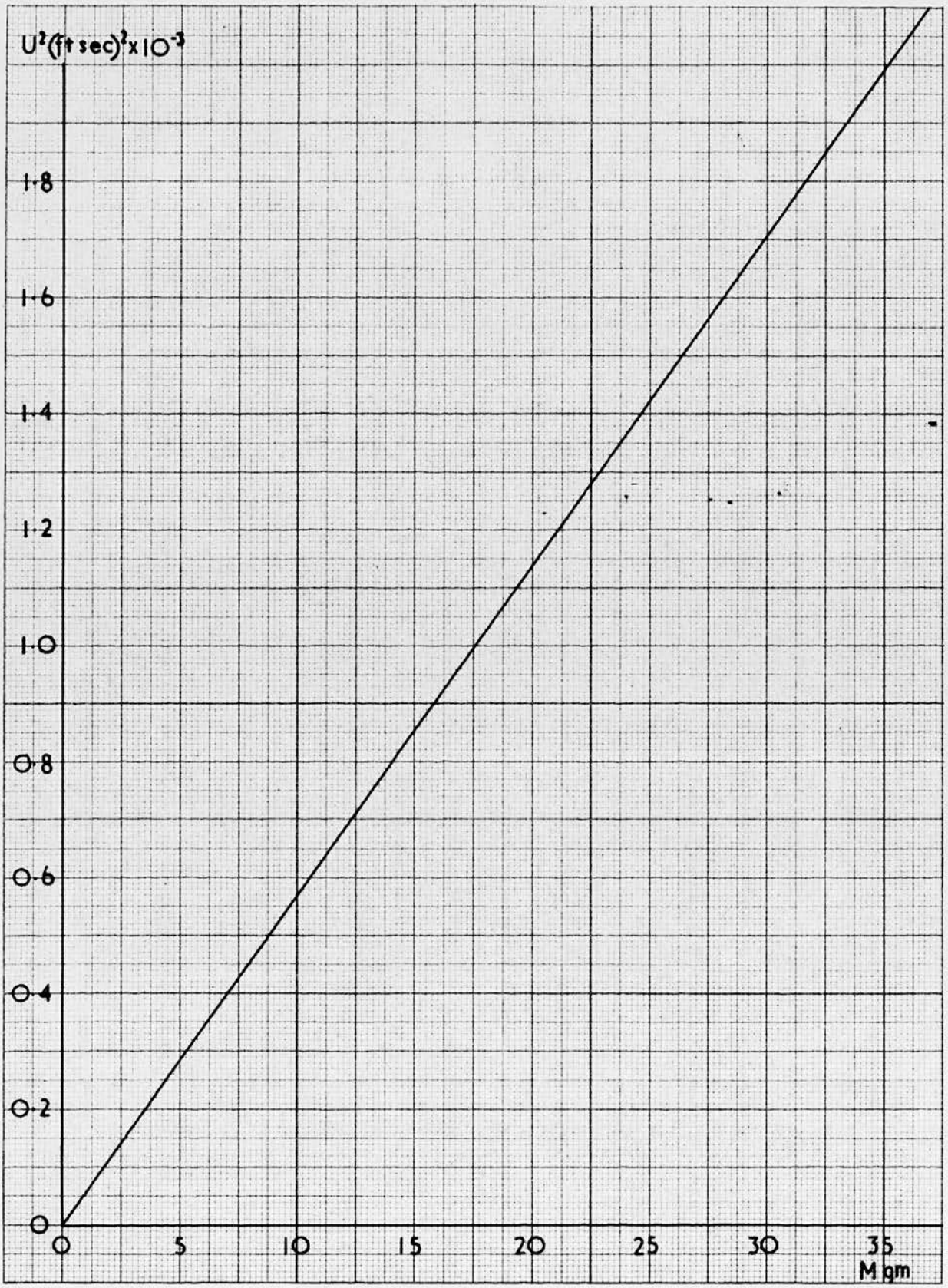

Figure 13

Calibration of pressure balance.

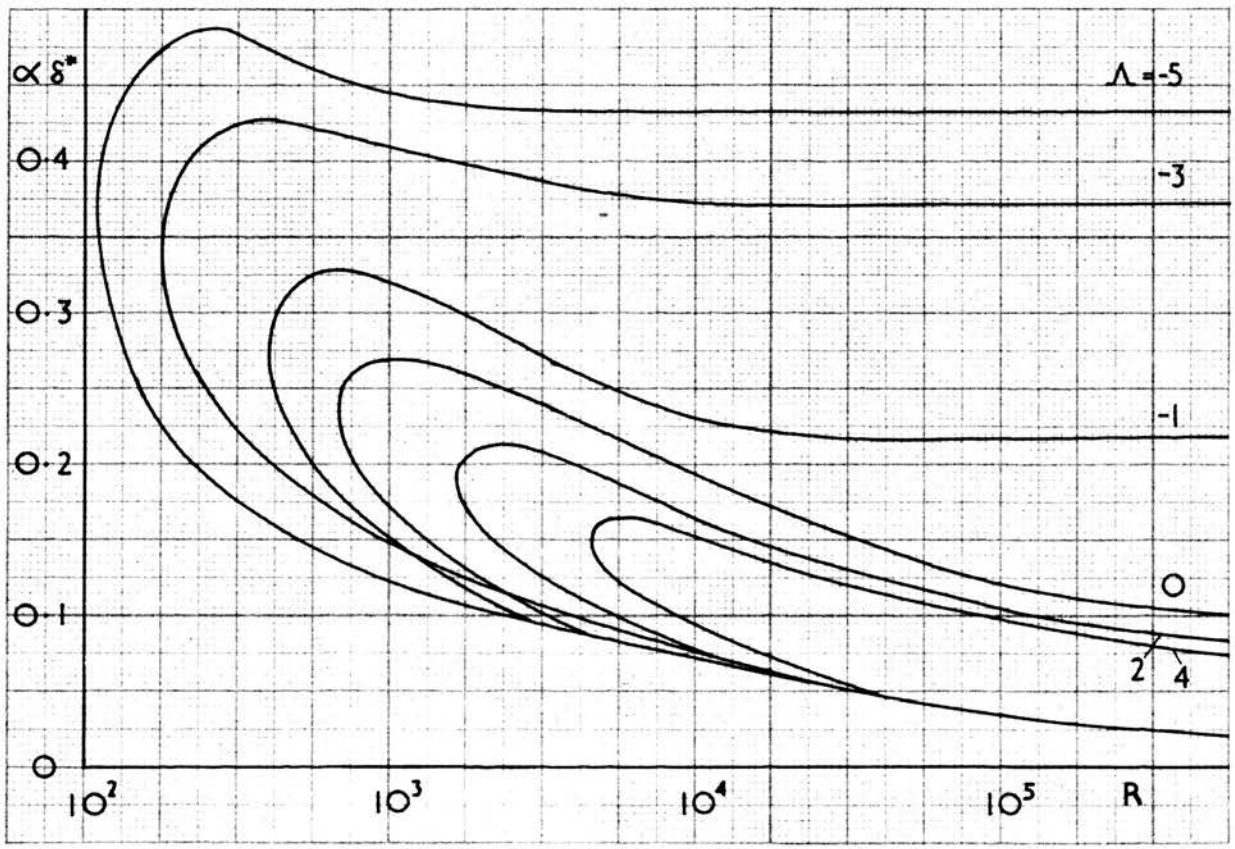

Figure 14

Neutral stability curves for various values of Λ according to Schlichting

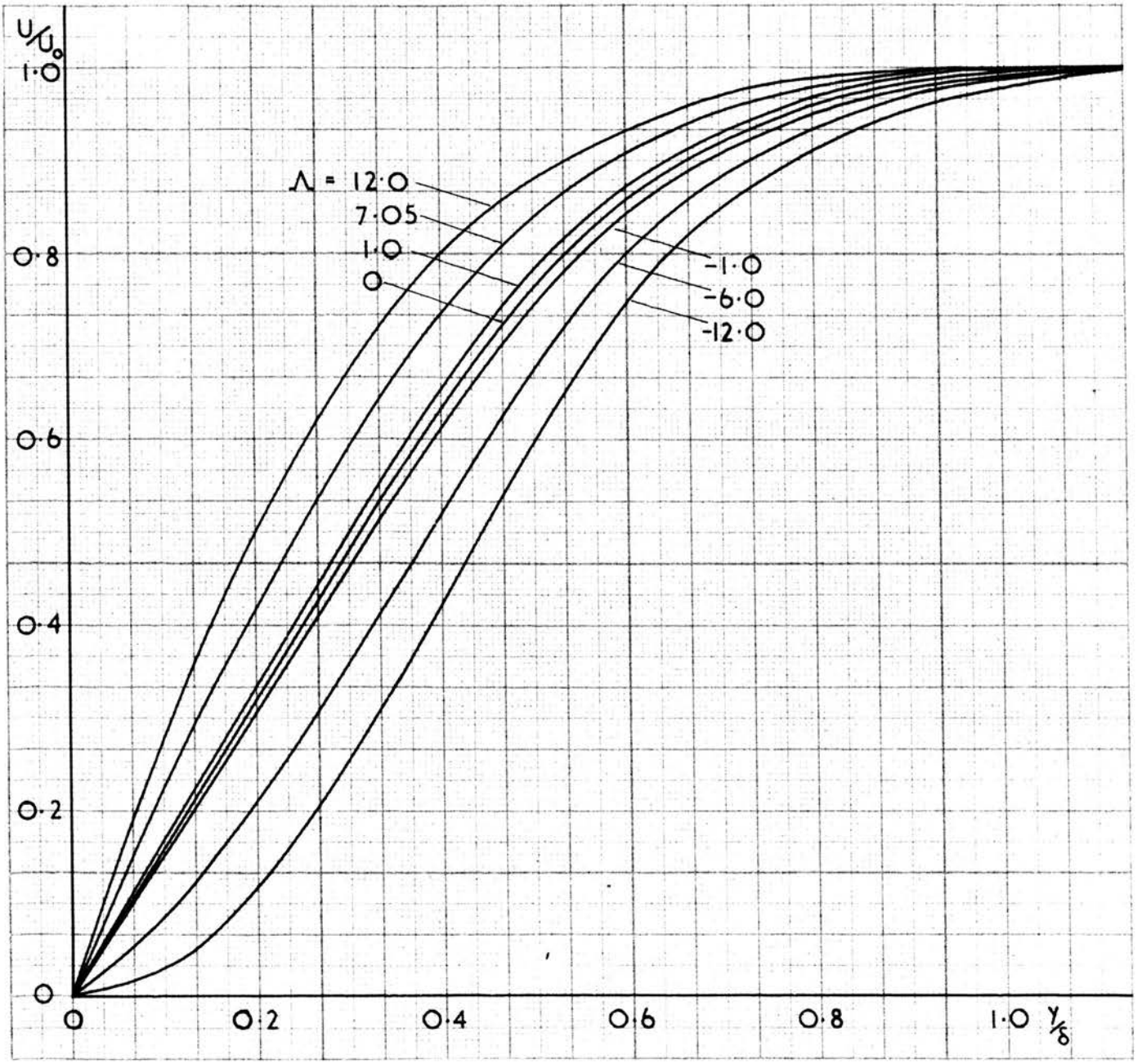

Figure 15

Boundary layer profiles for various values of Λ according to Schlichting

various values of the Polhausen parameter Λ, which is defined by the equation:-

$$\Lambda = \frac{\delta}{\nu} \frac{dU_o}{dx}$$

Figure 15 shows the shape of the boundary layer profile for various values of Λ. It was, therefore, considered important that variations in the pressure gradient along the flat plate, should be as small as possible.

The pressure gradient was measured using a static pressure tube 0.2 inches in diameter and mounted so that it could be moved parallel to the flat plate at a distance of 3 inches from it. The difference between the static pressure and a reference pressure, which was taken from a tapping in the side of the tunnel wall, was measured using a sloping tube manometer. Pressure readings were taken at intervals of 3 inches along the plate and the pressure gradient made as near zero as possible by adjusting the position of the false walls. The final result obtained is shown in figure 16; where the dimensionless quantity $(P - P_r)/\frac{1}{2}\rho U_o^2$ is plotted against x. A distance of one foot from the leading edge was chosen as a reference point and P_r was the pressure at this point.

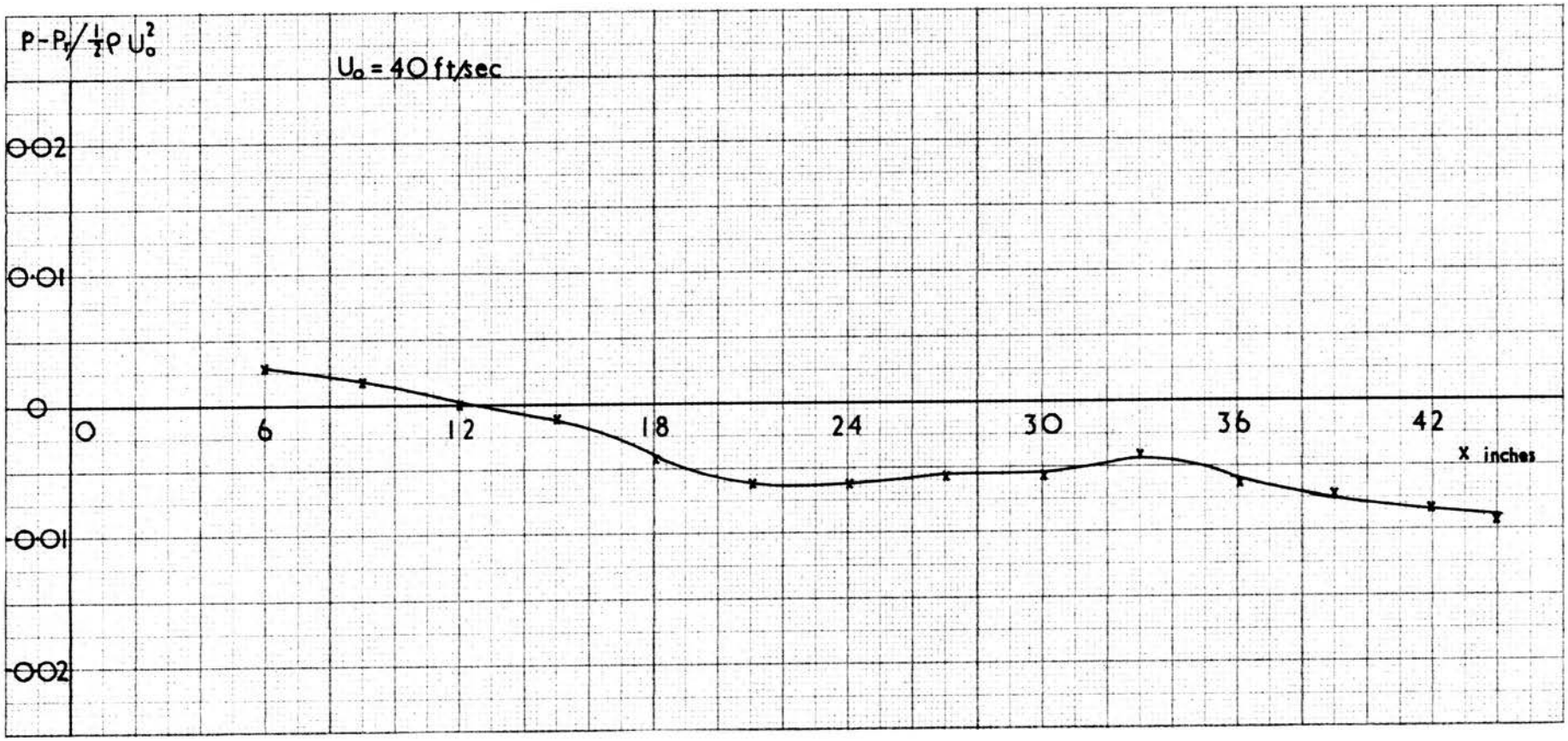

Figure 16

Variation of static pressure

along the flat plate

The maximum variation in the pressure gradient gave a Polhausen parameter of 0.04 which was small enough to have a negligible effect on the position of the neutral curve and the shape of the boundary layer profile.

III. 3. Investigation of Flow over the Flat Plate

Before any investigation of the boundary layer on the flat plate was carried out, the static flow conditions over the plate were determined. It was then seen which region of the plate was suitable for a detailed study of the boundary layer.

Total head and static pressure tubes, made of 0.04 inch diameter hypodermic tubing, were mounted in the tunnel. The end of the total head tube was flattened so that it formed a slit 0.004 inches wide with a wall thickness of 0.005 inches. The static pressure tube had a closed hemispherical end with six 0.008 inch diameter holes at a distance of 0.35 inches from the end, and it was positioned in the tunnel so that it remained outside the boundary layer at a distance of approximately two inches from the flat plate. The difference between the static and total head pressures was measured using the

sloping tube manometer.

Using these tubes, boundary layer profiles were measured at various x-positions along the centre line of the plate. These profiles are shown in figure 17. It is seen that the profiles are in good agreement with the Blasius curve up to a distance of 3 feet from the leading edge of the plate. After this the shape of the profiles alters owing to the onset of transition from laminar to turbulent flow, and at a distance of 4.5 feet from the leading edge, turbulence is well developed.

It can be seen from figure 17 that if the total head tube is traversed downstream, very close to the flat plate, from the laminar region, through transition, to the turbulent region, the pressure reading will at first drop very slowly due to the normal Blasius growth of the laminar boundary layer and when the transition is reached, the value will rise rapidly. The results of such an experiment are shown in figure 18. This experiment provides a simple method of examining the boundary layer and determining where transition from laminar to turbulent flow occurs. The onset of the transition region is taken as the point where the curve just starts to rise and the end of the transition region is taken as the point where the curve

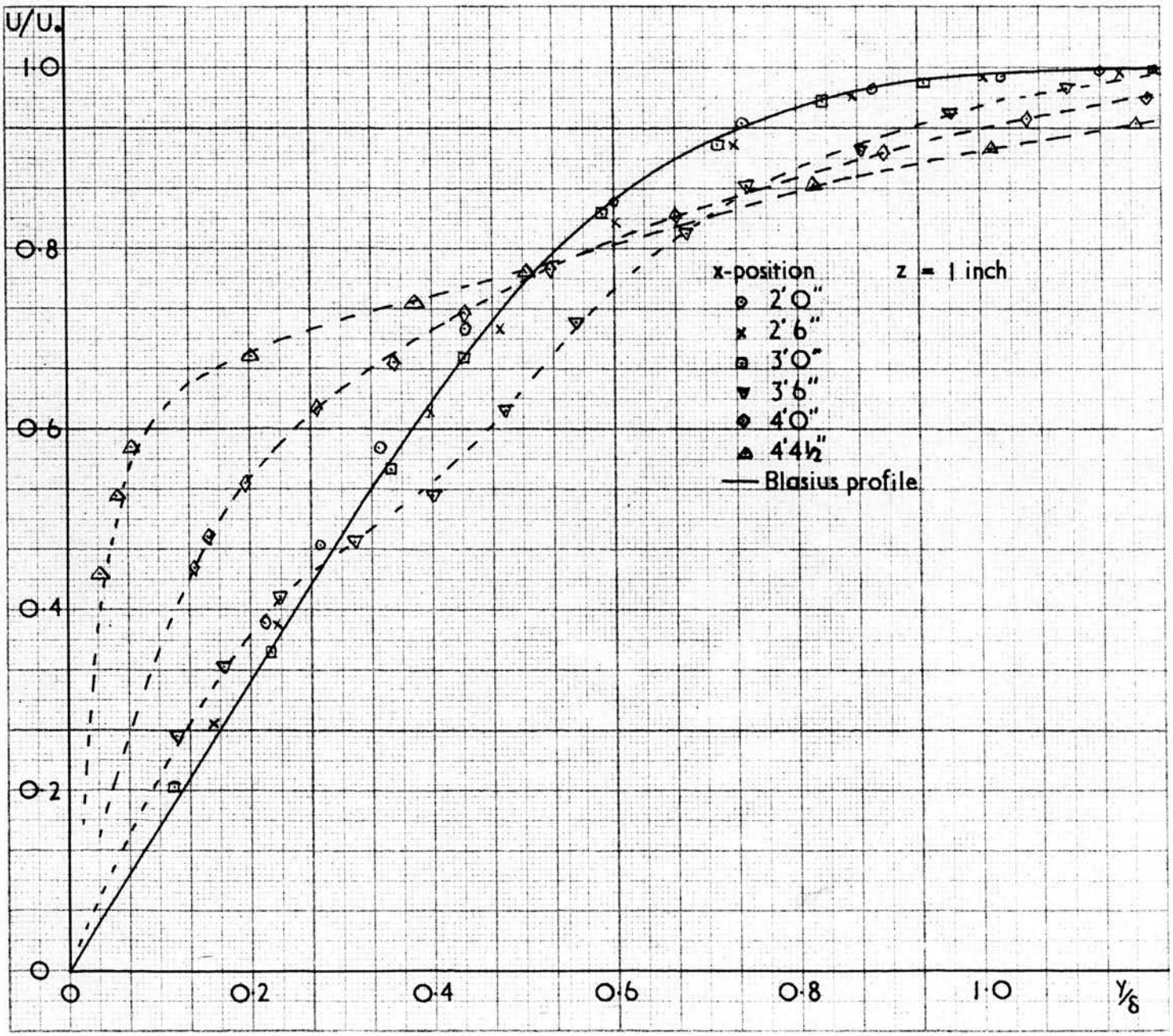

Figure 17

Boundary layer velocity profiles at various x - positions

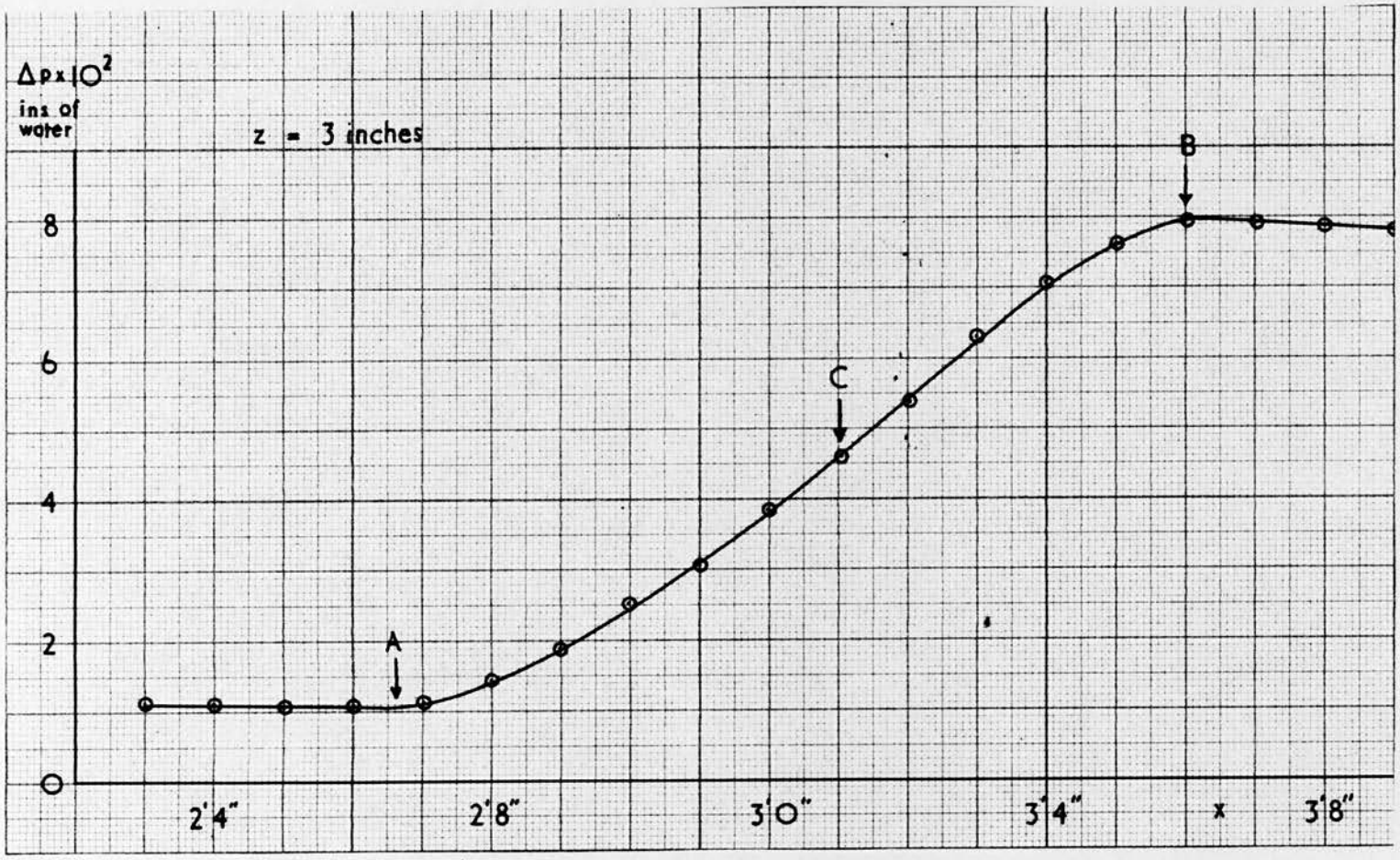

Figure 18

Variation of pressure reading as the total head tube is traversed through the transition region

reaches its maximum value. These are the points A & B in figure 18.

This method was used to study the flow over the plate at various z - positions and the result is shown in figure 19. The laminar part of the boundary layer flow forms a wedge-shaped area; this is because turbulence, caused by the top and bottom of the leading edge of the flat plate, grows towards the centre of the plate. The two turbulent regions meet at a distance of approximately 3.75 feet from the leading edge.

With a free stream turbulence of 0.3% and a wind speed of 100 ft/sec, it was estimated that natural transition would be complete at a distance of 4.65 feet from the leading edge. Since this was the maximum value of wind speed which could be obtained it is seen that natural transition could not be observed.

III. 4. The Oscillating Ribbon Technique

Artificial disturbances were introduced into the boundary layer by means of an oscillating ribbon. This method was first used by Schubauer and Skramstad (6) and has since been successfully used by a number of workers.

The ribbon used was of phosphor bronze 0.1 inches wide and 0.001 inches thick and two methods of mounting it were

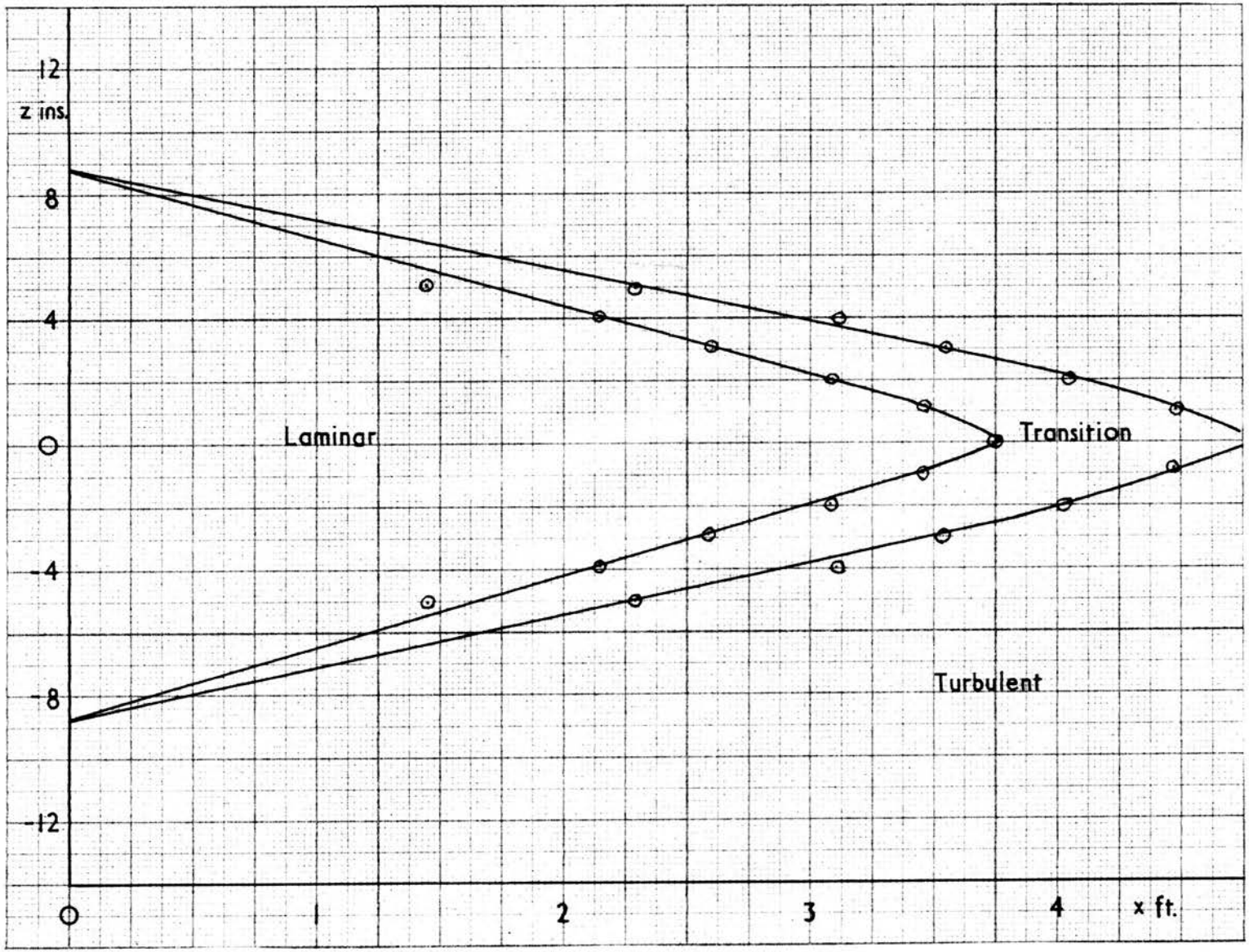

Figure 19

Diagram of static flow pattern on the flat plate

used at different stages of the work. In the earlier part of the work the ribbon was mounted completely inside the tunnel. The top of the ribbon was firmly anchored and at the bottom provision was made so that various weights could be attached, allowing the ribbon to be placed under any required tension. The central six inches of the ribbon was held away from the flat plate by two cylindrical glass bridges, 0.008 inches in diameter. To ensure that the ribbon passed over these bridges it was held against the flat plate by pieces of 'sellotape' just above the top bridge and just below the bottom bridge. The bottom piece of 'sellotape', however, had a small piece of paper stuck to its under side so that it did not stick to the ribbon. Thus the ribbon could move freely under the 'sellotape' and the tension on the ribbon remained constant. This was necessary since it was shown by Miss S.M. Whitelegg (33) that if the ribbon was stuck down at both ends, owing to the high thermal expansion of Perspex, the resonant frequency of the ribbon could alter by as much as 32% for a $1^{\circ}C$. change of temperature; but if the tension in the ribbon remained constant, the change in resonant frequency, with change in temperature, was negligible.

Fixed to the reverse side of the flat plate opposite the ribbon and placed symmetrically about the centre of the

flat plate, was a horse-shoe permanent magnet. The ribbon was therefore in a strong magnetic field parallel to the flat plate and it could be made to oscillate perpendicularly to the flat plate by passing an alternating current through the ribbon. The ribbon current was supplied by an audio-frequency signal generator, so that a control of both frequency and current was easily obtained. It was found that if the ribbon was made to vibrate within 20 cycles/sec. of its resonant frequency, the amplitude varied quite considerably, but on the other hand, if the vibrations were too far off resonance, distortion occurred. The resonant frequency of the ribbon was therefore adjusted, by altering the tension on the ribbon, so that the frequency of oscillation was approximately 30 cycles/sec. below the resonant frequency.

At a later stage in the work the length of the central, vibrating, part of the ribbon was increased to nine inches and three horse-shoe magnets were used instead of one. Small slits were made in the top and bottom of the tunnel to allow the ribbon to pass outside and the weights were attached to the ribbon outside the tunnel. A diagram of the ribbon mounted in the tunnel is given in figure 20.

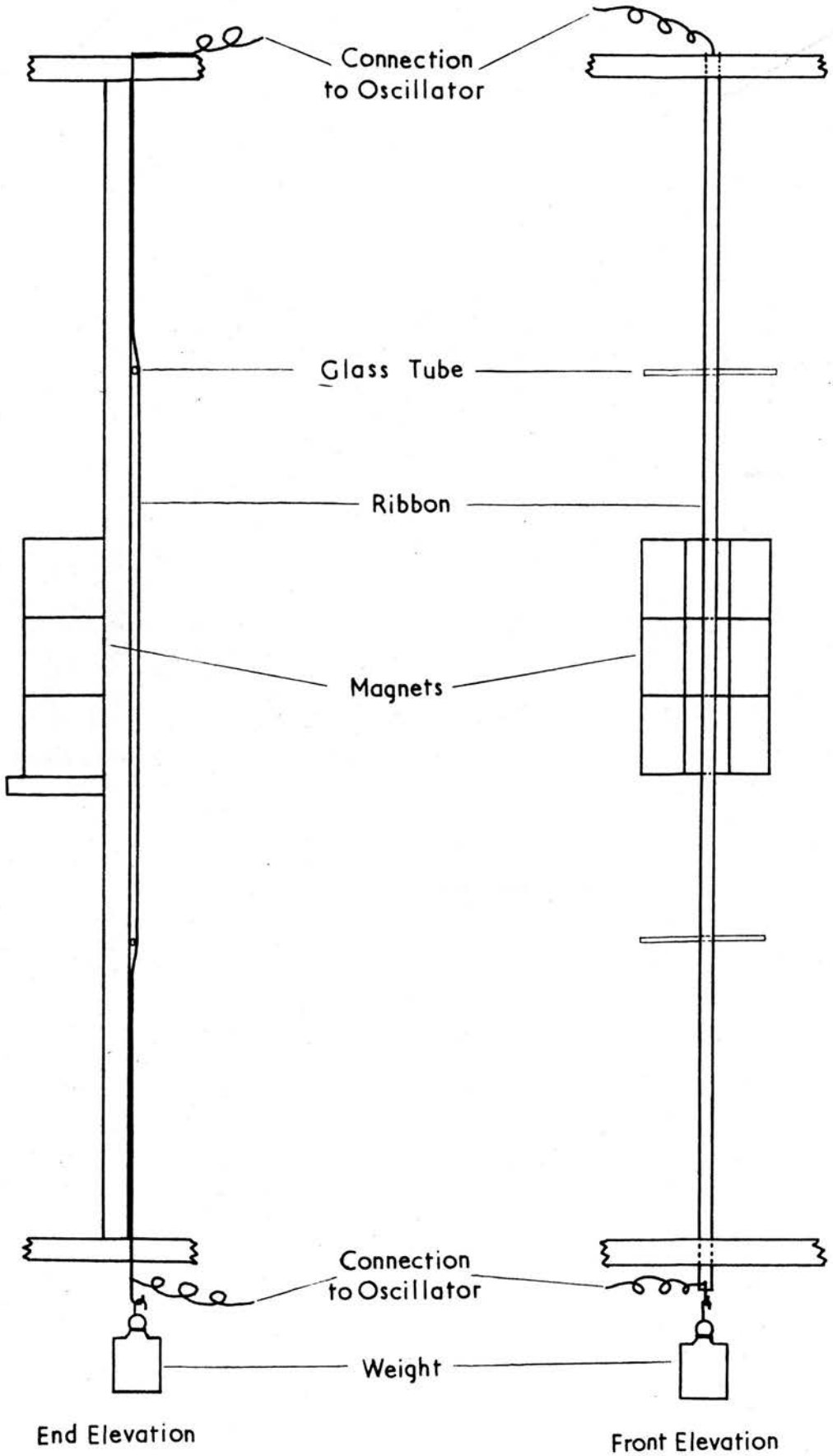

Figure 20

Diagram showing method of ribbon mounting

III. 5. Calibration of the Vibrating Ribbon

The calibration of the ribbon was carried out indirectly by setting up a ribbon on a sheet of Perspex outside the tunnel, in exactly the same manner as the ribbon on the flat plate. The motion of the ribbon was then examined using a travelling microscope. This method, however, proved unsatisfactory because of the difficulty involved in mounting the ribbon in exactly the same way as in the tunnel. The motion of the ribbon appeared to depend, to a great extent, on the manner in which the ribbon was mounted and great care had to be taken to ensure that it hung vertically, otherwise twisting occurred. This twisting appeared to be caused by an uneven distribution of tension across the ribbon which resulted in each side having a slightly different resonant frequency.

It was thought that if at all possible it would be of considerable advantage to have some method of measuring the amplitude of the ribbon so that it could be continuously monitored. This meant that a method had to be devised whereby the amplitude of the ribbon could be measured without disturbing the flow over the flat plate.

Several methods were examined but the most successful involved making the ribbon one plate of a capacitor, placing a fairly large voltage on it, and measuring the a.c. voltage on the other plate of the capacitor when the ribbon is vibrated. The principle of this method can be shown using the simple R-C circuit:-

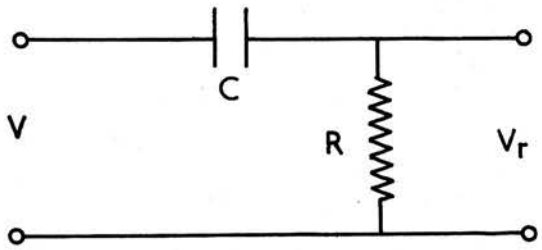

This is an ordinary differentiating circuit but instead of the voltage V varying the capacity C varies. It follows that provided the time constant RC is small then

$$V_r = iR = RV \frac{dC}{dt} .$$

But for a parallel plate condenser,

$$C = \frac{Ak}{4\pi D}$$

where A is the area of the plates, D is their separation and k is the dielectric constant of the medium between them. For convenience this can be written

$$C = \frac{K}{D} \quad \text{where} \quad K = \frac{Ak}{4\pi}$$

If one plate of the capacitor vibrates such that the distance between the plates can be expressed as $D = D_o + D_1 \cos \omega t$, then

$$C = \frac{K}{D_o + D_1 \cos \omega t}$$

and if $D_1 << D_o$, this can written

$$C = \frac{K}{D_o} \left(1 - \frac{D_1}{D_o} \cos \omega t \right)$$

$$\therefore \frac{dC}{dt} = \frac{KD_1}{D_o^2} \sin \omega t$$

$$\therefore Vr = RVK \frac{D_1}{D_o^2} \sin \omega t.$$

Thus provided that the amplitude of the ribbon is very much smaller than the distance between the ribbon and the other plate of the capacitor, the amplitude of the voltage measured across the resistance will be proportional to the amplitude of the ribbon.

The most suitable position for a small plate which with the ribbon would form a capacitor, was thought to be on the opposite side of the flat plate from the ribbon. A small piece of metal foil was therefore placed in this position and from it a resistance was taken to earth. The a.c. voltage across this resistance was extremely small and although the amplifiers available allowed an amplification of 60,000 times, a d.c. voltage of 1,400 volts

had to be applied to the ribbon before a measurable signal was obtained for the lowest ribbon amplitude required. This seemed satisfactory and the condition, that the distance between the plates should be very much greater than the amplitude of the ribbon, was satisfied, since the flat plate was 0.25 inches thick and the maximum ribbon amplitude which could be obtained was 0.008 inches.

When a calibration of the ribbon was attempted, it was discovered that the output voltage varied considerably from one day to the next. The cause of this was eventually traced to the accumulation of charge on the flat plate between the ribbon and the metal foil. An attempt was made to find some method of removing this charge but a permanent removal seemed to be impossible.

It was thought that the difficulty arising from this accumulation of charge could be averted if the capacitor plate was on the working side of the flat plate; however, in order that the flow should remain undisturbed the only possible position for the plate was on the surface of the flat plate, underneath the ribbon. A small probe was taken from the opposite side of the flat plate, underneath

the ribbon and made flush with the surface of the plate. A thin layer of 'Aquadag' (this is a suspension of graphite in water) was then painted on the surface of the plate over this probe and when the water avaporated a very thin layer of graphite was left. This layer of graphite and the ribbon then formed the plates of a capacitor - electrical contact being made to the graphite by means of the probe. The voltage now obtained across the resistance connected from the probe to earth, was considerably greater and a measurable signal was obtained with 120 volts on the ribbon. The signal, however, was no longer sinusoidal, but was more inclined to be of a saw-tooth shape. This was due to the fact that in bringing the condenser plate to the working side of the plate, the distance between the plates was now of the same order of magnitude as the ribbon amplitude, and the output signal was therefore no longer proportional to the ribbon amplitude.

Despite this drawback the method still proved to be extremely useful, because even although the signal was distorted it remained constant for each ribbon amplitude and once this amplitude was set the reading could

be constantly monitored to ensure that it remained constant throughout each experiment.

With the development of the 'hot wire', the calibration of the ribbon was not essential, but it was still extremely useful to be able to keep a continual check on the ribbon performance throughout an experiment.

CHAPTER IV

The Hot Wire Anemometer

IV. 1. Introduction

Crude hot-wire instruments were first used in about the year 1900, to measure wind velocities. Since then the technique has been developed considerably, and hot-wire anemometers are now used extensively for the measurement of the instantaneous velocity component of a fluid stream.

The hot-wire method depends essentially on the fact that the loss of heat from a heated wire placed in a fluid stream, is a function of the velocity of the stream. The hot-wire is usually a very thin piece of either tungsten or platinum wire and is heated by means of an electric current. There are two types of instruments used; one in which the wire current is kept constant, the other in which the wire temperature is kept constant. In the constant current type, the current in the wire is kept constant, by placing a large fixed resistance in series with the hot-wire, and the voltage across the wire is

then examined. In this system, if the fluctuation frequency is large, the response of the hot-wire is modified by the heat capacity of the wire; however, it is possible to include a circuit in the system which will compensate for this effect. The constant temperature type system employs a feed-back circuit which maintains the wire at constant resistance and therefore constant temperature. The electrical energy input to the wire is then a measure of the instantaneous fluid velocity.

Although the constant temperature system has theoretical advantages over the constant current system, it is subject to some serious design limitations. Noise levels are generally higher and the high gain d.c. amplifiers must be carefully controlled for drift. High capacity power supplies must be regulated to better that 0.001%, which implies great expense and bulk. For these reasons the constant current type instrument is more commonly used.

IV. 2. Theoretical Approach to the Flow of Air over a Heated Wire.

Consider a thin wire which is heated electrically, immersed in a fluid stream. Let the wire axis be

perpendicular to the direction of the fluid velocity. The heat lost by the wire, by transfer to the stream, can be represented by the formula;

$$H = L(Tw - Te)(A\sqrt{U} + B) \quad \ldots\ (1)$$

where H - heat loss of wire per unit time.

L - hot-wire length.

Tw - wire temperature when heated.

Te - wire temperature when unheated.

A&B - convection constants.

U - stream velocity.

This formula was first derived by King (34) in 1914 and is generally referred to as King's Law.

According to the law of conservation of energy, the difference between the heat generated in the wire and the heat lost to the air will be equal to the thermal energy, accumulated in the wire;

$$\therefore \quad I^2Rw - L(Tw - Te)(A\sqrt{U} + B) = C_T \frac{dTw}{dt} \quad \ldots\ (2)$$

where I - wire current.

Rw - wire resistance at temperature Tw.

C_T - thermal capacity of the wire.

If the mass of the wire is small and the velocity fluctuations are slow, then the right hand side of the equation can be neglected;

$$\therefore I^2Rw = L(Tw - Te)(A\sqrt{U} + B) \quad .... (3)$$

If α_o denotes the temperature coefficient of resistance of the wire then,

$$R = Ro\left[1 + \alpha o(T - To)\right] \quad .... (4)$$

where Ro is the wire resistance at temperature To and R is the wire resistance at temperature T. The product $\alpha o Ro$ is the slope of the resistance-temperature curve at To and is nearly constant over a wide range of To for most wire materials.

$$\therefore Rw - Re = Ro\,\alpha o(Tw - Te) \quad .... (5)$$

where Re is the wire resistance at temperature Te and Ro is its resistance at a reference temperature To. Substituting for (Tw - Te) in equation (3) gives

$$I^2Rw = \frac{L(Rw - Re)}{Ro\,\alpha o}(A\sqrt{U} + B)$$

$$\therefore \frac{Rw}{Rw - Re} = \frac{L}{I^2Ro\,\alpha o}(A\sqrt{U} + B) \quad .... (6)$$

putting $\rho = \frac{Rw}{Rw - Re}$

$$A' = \frac{LA}{I^2 Ro \alpha o}$$

$$\rho o = \frac{LB}{I^2 Ro \alpha o}$$

equation (6) becomes

$$\rho = A' \sqrt{U} + \rho o \qquad \ldots\ldots (7)$$

If I is constant, then A' and ρo are also constant and there is therefore a linear relationship between ρ and $\sqrt{U}$. Once this relationship has been obtained the hot-wire can be used to measure the constant velocity of a fluid stream.

Variations in the temperature of the wire, caused by fluctuations in the velocity of the stream, result in variations of the resistance of the wire and these resistance variations can then be measured as a fluctuating voltage. By differentiating equation (7) the resistance fluctuations can be represented by the equation

$$\frac{d\rho}{(\rho - \rho o)} = \frac{1}{2} \frac{dU}{U}$$

but $d\rho = \frac{Re}{(Rw - Re)^2} dRw$

$$\therefore \quad \frac{dRw\ Re}{(Rw - Re)^2(\rho - \rho o)} = \frac{1}{2} \frac{dU}{U} \qquad \ldots\ (8)$$

Expressing the voltage fluctuations as $\tilde{e} = I\ dRw$ then equation (8) becomes

$$\frac{\tilde{e}}{I\ Re} \frac{2(\rho - 1)^2}{(\rho - \rho o)} = \frac{dU}{U} \qquad \ldots\ (9)$$

If, using equation (7) the wire is first calibrated for several values of U, and ρo found, then the fluctuating velocity can be calculated from equation (9).

It has been suggested by Collis and Williams (35), that if the velocity range is fairly large, then in King's Law the power of U should be 0.45 rather than 0.5. This means that equation (7) becomes

$$\rho = A' U^{0.45} + \rho o \qquad \ldots\ (10)$$

and equation (9) becomes

$$\frac{\tilde{e}\ (\rho - 1)^2}{0.45 I Re(\rho - \rho o)} = \frac{dU}{U} \qquad \ldots\ (11)$$

In practice, it was found when calibrating hot-wires, that a linear relationship between ρ and U was only obtained if the 0.45 power of U was used. Equations (10) and (11) were therefore always used in the calculation of the fluctuating velocity component.

IV. 3. Details of the hot-wire circuit

The hot-wire system was of the constant current type, with the heating current supplied from a transistor circuit. Currents within the range 0 - 100 m.a. in hot wires with resistances in the range 0 - 100 ohms were then obtainable using a 12 volt d.c. supply. A two channel system with compensation stages was available but for the present work only one channel was used. The basic circuit is shown in figure 21.

The current through the transistor and therefore through the hot-wire, was controlled by the variable resistors R_2 and R_3, and the fixed resistor R_1 ensured that the resistance in the circuit was never zero. A very small current could be passed through the hot-wire by switching in the large resistance R_4; this enabled the 'cold' resistance of the wire to be measured. The voltage across

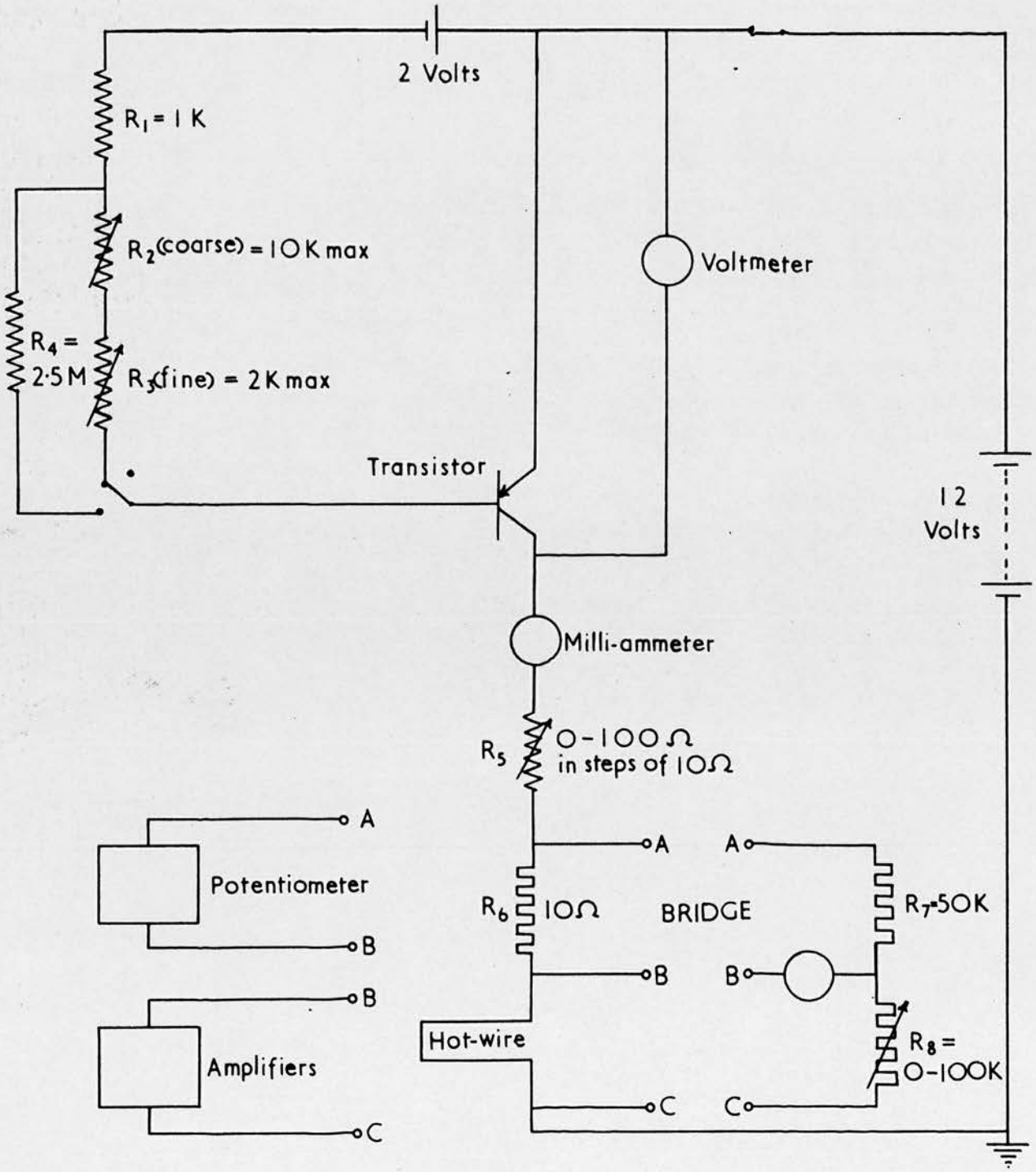

Figure 21

Circuit diagram of hot-wire system

the transistor was measured on the voltmeter and its value controlled by the variable resistor R_5. The current through the hot-wire as read on the milli-ammeter was set approximately, and then measured accurately by connecting a potentiometer across the standard 10 ohm resistor, R_6. The resistance of the hot-wire was measured by connecting A, B and C into the bridge circuit and allowing the hot-wire current to flow through this bridge. To avoid any change in the hot-wire resistance during this process, the resistances R_7 and R_8 were made large, and of the order of 10^5 times the resistances of the hot-wire and R_6.

The measurement of the 'cold' resistance of the wire was made in the same way, using in this case the 'cold' resistance current to balance the bridge. Because this current was small, the 'cold' resistance was the least accurate resistance measurement having an error of $\pm$ 0.5%. The error in 'hot'-wire resistance was negligible by comparison with the 'cold' resistance and the current measurement was correct to $\pm$ 0.1%. The current was constant, with respect to change of wire resistance, to 1 part in 300; i.e. for a 1% change in wire resistance the current changed by 1/300%.

The fluctuating voltage across the hot-wire was amplified

and fed to a valve voltmeter. A valve voltmeter operates by the charging of its input capacitor and its dial is calibrated to read r.m.s. voltage from the peak of the signal. Such an instrument reads accurately only on a sinusoidal signal. It was originally thought that since the hot-wire was detecting signals produced by injecting sinusoidal disturbances, the valve voltmeter would function correctly. During the course of the work, however, evidence was found which indicated that harmonics of the sinusoidal disturbance were present. After this the valve voltmeter was replaced by a linear recording system using photographic recording of a C.R.O. trace.

The amplifiers used were Solartron d.c. decade amplifiers, type A.A. 900. These are low noise, low drift, wide band d.c. amplifiers which provide accurate amplification of low level signals.

IV. 4. The hot-wire probe

In designing the hot-wire probe care had to be taken to ensure that it did not cause any undue blockage of the air-stream, and that the upstream influence of vortex shedding from the probe components was negligible. This entailed keeping the probe as small as possible and streamlining it in the direction of the air flow.

The body of the probe was made of ¼ inch diameter brass tubing with two steel sewing needles forming the prongs. One needle was soldered to the inside of the tube, the other passed through the tube and was insulated from it by 'araldite'. The end of the body was machined so that it fitted into another brass tube which formed a support for the probe. Connected to the other end of this tube was a coaxial cable whose central wire passed through the tube and was fixed so that it made electrical contact with the central needle of the probe. In this way the hot-wire circuit was screened except for the short distance of the length of the prongs. The probe with the supporting tube was fixed to the traversing mechanism and could be placed at any desired position in the boundary layer.

A diagram of the probe is given in figure 22.

IV. 5. Manufacture of hot-wires

The hot-wires were manufactured from 0.0002 inch diameter tungsten wire, although some workers have used platinum for this purpose. Tungsten is however about five times as strong as platinum and moreover it was thought that with an open circuit tunnel the dust content of the air-stream was likely to be greater than for a closed circuit tunnel and previous workers have found that platinum wires

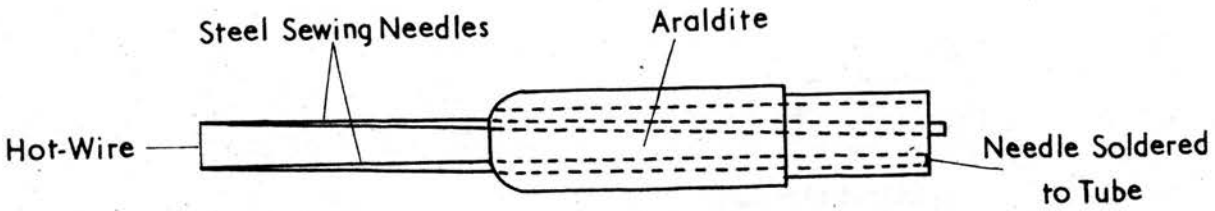

Figure 22

Diagram of hot-wire probe

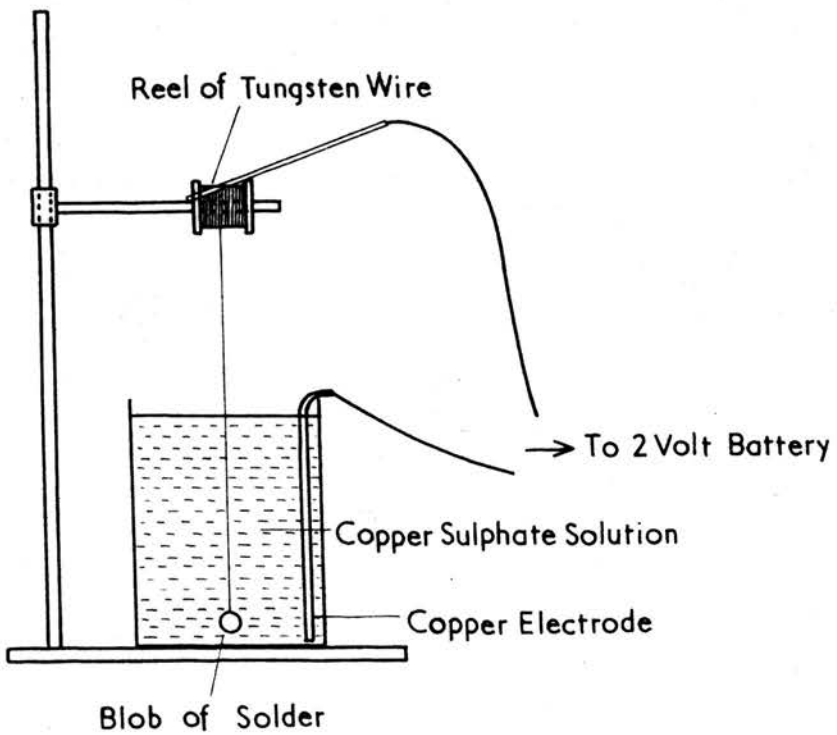

Figure 23

Diagram of copper plating system

are easily destroyed by dust in the air-stream.

Since tungsten does not solder, it was first plated with copper so that it could be soldered to the prongs of the probe and then the copper was etched away from the central part of the wire. It is possible to weld the tungsten wire to the prongs by discharging a capacitor as contact is made, but this method was not attempted. The technique for plating and etching tungsten wire is described in detail by Bradshaw (36), and, in principle, his method was followed.

The wire was first cleaned by making it the anode in a bath of strong solium carbonate solution, using a platinum cathode, and passing a current for a few minutes. Bradshaw recommends a current of 5 milli-amps for a 3 inch length of 0.0002 inch diameter tungsten wire, but it was found that with this current the wire broke after a few seconds. A current of 1 milli-amp was found more suitable. The wire was then washed in distilled water and placed in a plating bath of saturated copper sulphate solution with 10% by volume of concentrated sulphuric acid, and a pure copper electrode. Bradshaw's recommended current of 0.3 milli-amps for a 3 inch length of 0.0002 inch diameter wire was satisfactory, the wire being sufficiently plated after a

period of a few hours. It was found that if the plated wire was too thick it became brittle and very difficult to manage, so for this reason the wire was never plated to more than two or three times its original diameter. For convenience a small piece of solder was attached to the end of the wire and the wire suspended from its reel over the cleaning and plating baths. Electrical contact was then made to the wire by touching the reel. A diagram of the plating system is shown in figure 23.

A piece of the plated wire was then soldered across the prongs of the probe, as near the tips as possible. This proved to be rather a delicate operation, but after a little practice it became fairly routine. Etching of the wire was carried out by directing a fine jet of 10% nitric acid on the wire; the jet was obtained from a small burette mounted above the wire. If a voltage of about 6 volts was applied to the wire, the electrical circuit being made through an electrode in the burette, then the etching process only took a few seconds. The probe was mounted on a stand which allowed a fairly fine movement of the wire through the jet, enabling the length of etched portion of the wire to be controlled easily.

IV. 6. Development of apparatus to determine the y - position of the hot-wire

When the hot-wire was mounted on the traversing mechanism, its movement perpendicular to the flat plate could be measured accurately on the clock gauge, but its actual distance from the flat plate could not be determined. It was therefore essential that a method should be devised to measure this distance.

The position of the prongs in the boundary layer was determined by an optical method. A narrow plane mirror was placed at the bottom of the tunnel at 45° to the flat plate and touching it. The mirror was directly below the hot-wire probe so that with proper illumination the probe, and its reflection in the perspex flat plate, could be viewed by means of the mirror, through a telescope mounted outside the tunnel. This arrangement is shown in figure 24. The reading on the clock gauge when the prongs just touched the flat plate was then determined. However, because of the impossibility of placing each hot-wire in exactly the same position on the prongs, there was still an amount of uncertainity as to the position of the hot-wire.

To overcome this problem it was necessary to measure the distance of the hot-wire from the plate when the prongs

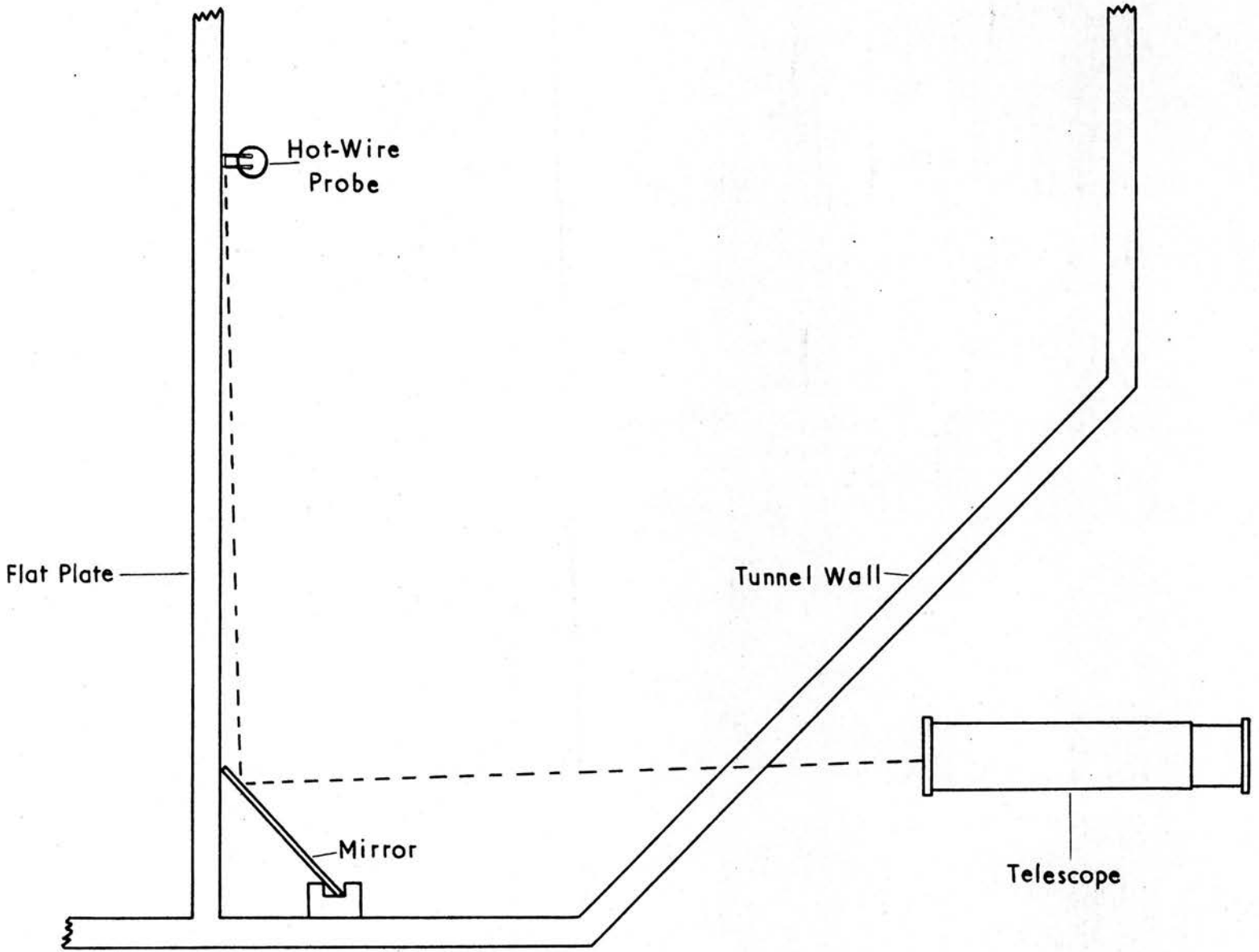

Figure 24

Diagram of method used to position the hot-wire prongs

were just touching it, the plate, and a method of measuring this distance was devised. A diagram illustrating this method is given in figure 25. A piece of brass tubing was fixed to a pivot on a small perspex plate mounted outside the tunnel. The hot-wire probe was fitted to one end of the tube and the other end was attached to a micrometer screw so that the probe could be moved perpendicularly to the perspex plate, in the same manner as in the tunnel. The prongs and hot-wire were then examined, using a travelling microscope, and the distance of the hot-wire from the plate when the prongs were just touching it was determined. Knowing this distance and the clock gauge reading when the prongs touch the flat plate, the actual y - position of the hot-wire could be calculated.

IV. 7. Calibration of the hot-wire

It has been shown previously, in section IV. 2, that before a hot-wire can be used to measure the fluctuating velocity component, the calibration curve of equation (10) for constant velocity conditions must be determined. Since equation (10) represents a straight line, the calibration is easily carried out by placing the hot-wire in the free stream and measuring its resistance for a

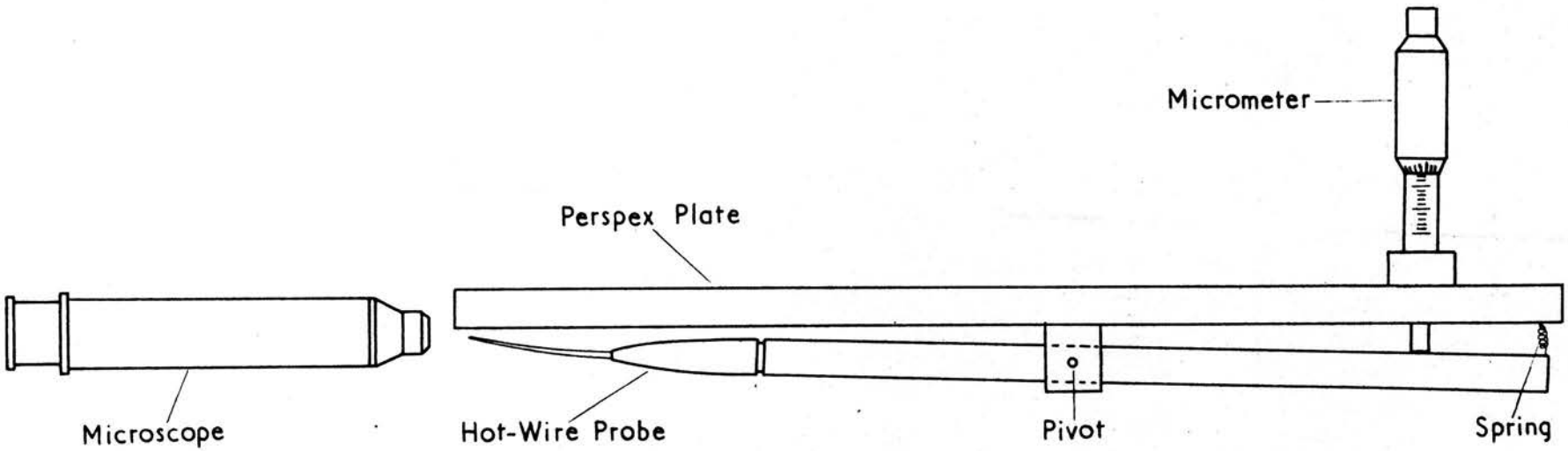

Figure 25

Diagram of method used to measure the distance of the hot-wire from the plate when the prongs were just touching the plate

series of windspeeds.

After a hot-wire was manufactured, it was placed in position in the tunnel and a current of approximately 20 milli-amps was passed through it for a period of about one hour. This helped to prevent drifting after the wire was calibrated. The 'cold' resistance of the wire was then measured, and the current which was required to double the 'cold' resistance was used as the working current. For a wire with 'cold' resistance of 8 ohms this was approximately 40 milli-amps. The resistance of the wire was then measured with free-stream velocities of 15, 20, 25, 30, 35, 40 and 45 ft/sec., and the value of $\rho = Rw/(Rw - Re)$ calculated for each wind-speed. ρ was then plotted against $U^{0.45}$ and a straight line graph was obtained. A typical calibration is given in figure 26. To demonstrate the difference between using $U^{0.45}$ instead $U^{0.5}$, figure 26 also shows the same set of results with ρ plotted against $U^{0.5}$ and it is seen that the points do not lie on a straight line.

As a check on the calibration obtained as described above, it was decided to compare the velocity profiles as measured by Pitot tube and by hot-wire anemometer since

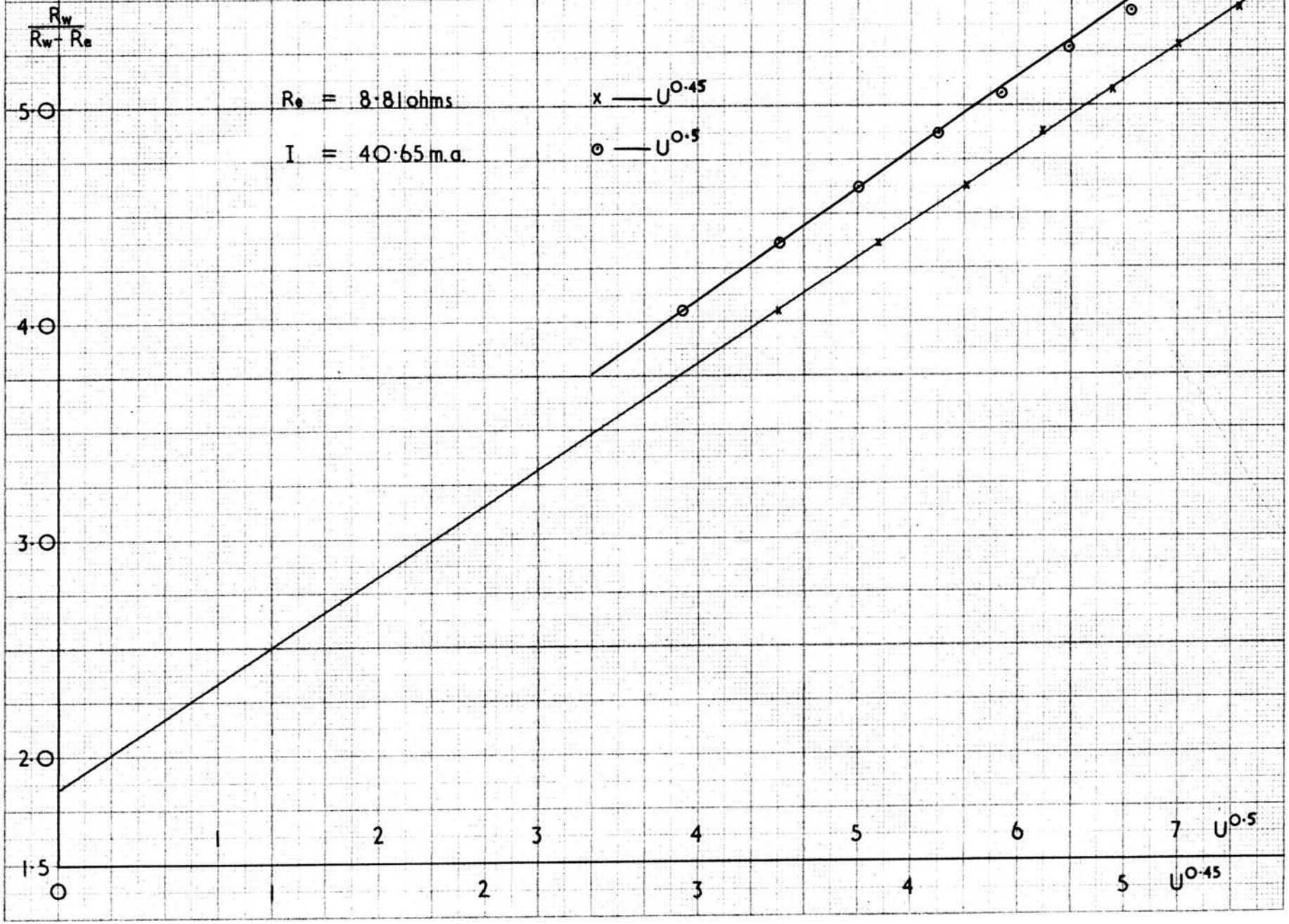

Figure 26

Typical calibration graph of hot-wire

the profiles obtained from Pitot tube measurements were in good agreement with the Blasius distribution and they were therefore regarded as good measurements. The hot-wire was therefore traversed through the boundary layer and its resistance was measured at y - intervals of 0.01 inches. From the calibration, the value of the velocity was determined for each position and the velocity profile obtained. Figure 27 shows a typical result obtained with the hot-wire and this is seen to be in good agreement with the Blasius curve.

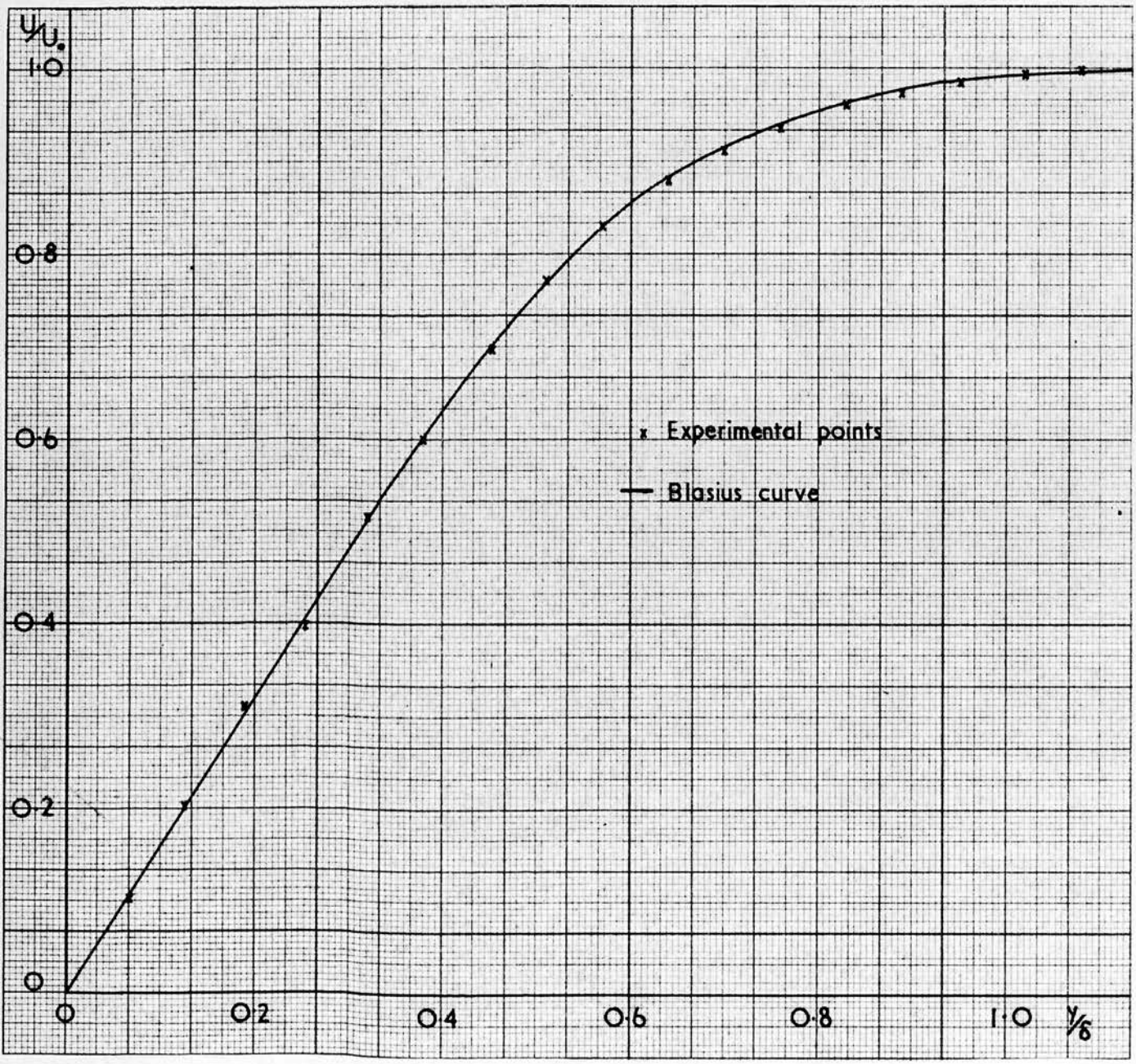

Figure 27

Velocity profile obtained with hot-wire.

CHAPTER V

BOUNDARY LAYER MEASUREMENTS

V.1. Transition caused by vibrating ribbon

In section III. 3, it was pointed out that, because of the size of the tunnel, natural transition could not be observed; in order to study transition it was therefore necessary to produce it artificially. The oscillating ribbon (see Chapter III. 4.) was used to inject disturbances into the boundary layer and, depending on the amplitude and frequency of the ribbon vibrations, the x - position of the transition from laminar to turbulent flow could be varied over quite a wide range. To demonstrate this, boundary layer profiles were measured at a fixed x - position, with one frequency and several amplitudes of ribbon vibration. A set of typical profiles are illustrated in figure 28. This shows that for the smallest ribbon amplitude the boundary layer remains laminar, and that, as the amplitude, is increased, the profiles indicate that turbulence is gradually developed, until at the largest amplitude the boundary layer is fully turbulent.

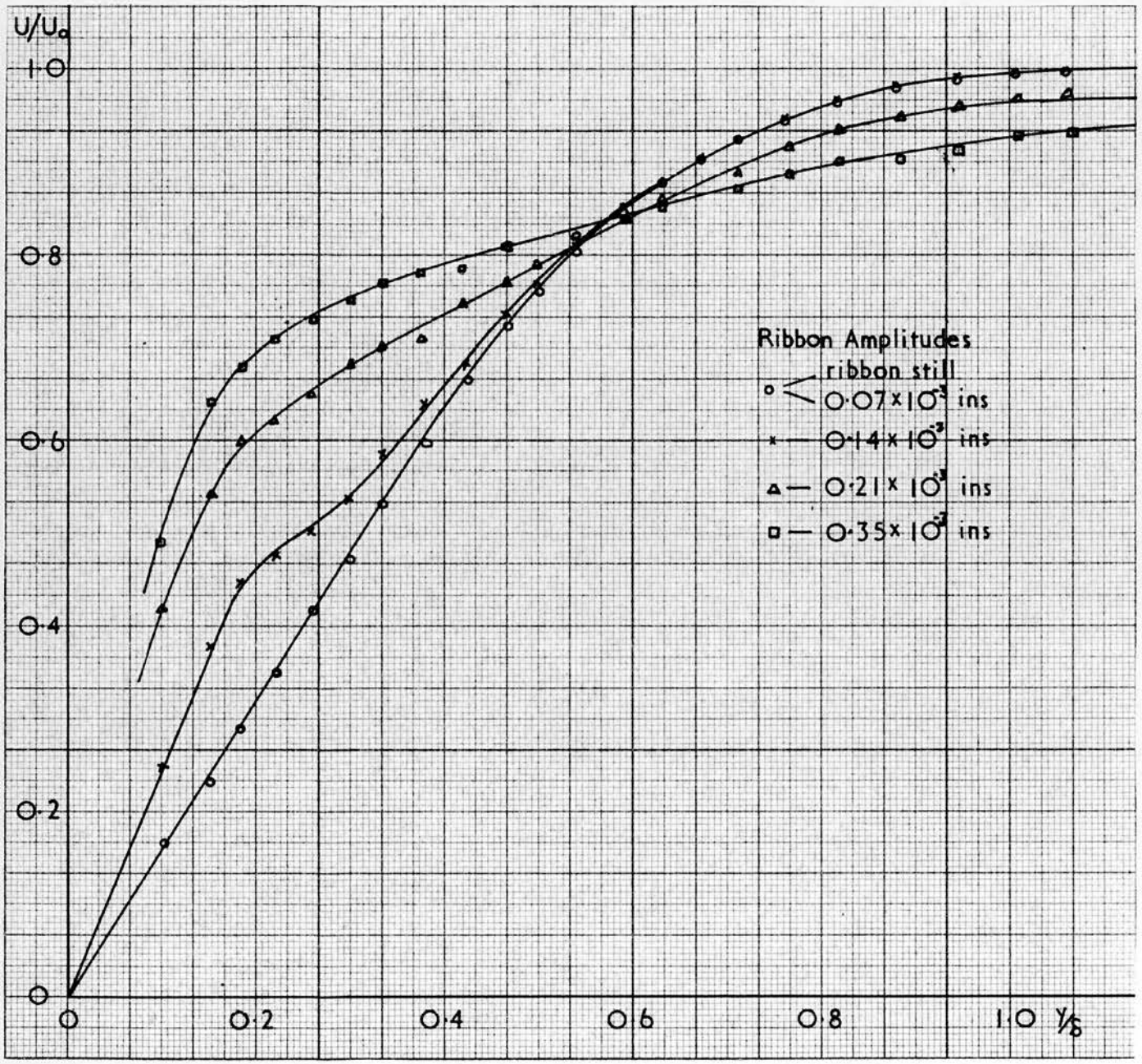

Figure 28

Boundary layer profiles showing transition caused by vibrating ribbon.

These results indicated that the position of the transition region could be altered by varying the amplitude of the disturbance produced by the oscillating ribbon. Since the amplitude of the ribbon vibration was not the only parameter involved, (others obviously are the frequency of ribbon vibration and the main stream velocity), it was decided that a detailed study of the effect of the ribbon vibrations on the position of the transition might prove to be useful. If the onset of transition is defined to occur at the point where the velocity profile begins to deviate from the Blasius distribution, then it can be measured conveniently using the method described in section III. 3, paragraph 4. Before carrying out this study however, it was decided to make a preliminary examination of the three-dimensional nature of the boundary layer.

V. 2. Three-dimensional nature of the boundary layer

In 1959 Klebanoff and Tidstrom (30) noticed that the boundary layer flow over a flat plate was not strictly two-dimensional. They observed variations of boundary layer thickness in the z - direction and suggested that this three-dimensionality played an important part in the

transition process.

In our tunnel, measurements could be made over a range of z which was severely limited owing to the small width of the working section and the presence of the turbulent wedges. It was nevertheless thought worth while to examine the boundary layer in this tunnel to see whether thickness fluctations like those observed by Klebanoff and Tidstrom could be found. Using the static and Pitot tubes described in section III. 3, complete velocity profiles were therefore taken for several z - positions within the range - 1.5 inches $< z <$ + 1.5 inches, and the boundary layer thickness was calculated in each case from the point where the velocity reached 99% of the free-stream value. Variations of the type observed by Klebanoff and Tidstrom were found, and figure 29 shows these variations for two x - positions. Figure 30 shows how the velocity in the boundary layer at a constant distance from the flat plate, varies with z - position. It is seen from these graphs that at $z = 0$ the boundary layer thickness is near a maximum and the velocity in the boundary layer at a given value of y is therefore near a minimum. Such conditions are called a 'valley' by Klebanoff and Tidstrom.

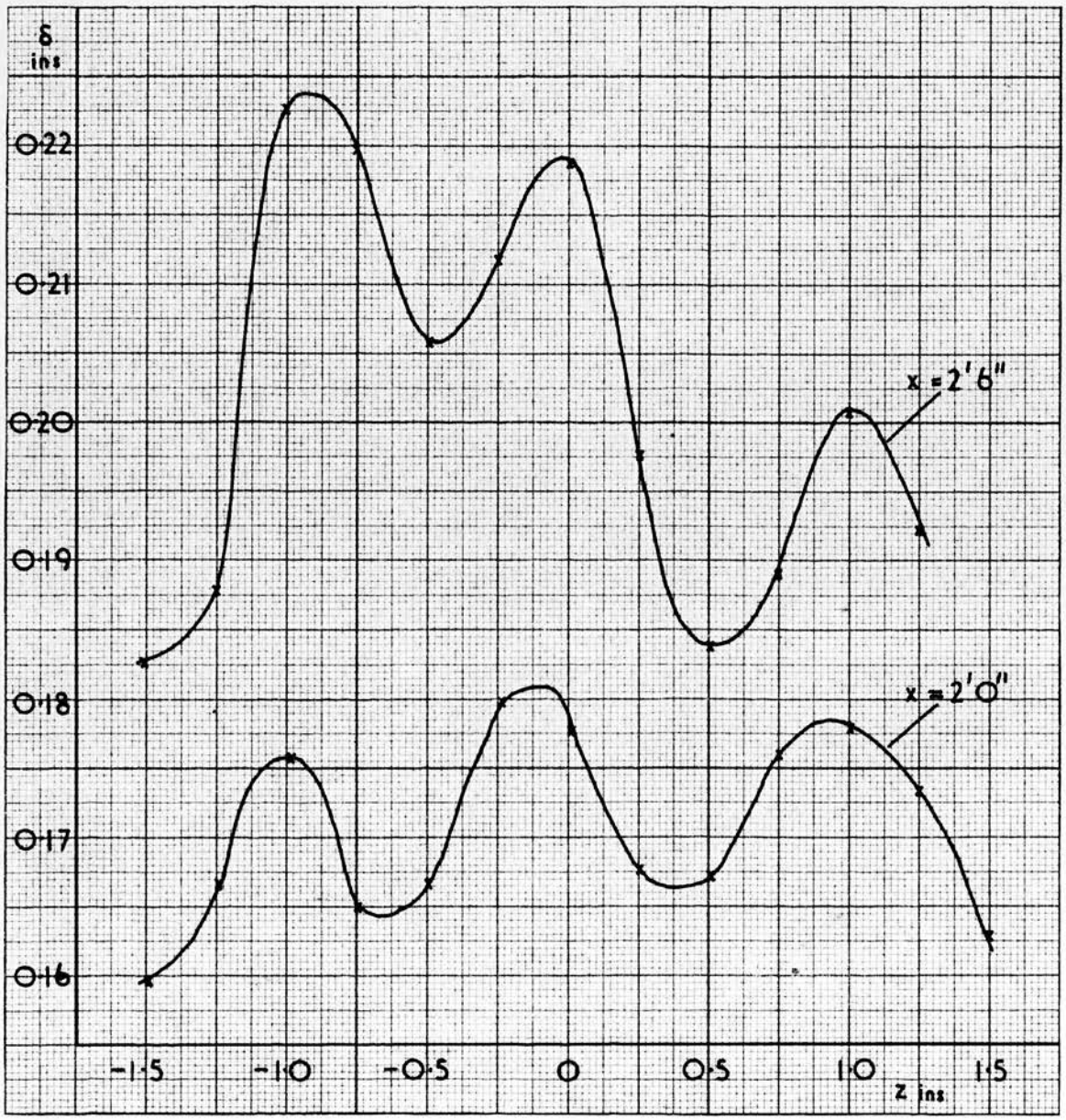

Figure 29

Boundary layer thickness variations for two x - positions.

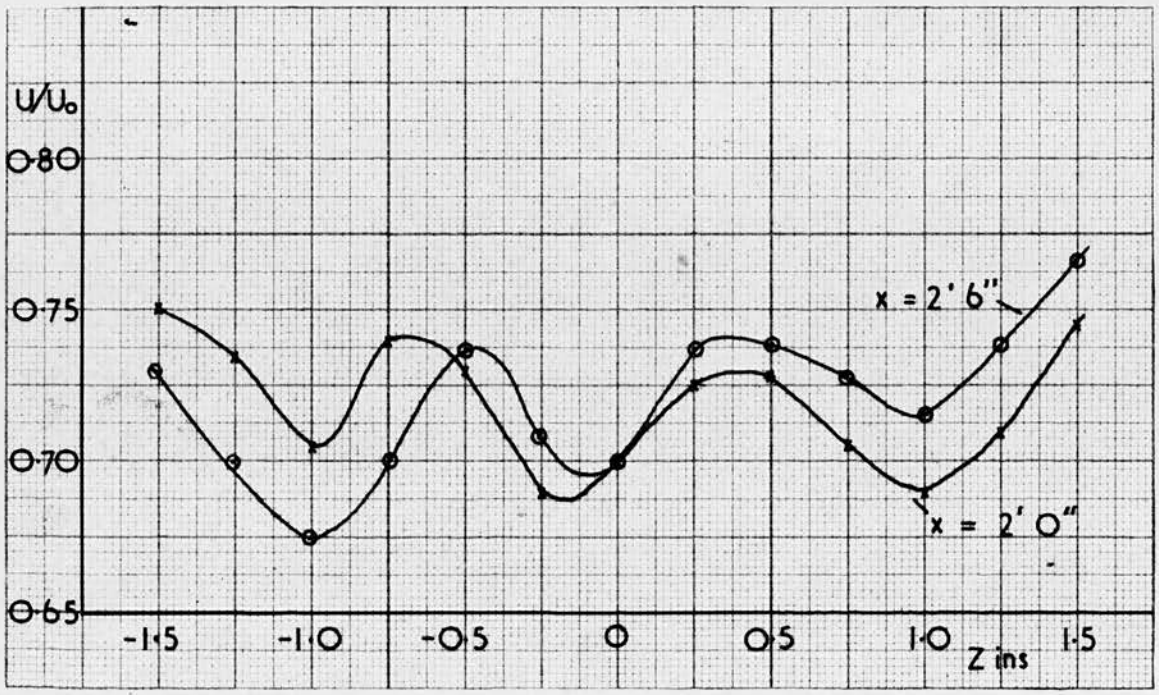

Figure 30

Variation of velocity in the boundary layer at a constant distance from the flat plate

Since variations in boundary layer thickness were present before the boundary layer was artificially disturbed, the position of breakdown might be expected to vary with z. It was thought that any such change in the x - position of breakdown as a function of z could be detected most sensitively by using the point of inflection of the curve in figure 18, i.e., the point marked C on that curve. The surface pitot tube can be set initially at this x - position on the centre line of the tunnel, and then traversed in the z - direction. The pressure reading as a function of z should then be sensitive to the x - position of the onset of transition. This experiment was therefore carried out.

A surface pitot tube was placed at an x - position of 2'6" on the centre line of the plate i.e., at z = 0. The windspeed was set at 40 ft/sec. and the ribbon vibrated at a frequency of 80 c/s. The amplitude of the ribbon was adjusted so that in this position the pitot tube was at point C the position of maximum pressure gradient. The tube was then traversed in the z - direction at $\frac{1}{4}$ inch within the range - 1.5 inches $< z <$ + 1.5 inches.

Figure 31 shows the results obtained and it is seen that the points form a regular curve with a single maximum

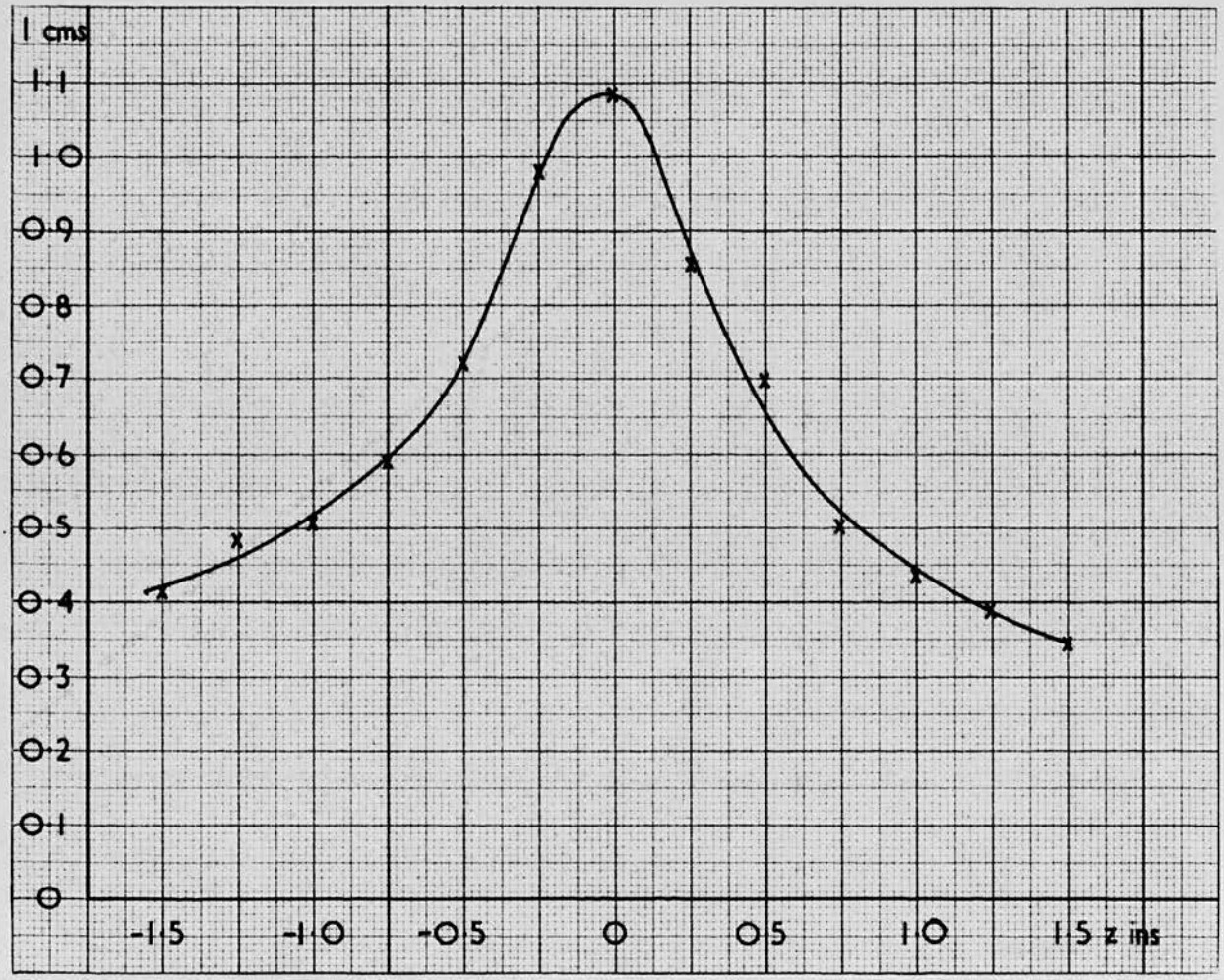

Figure 31

Graph showing the variation in pressure readings for a z - traverse through the centre of the transition region

at $z \approx 0$. This indicates that transition occurs soonest on the centre line of the plate and gradually moves down stream as the distance from the centre line is increased. The reason for this is that the initial disturbance is not two-dimensional, since the ribbon is in the form of a loop the maximum amplitude is at the centre and decreases to zero at the bridges. There is therefore a gradual decrease in the amplitude of the injected disturbance away from the centre line and the position of transition will be delayed.

The original three-dimensionality of the boundary layer may affect the position of breakdown but the effect will be masked by the three-dimensional nature of the injected disturbance. For this reason all other readings were confined to the centre line of the plate.

V. 3. Detailed study of the effect of the ribbon vibrations on the position of the transition region

We were now ready to undertake a more general investigation of the onset of transition by the method already described in section III. 3. With the total head tube in contact with the plate and the static tube outside the boundary layer approximately 2 inches from the flat plate, the total head and static pressure tubes were traversed at two inch intervals in the x - direction. The

pressure difference between the two tubes was measured on the sloping tube manometer, and the accuracy of the pressure measurements was improved by viewing the manometer through a microscope which allowed the position of the paraffin to be read to an accuracy of 0.01 centimetres, which corresponds to a velocity of 1.4 ft/sec. The ribbon was positioned 13 inches from the leading edge of the flat plate, and was made to vibrate over a range of frequencies from 40 cycles/second to 160 cycles/second in steps 10 cycles/second. The frequency of vibration was kept within the permitted range of the resonant frequency by adjusting the tension on the ribbon. Ribbon amplitudes of 0.7, 1.4, 2.1, 2.8 and 3.5 x 10^{-3} inches were used for each frequency and the experiment was carried out with windspeeds of 25, 30, 35 and 40 ft/sec.

A graph showing a typical set of curves for a given U_o and frequency is shown in figure 32. The positions of the onset of transition were read as the points where the curves diverge from the curve L M for the undisturbed laminar boundary layer. In figure 32 the points of divergence are indicated by letters A, B, C, D and E.

During this study of the transition region it was

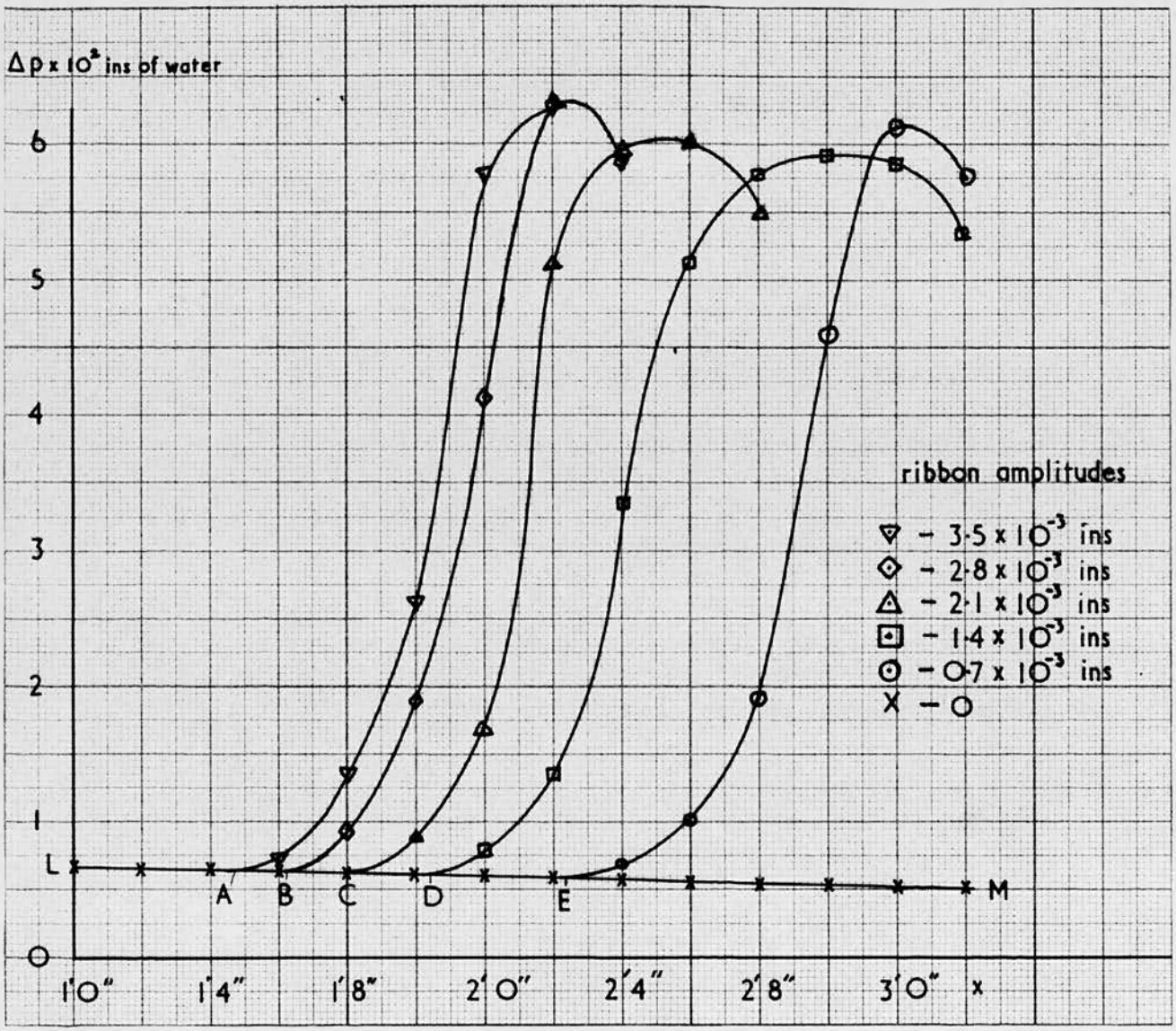

Figure 32

Graph showing one set of pressure readings for transition induced by various amplitudes of the ribbon.

U_o = 40 ft/sec, f = 160 c/s.

noticed that irregular velocity fluctuations occurred at any one point and these were greatest at the centre of the transition region. The maximum observed fluctuations were of the order of 3 ft/sec. when the free-stream velocity was of the order of 40 ft/sec. and they could therefore not be ignored. Such fluctuations could be caused by short period variations in U_o or in the free-stream turbulence but they were not considered to be associated with variations of ribbon amplitude because this was continuously monitored. A mean reading of the manometer was taken so that the average position of the transition region was obtained.

The whole experiment was carried out a second time for all sets of conditions and it was found that the positions of the onset of transition obtained from the second set of observations agreed with the first set to within $\pm$ 1 inch in x. It was thought that this variation was probably within the limits of experimental error, i.e., that the discrepancies could be accounted for by slight changes in free-stream turbulence, in the settings of windspeed, and of amplitude and frequency of the ribbon vibration.

Tables 1, to IV give the position of the onset of

transition for each set of readings and the Reynolds numbers, R_{δ^*}, corresponding to these positions. Curves showing the position of the onset of the transition region for constant ribbon amplitude can be drawn in the $\beta_r \nu / U_o^2$, R_{δ^*} plane and these curves are shown in figures 33 to 36.

V. 4. Comparison of experimental results with Shen's calculations.

Figures 33 to 36 show the R_{δ^*} positions at which the disturbances have grown sufficiently to produce distortion of the mean flow; the amplifications are considerable and the small disturbance theory cannot be expected to hold. Since there is as yet no satisfactory method of dealing with large disturbances, the results were examined to see if they could be related in any way to the predictions of the small disturbance theory. The best theoretical calculations to date, for the small disturbance theory, are those due to Shen whose results are summarised in figure 4. Each curve in this graph shows the $\log_e$ of the total amplification of a disturbance from branch I of the neutral curve. The different curves correspond to different values of $\beta_r \nu / U_o^2$, the non-dimensional frequency parameter. In our experiments the only amplitude which is known is the amplitude of the ribbon but if we assume that for any particular frequency breakdown occurs at a definite

TABLE I

$f_{c/s}$	$\frac{10^6 \beta_r \nu}{U_o^2}$	a=0.7x10^{-3}"		a=1.4x10^{-3}"		a=2.1x10^{-3}"		a=2.8x10^{-3}"		a=3.5x10^{-3}"	
		Xm	R	Xm	R	Xm	R	Xm	R	Xm	R
40	24.4	-	-	-	-	-	-	-	-	3'1"	1535
50	30.5	-	-	-	-	-	-	3'1"	1535	2'10"	1470
60	36.5	-	-	-	-	3'0½"	1525	2'8½"	1440	2'5½"	1370
70	42.6	-	-	3'1½"	1545	2'9½"	1460	2'5½"	1370	2'3½"	1320
80	48.7	-	-	2'9"	1450	2'5"	1360	2'1½"	1270	1'11"	1210
90	54.8	2'11"	1490	2'7½"	1415	2'4"	1335	2'1½"	1270	1'9½"	1170
100	60.8	2'9½"	1460	2'7½"	1415	2'3½"	1320	2'0½"	1250	1'11"	1210
110	67.0	2'8"	1425	2'4½"	1345	2'1½"	1270	1'11½"	1220	1'9½"	1170
120	73.1	2'6½"	1390	2'2"	1285	1'11"	1210	1'10"	1182	1'8½"	1140
130	79.2	2'5½"	1370	2'0"	1236	1'10½"	1195	1'9½"	1170	1'8½"	1140
140	85.2	2'3½"	1320	2'0"	1236	1'10"	1182	1'8"	1127	1'7"	1100
150	91.3	2'3"	1310	1'11"	1210	1'8½"	1140	1'7½"	1115	1'6"	1070
160	97.4	2'3½"	1320	1'10½"	1195	1'8"	1127	1'6"	1070	1'5"	1040

Xm - average reading of the start of the transition region.

R - $1.72\sqrt{\frac{U_o \, Xm}{\nu}}$

U_o = 40 ft/sec.

TABLE II

f_{cps}	$\frac{\beta \nu}{U_o^2} \times 10^6$	a=0.7x10^{-3}"		a=1.4x10^{-3}"		a=2.1x10^{-3}"		a=2.8x10^{-3}"		a=3.5x10^{-3}"	
		Xm	R	Xm	R	Xm	R	Xm	R	Xm	R
40	31.8	-	-	-	-	-	-	-	-	-	-
50	39.8	-	-	-	-	-	-	-	-	-	-
60	47.7	-	-	-	-	-	-	-	-	-	-
70	55.7	-	-	-	-	-	-	-	-	3'0"	1416
80	63.6	-	-	3'1"	1436	2'10"	1376	2'8"	1336	2'4½"	1260
90	71.6	3'1"	1436	2'8"	1336	2'5"	1271	2'3½"	1238	2'2"	1203
100	79.5	2'10½"	1387	2'5½"	1282	2'3"	1227	2'1½"	1192	2'0"	1156
110	87.4	2'8½"	1346	2'4½"	1260	2'2"	1203	2'0½"	1168	1'10½"	1120
120	95.4	2'9½"	1366	2'4"	1250	2'1½"	1192	1'11"	1132	1'10"	1108
130	103.3	2'11½"	1406	2'4"	1250	2'0"	1156	1'10"	1108	1'9"	1082
140	111.5	3'0½"	1427	2'5"	1271	2'0"	1156	1'10"	1108	1'8"	1056
150	119.2	3'1½"	1446	2'9"	1356	2'1½"	1192	1'10"	1108	1'8"	1056
160	127.2	-	-	3'0½"	1427	2'3½"	1304	1'11½"	1144	1'8½"	1068

U_o = 35 ft/sec.

R = 8507 ✓
(833)

TABLE III

f_{cds}	$\frac{\beta_r \nu}{U_o^2} \times 10^6$	$a=0.7\times10^{-3}$"		$a=1.4\times10^{-3}$"		$a=2.1\times10^{-3}$"		$a=2.8\times10^{-3}$"		$a=3.5\times10^{-3}$"	
		Xm	R	Xm	R	Xm	R	Xm	R	Xm	R
40	43.3	-	-	-	-	-	-	-	-	-	-
50	54.1.	-	-	-	-	-	-	-	-	3'1"	1330
60	65.0	-	-	-	-	-	-	3'1½"	1321	2'11½"	1302
70	75.8	-	-	-	-	3'0"	1312	2'9½"	1266	2'7"	1217
80	86.7	-	-	3'1½"	1321	2'9½"	1266	2'7"	1217	2'5"	1178
90	97.5	-	-	3'0"	1312	2'8½"	1247	2'6"	1199	2'3"	1138
100	108.2	-	-	2'11"	1293	2'5½"	1188	2'3"	1138	2'1"	1093
110	119.1	-	-	3'0"	1312	2'5½"	1188	2'2"	1116	2'0"	1070
120	129.9	-	-	-	-	2'11"	1293	2'4½"	1168	2'1½"	1105
130	140.7	-	-	-	-	-	-	2'9½"	1266	2'4½"	1168
140	151.6	-	-	-	-	-	-	-	-	2'11"	1293
150	162.5	-	-	-	-	-	-	-	-	-	-
160	173.2.	-	-	-	-	-	-	-	-	-	-

U_o = 30 ft/sec.

TABLE IV

f_{cs}	$\frac{\beta\nu}{U_o^2} \times 10^6$	a=0.7x10^{-3}"		a=1.4x10^{-3}"		a=2.1x10^{-3}"		a=2.8x10^{-3}"		a=3.5x10^{-3}"	
		Xm	R	Xm	R	Xm	R	Xm	R	Xm	R
40	62.3	-	-	-	-	-	-	-	-	-	-
50	78.0	-	-	-	-	-	-	-	-	-	-
60	93.5	-	-	-	-	-	-	3'1"	1210	2'11"	1180
70	109.0	-	-	-	-	-	-	2'10"	1160	2'8"	1127
80	124.5	-	-	-	-	3'0½"	1205	2'8"	1127	2'4½"	1045
90	140.0	-	-	-	-	3'1"	1210	2'10½"	1170	2'5"	1055
100	156.0	-	-	-	-	-	-	3'1½"	1220	2'10½"	1170
110	171.3	-	-	-	-	-	-	-	-	-	-
120	187.0	-	-	-	-	-	-	-	-	-	-
130	202.5	-	-	-	-	-	-	-	-	-	-
140	218.0	-	-	-	-	-	-	-	-	-	-

U_o = 25 ft/sec

Figures 33 to 36

Graphs showing the start of the transition region under different conditions.

Key

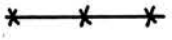 position of the oscillating ribbon.

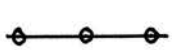 start of transition when ribbon amplitude = 0.0035 ins.

 start of transition when ribbon amplitude = 0.0028 ins.

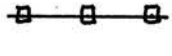 start of transition when ribbon amplitude = 0.0021 ins.

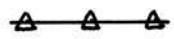 start of transition when ribbon amplitude = 0.0014 ins.

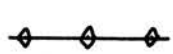 start of transition when ribbon amplitude = 0.0007 ins.

Figure 33 U_o = 40 ft/sec.

34 U_o = 35 ft/sec.

35 U_o = 30 ft/sec.

36 U_o = 25 ft/sec.

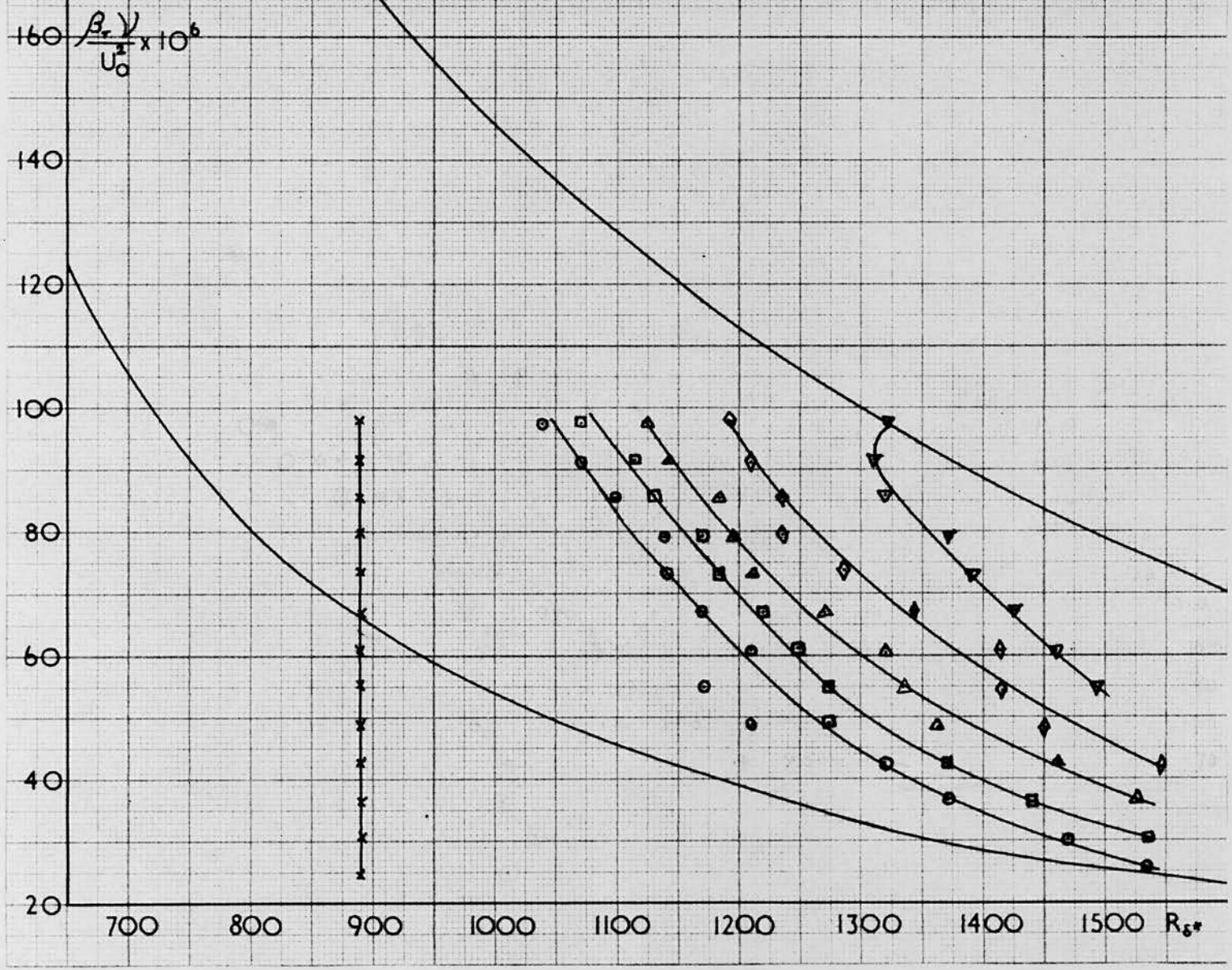
$\frac{\beta_r \nu}{U_0^2} \times 10^6$
160
140
120
100
80
60
40
20
700
800
900
1000
1100
1200
1300
1400
1500
R_{δ^*}

Figure 33

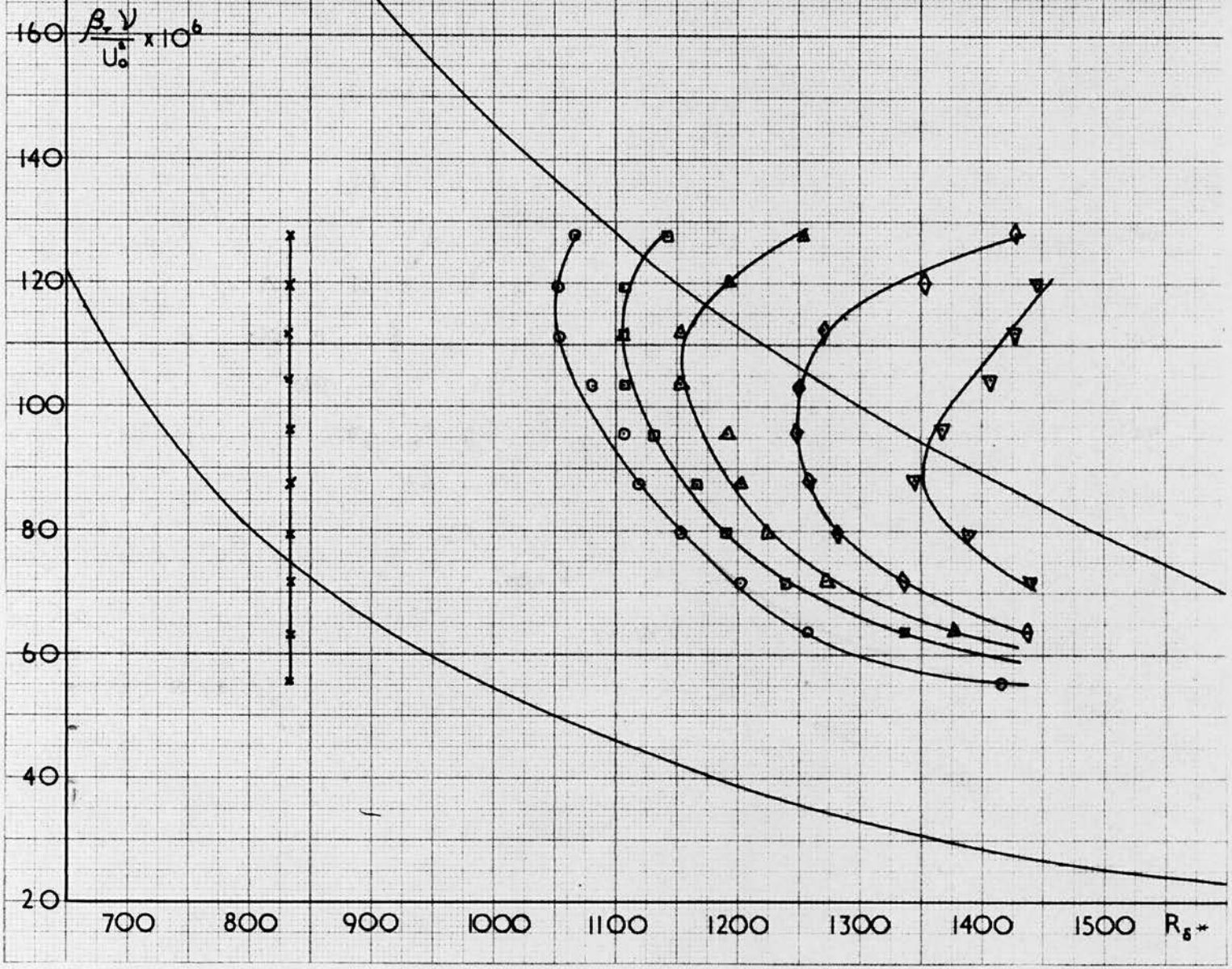
$\frac{\beta_x \nu}{U_o^2} \times 10^6$
160
140
120
100
80
60
40
20
700
800
900
1000
1100
1200
1300
1400
1500
R_{δ^*}

Figure 34

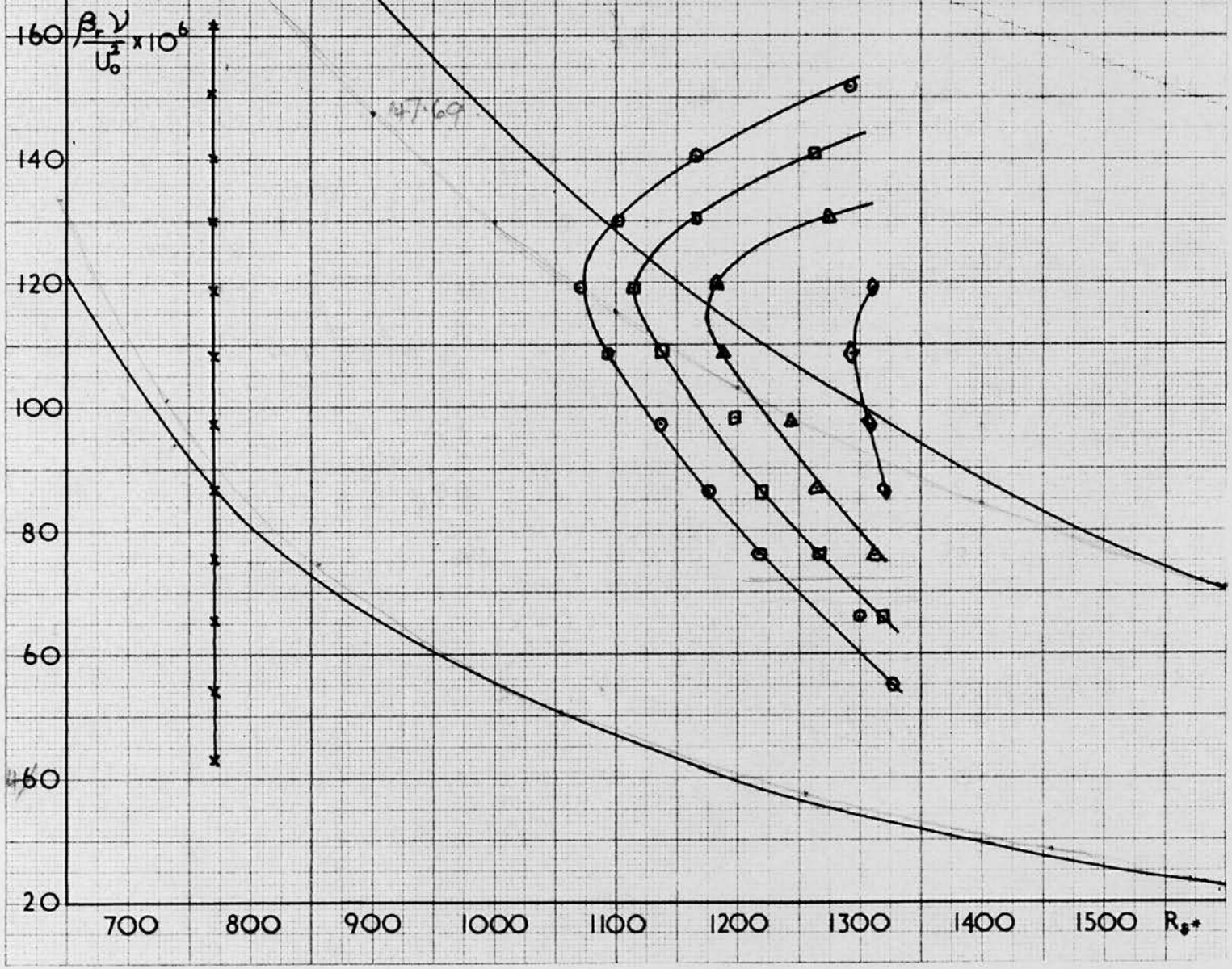
$\frac{\beta_r \nu}{U_0^2} \times 10^6$
160
140
120
100
80
60
40
20
700
800
900
1000
1100
1200
1300
1400
1500
R_{δ^*}

Figure 35

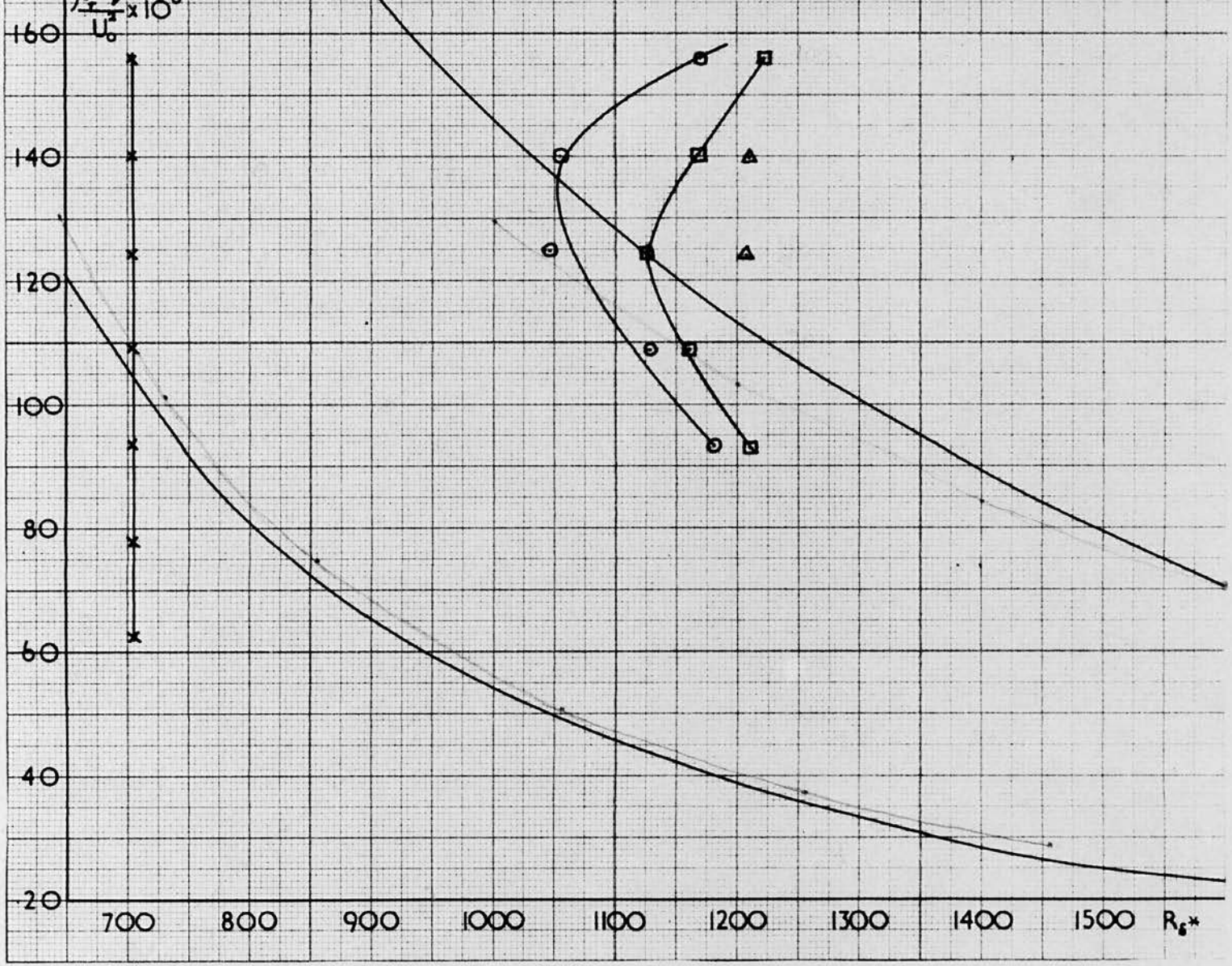
$\frac{\nu}{U_0^2} \times 10^6$
160
140
120
100
80
60
40
20
700
800
900
1000
1100
1200
1300
1400
1500
R_{δ^*}

Figure 36

amplitude, then we can determine the amplification rate from the spacing between the curves of figures 33 to 36.

Since we do not know the amplitude of the disturbance at the neutral curve we must fix one point on the curve of total amplification and from it calculate the others e.g. In figure 33, (for a windspeed of 40 ft/sec.) at a $\beta_r \nu/U_o^2$ value of 80×10^{-6} the largest initial amplitude of disturbance causes breakdown at a Reynolds number of 1110 and on Shen's curve of $\beta_r \nu/U_o^2 = 80 \times 10^{-6}$ this Reynolds number corresponds to a $\log_e A/A_o$ value of 1.4, where A is the amplitude of the disturbance at the point and A_o is the amplitude at the neutral curve. This ~~fixes one point on the curve and~~ point is now taken as the starting point for drawing an experimental curve of $\log_e A/A_o$ against R. If we assume that for the other points of breakdown on a line of $\beta_r \nu/U_o^2 = 80 \times 10^{-6}$ the amplification required ~~is in the same ratio~~ is inversely as the initial amplitudes, then a point can be obtained for each amplitude. This was done for $\beta_r \nu/U_o^2$ values of 100, 80, 60 and 40×10^{-6} using the curves of figure 33 and the results ~~obtained are~~ as plotted points shown in figure 37. The curves shown on this figure are those calculated by Shen.

It appears that ~~the general shape of curves drawn through the calculated points is the same as those of Shen's but they are~~ if curves were drawn through the calculated points, their shape would be similar to those of Shen but displaced along the direction of the curves. ~~In~~

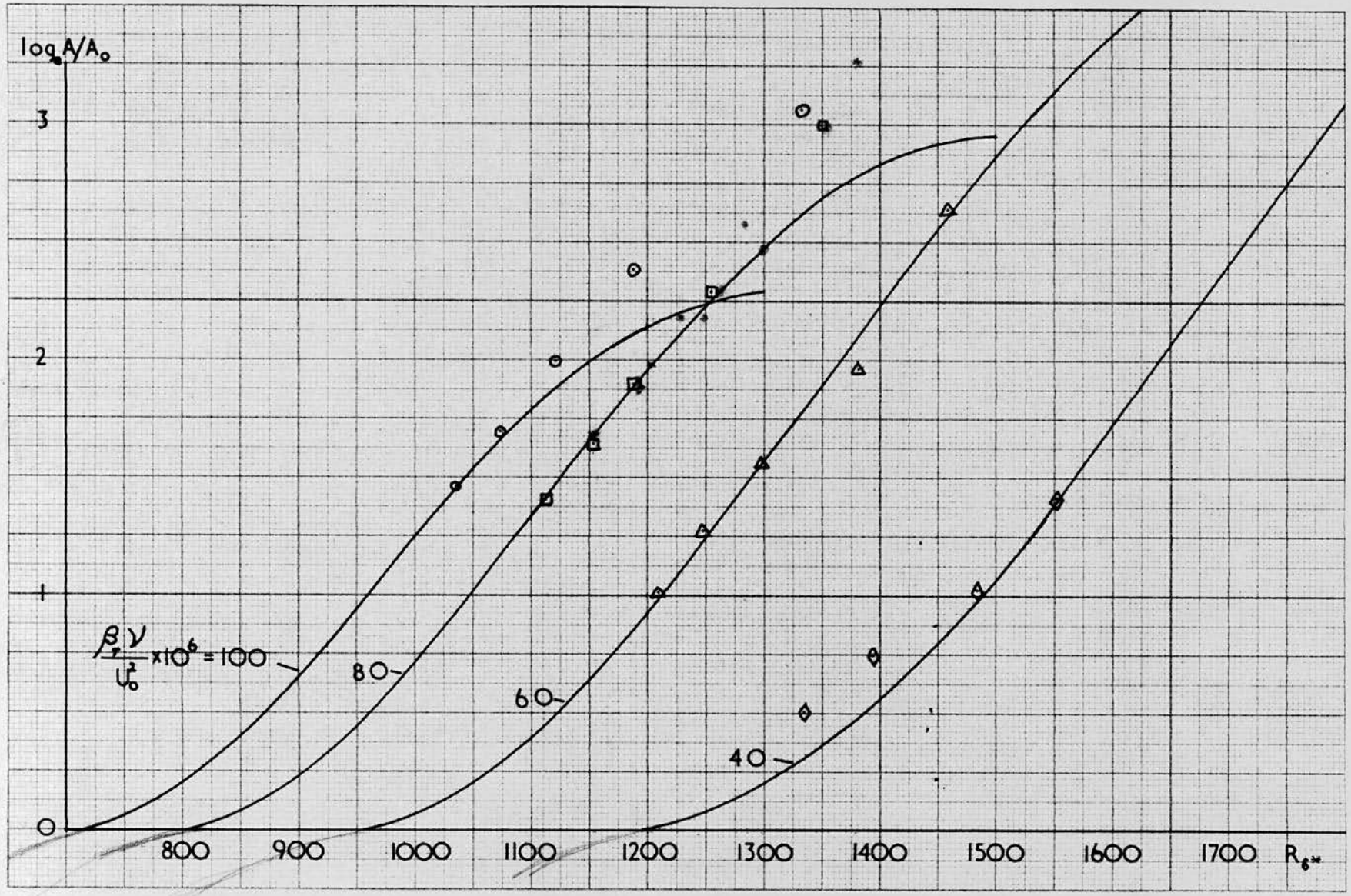

Figure 37

Comparison of experimental growth of disturbance with Shen's theoretical calculations.

~~other words if the experimental points of breakdown were~~ If the Reynolds number of the first plotted point ~~displaced by a fixed amount in the direction of lower~~ had been lower, and the other plotted points ~~Reynolds number then points could be obtained which would~~ had retained their Reynolds number spacing relative ~~correspond to Shen's curves. It was now thought that if~~ to the first point, a better fit would have been ~~the spacing between the experimental curves could be~~ obtained. This change is equivalent to moving ~~related to Shen's curves at a lower Reynolds number then~~ the curves in figure 33 bodily to a lower ~~it might be possible to extend this and obtain a set of~~ Reynolds number.

~~curves which correspond to the experimental curves if moved~~ This line of thought suggested that it might ~~by a fixed amount in the direction of increasing Reynolds~~ be possible to obtain a set of curves of constant ~~number. From Shen's curves it is a fairly easy matter to~~ non-dimensional amplitude, lying at lower Reynolds ~~calculate curves of constant disturbance amplitude,~~ number than the curves in figure 33 and having ~~remembering of course that the disturbance starts at the~~ the same shape as the experimental curves ~~ribbon and not at the neutral curve, but since there is no~~ shown there. The non-dimensional amplitude ~~data for the damping region we are restricted to the cases~~ parameter selected for this purpose was $a\beta_r/U_0$ ~~where the ribbon is in the amplifying region.~~ where 'a' is the amplitude obtained from the

~~A number of curves of constant disturbance amplitude~~ ribbon amplitude after it has been amplified in ~~were calculated but it was obvious from their general shape~~ the boundary layer in accordance with Shen's ~~that moving them to a higher Reynolds number would not make~~ calculations.

~~them coincide with the experimental curves. The shape of~~

~~the curves however could be changed if, instead of keeping~~

~~the amplitude constant, a term which included frequency~~

~~was kept constant. The obvious combination to use was the~~

Since in figure 33 U_o is constant ~~product of amplitude and frequency so~~ curves of constant $a\beta_r$ were calculated, ~~(where 'a' is the amplitude of the disturbance)~~ in the first instance and a set of these is shown in figure 38. The value of $a\beta_r^*$ chosen was quite arbitrary, the final choice being the result of trial and error until a set of curves ~~was obtained which corresponded fairly well with the experimental curves. Figure 39, gives the same set of~~ was obtained whose shape was closely similar to the experimental curves but with a lower Reynolds number. The five curves in figure 38 correspond to ribbon amplitudes in the ratio 5:4:3:2:1 as used in the experiment. Figure 39 gives the same set of curves with the Reynolds number of each point increased by 100 and also shown on the graph are the experimental points of breakdown corresponding to this windspeed. It is seen that good agreement between the experimental points and the calculated curves is obtained for the higher ribbon amplitudes but the calculated curves spread out more, so that for the smallest amplitude they do not coincide. It was also found that for the various windspeeds, to obtain the best agreement with the experimental points, a different value of $a\beta_r$ had to be used in each case and there was no obvious relation between the shifts required.

Although the agreement between the calculated and experimental curves was quite good it was felt that an improvement could be made. The curves corresponding to the smaller ribbon amplitudes required to be moved to a lower

* This value was 0.5 ft/sec

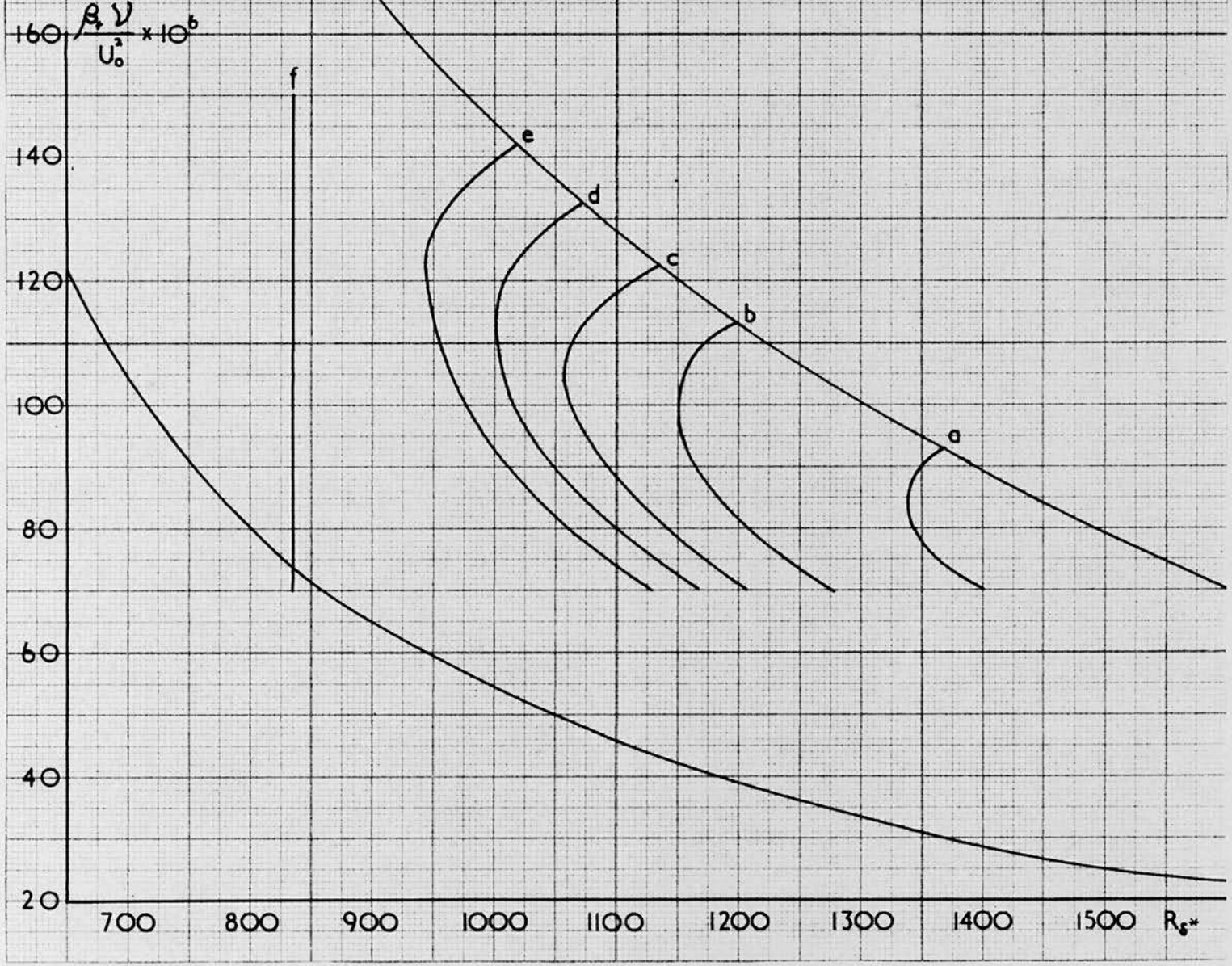

Figure 38

Calculated curves of constant $\alpha\beta_r$ for different ribbon amplitudes.

U_o = 35 ft/sec.

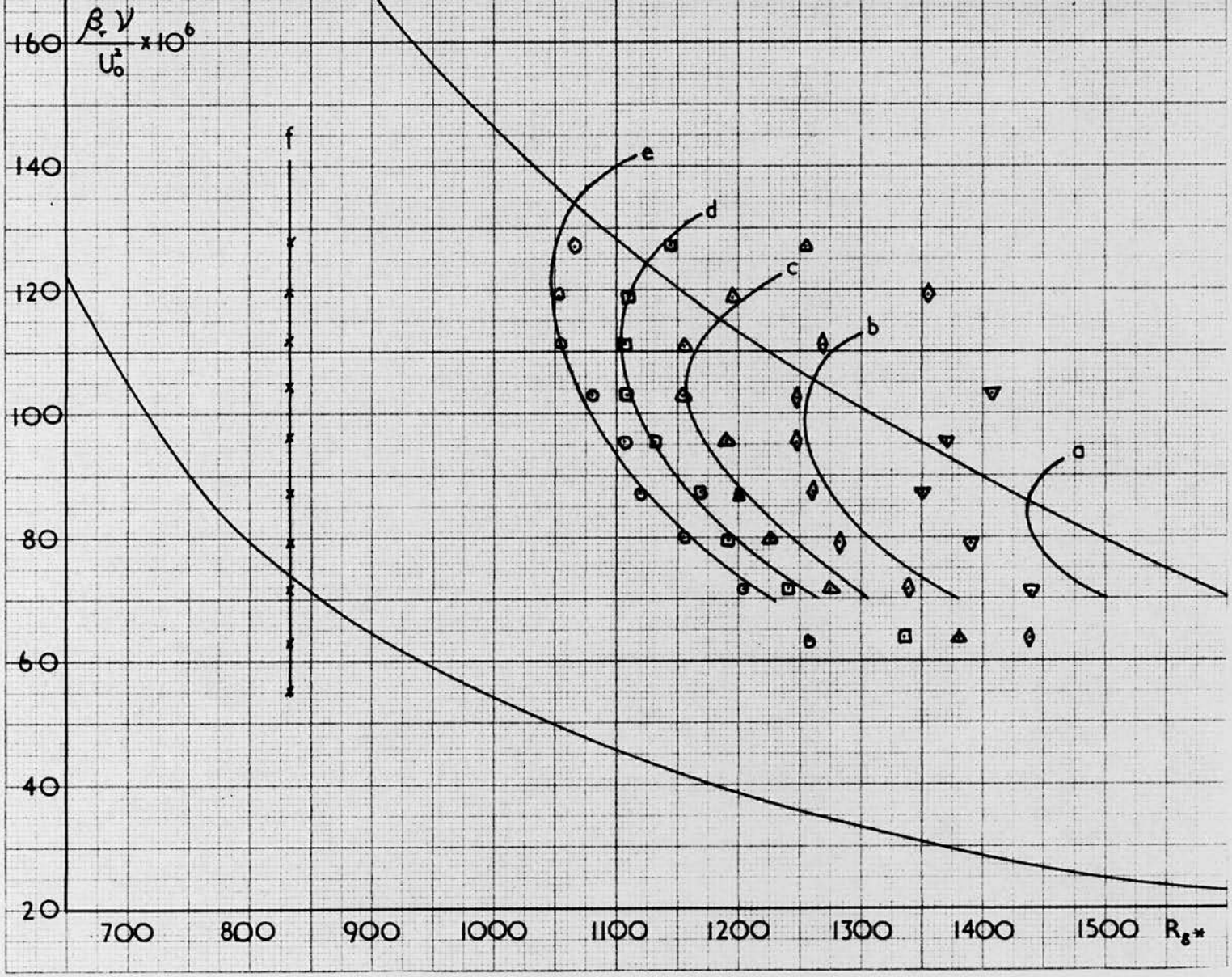

Figure 39

Curves of constant $\alpha\beta_r$ moved to correspond to experimental points.

U_o = 35 ft/sec.

Reynolds number and this could be achieved, without significantly changing their shape, if the Reynolds number was included in the parameter to be kept constant, i.e. we would now calculate curves of constant $(\alpha\beta_r R_\delta)$. However, if Reynolds number is to be introduced it is better that the parameter be kept dimensionless and the obvious thing to do is to divide by U_o the free stream velocity, this will alter the value of the constant but in no way alter the shapes of the curves.

Curves of constant $(\alpha\beta_r/U_o) \times R_\delta$ where now calculated for the five ribbon amplitudes used in the experiment and the results are shown in figures (40) to (43). Figures (44) to (47) show the same curves shifted to a higher Reynolds number so that they correspond to the experimental points and it is seen that the curves corresponding to all amplitudes now agree well with experiment. The constant value* of $(\alpha\beta_r/U_o) \times R_\delta$ was quite arbitrary being chosen as the value which gave the best agreement with the experimental points and this time it was found that the same value could be used for all windspeeds. The Reynolds number by which each set of curves had to be increased so that they corresponded to the experimental points was different for

* this constant value was 16.

Figures 40 to 43

Calculated curves of constant $(\alpha\beta_r/U_0) \times R_{\delta^*}$ for varies windspeeds.

Figures 44 to 47

Calculated curves of constant $(\alpha\beta_r/U_0) \times R_{\delta^*}$ shifted so as to correspond to the experimental points of Figures 33 to 36.

Figure 44 - R values increased by 60, U_0 = 40 ft/sec.

45 - R values increased by 85, U_0 = 35 ft/sec.

46 - R values increased by 120, U_0 = 30 ft/sec.

47 - R values increased by 150, U_0 = 25 ft/sec.

Key

a - amplitude of disturbance at ribbon position = 0.0007 ins.

b - amplitude of disturbance at ribbon position = 0.0014 ins.

c - amplitude of disturbance at ribbon position = 0.0021 ins.

d - amplitude of disturbance at ribbon position = 0.0028 ins.

e - amplitude of disturbance at ribbon position = 0.0035 ins.

f - position of ribbon

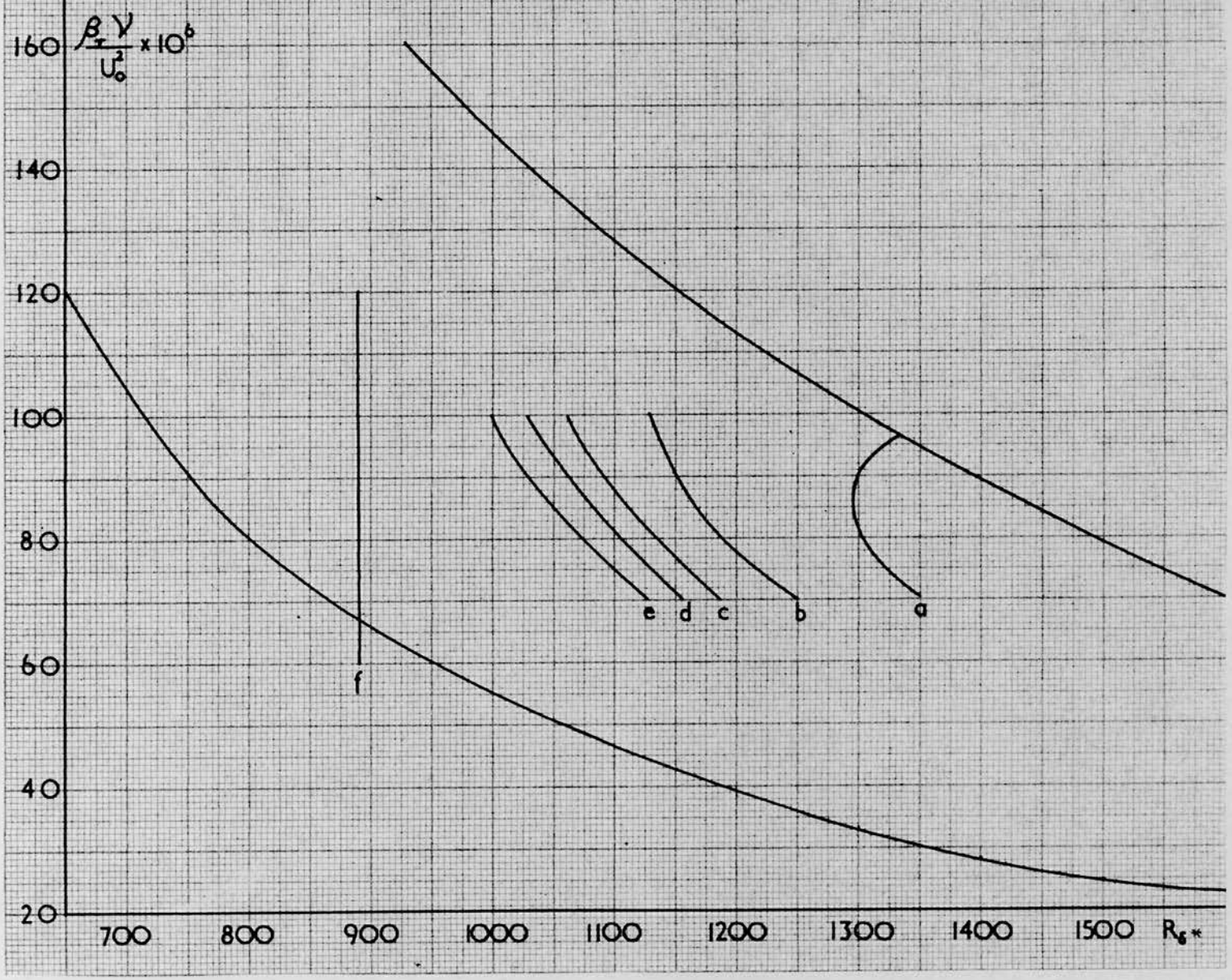

Figure 40

Calculated curves of constant $(a\beta_r/U_o) \times R_{\delta^*}$

U_o = 40 ft/sec.

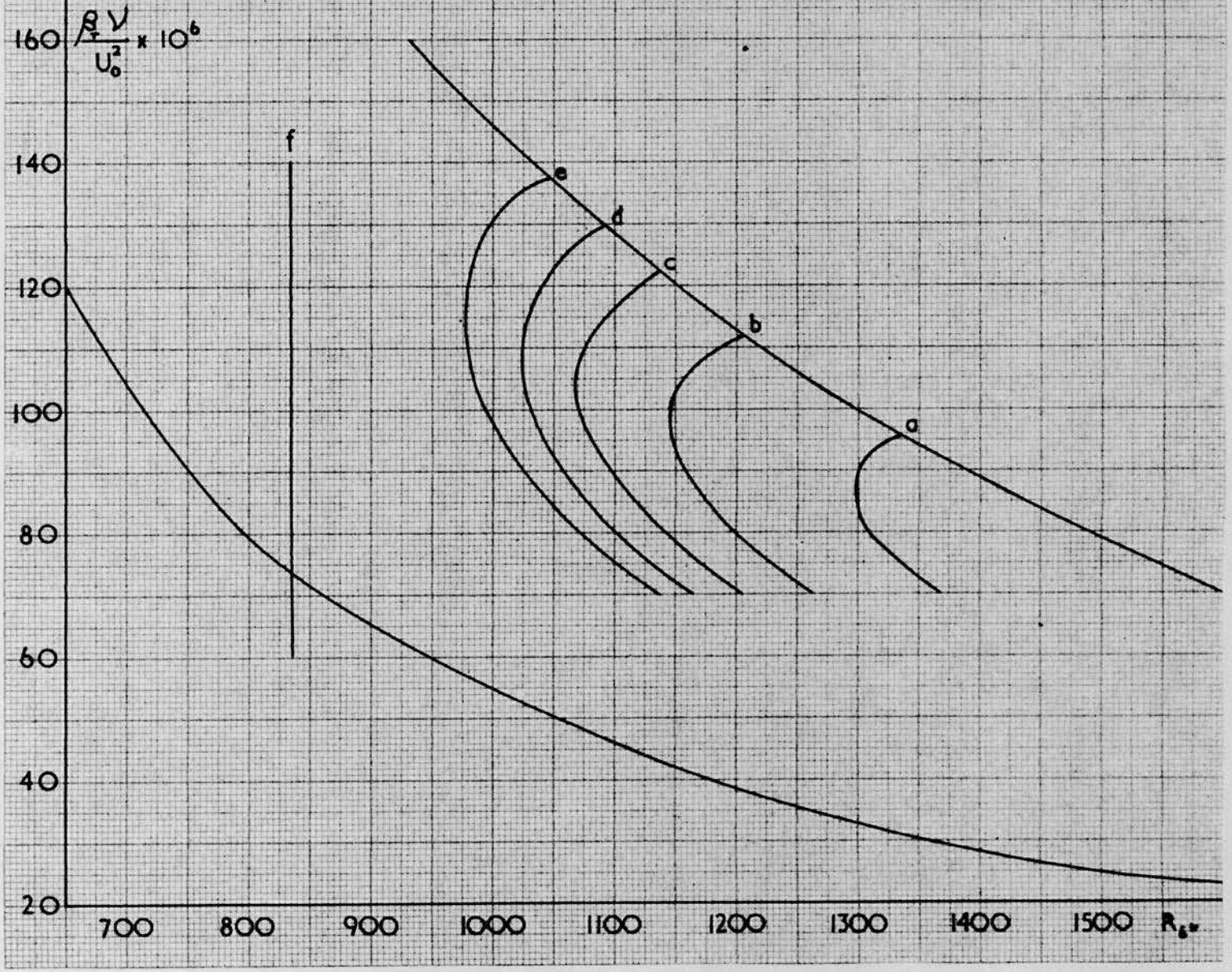

Figure 41

Calculated curves of constant $(a\beta_r/U_o) \times R_{\delta^*}$

U_o = 35 ft/sec.

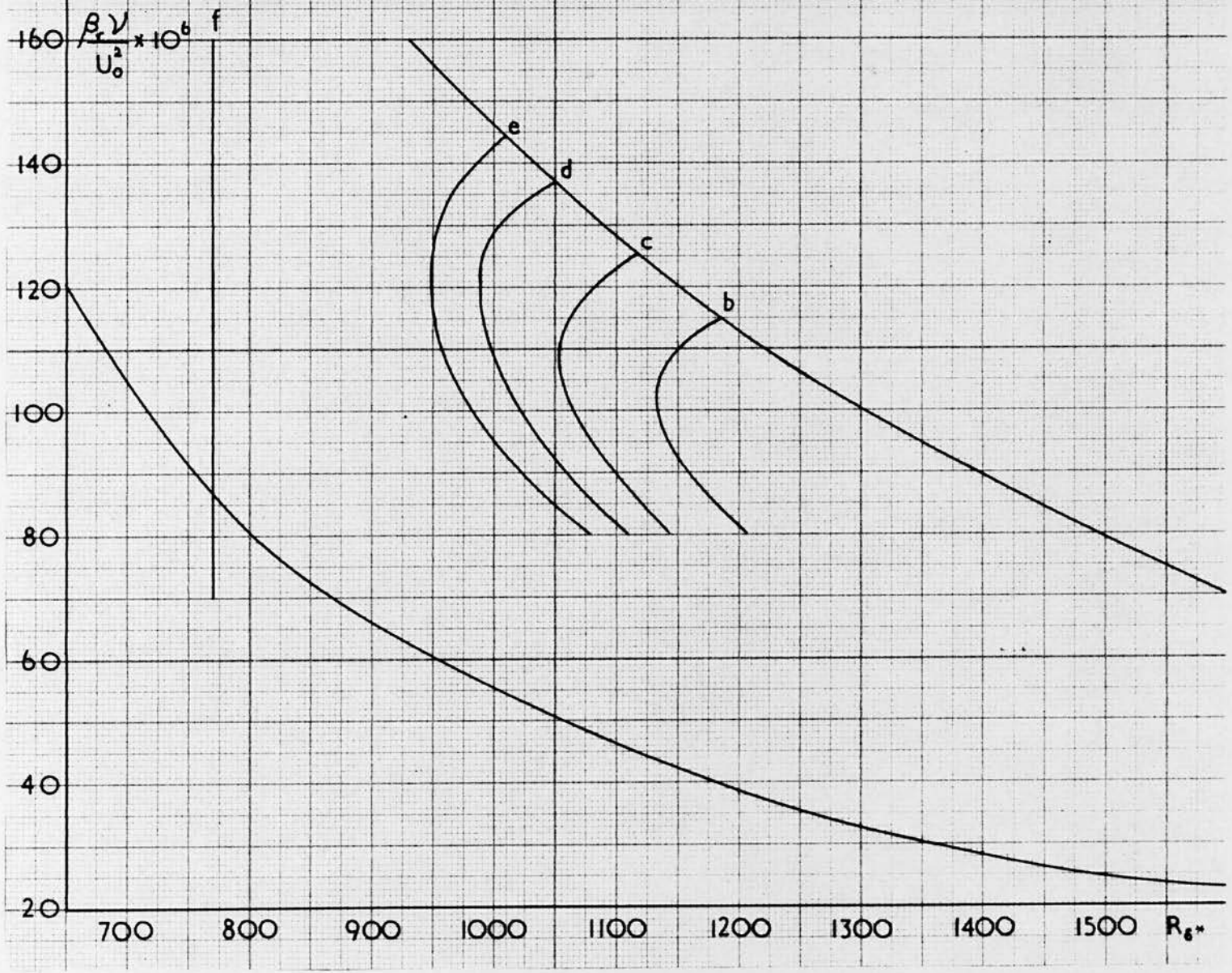

Figure 42

Calculated curves of constant $(\alpha \beta_r / U_0) \times R_{\delta^*}$

U_0 = 30 ft/sec.

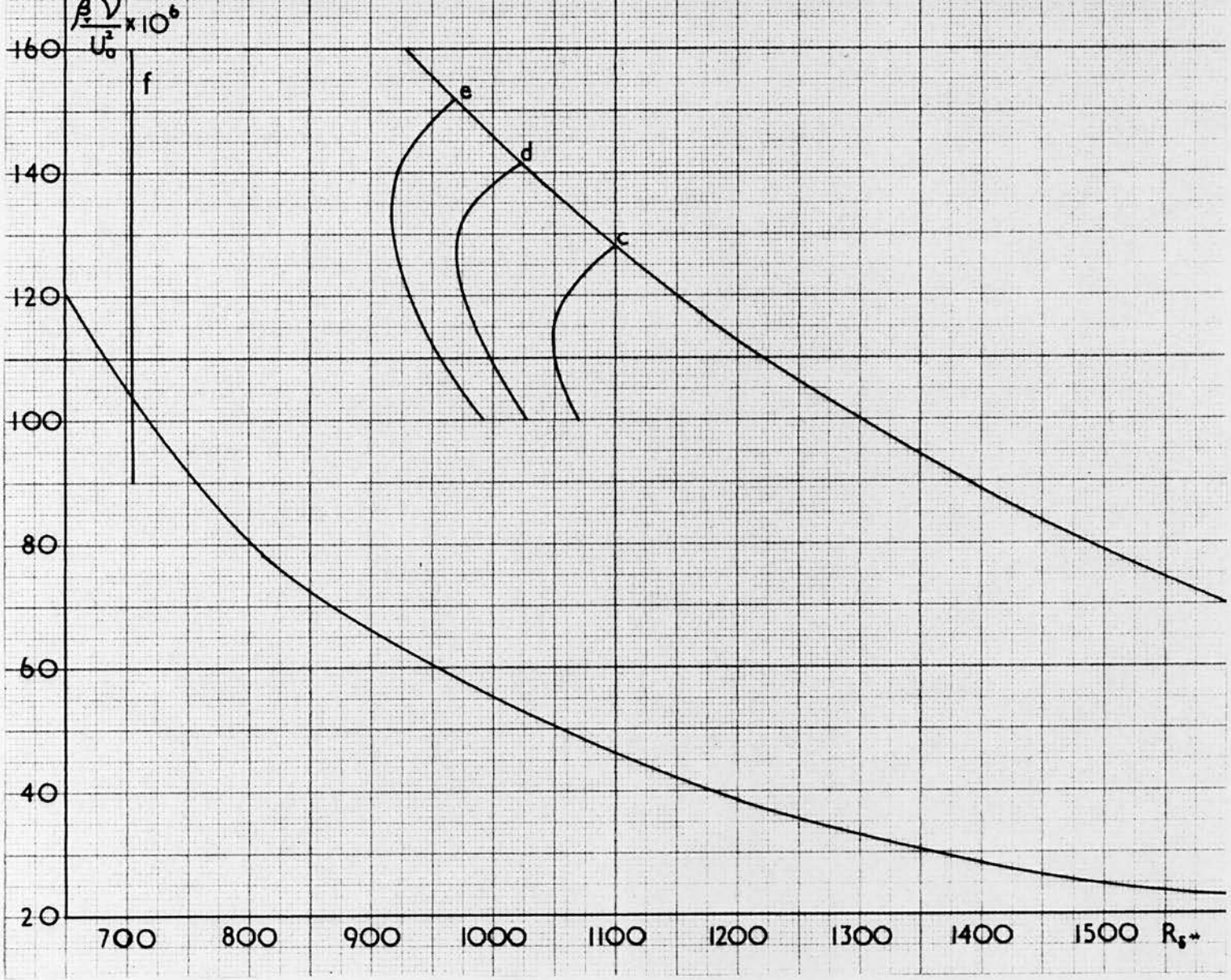

Figure 43

Calculated curves of constant $(a\beta_\tau/U_0) \times R_{\delta^*}$

U_0 = 25 ft/sec.

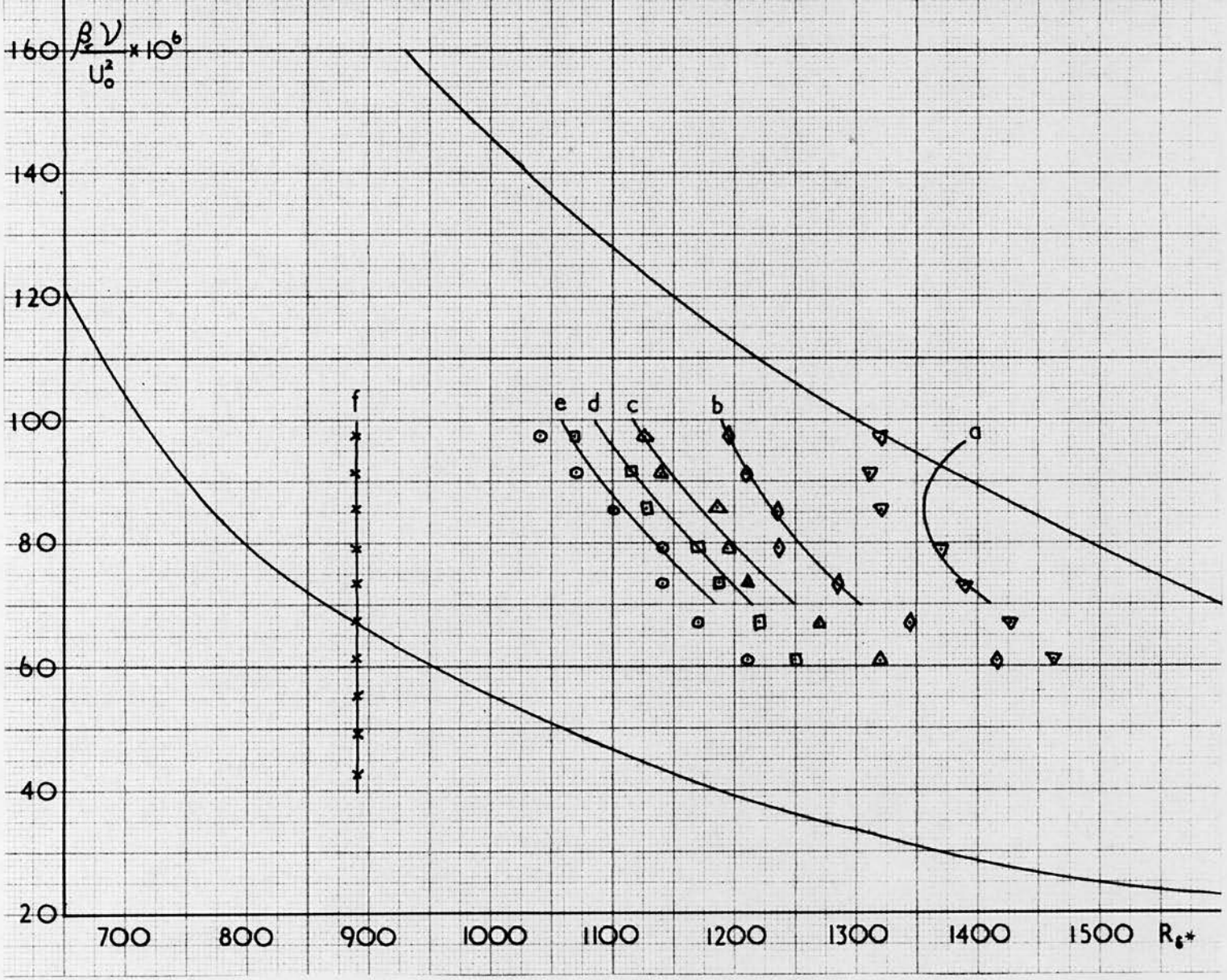
$\frac{\beta_x V}{U_0^2} \times 10^6$
160
140
120
100
80
60
40
20
700
800
900
1000
1100
1200
1300
1400
1500
R_{δ^*}
a
b
c
d
e
f

Figure 44

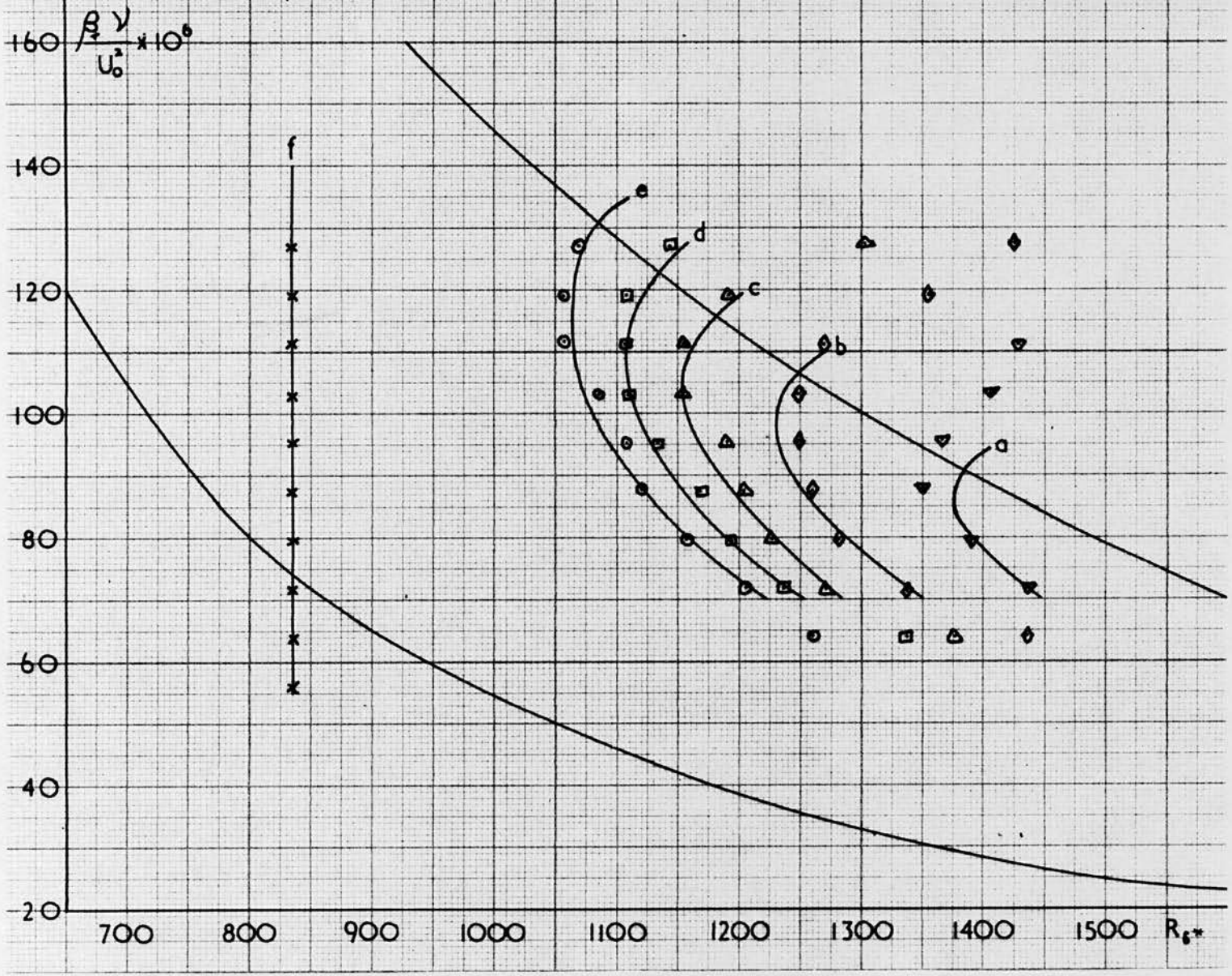
$\frac{\beta_z \nu}{U_0^2} \times 10^6$
160
140
120
100
80
60
40
20
700
800
900
1000
1100
1200
1300
1400
1500
R_{δ^*}
a
b
c
d
e
f

Figure 45

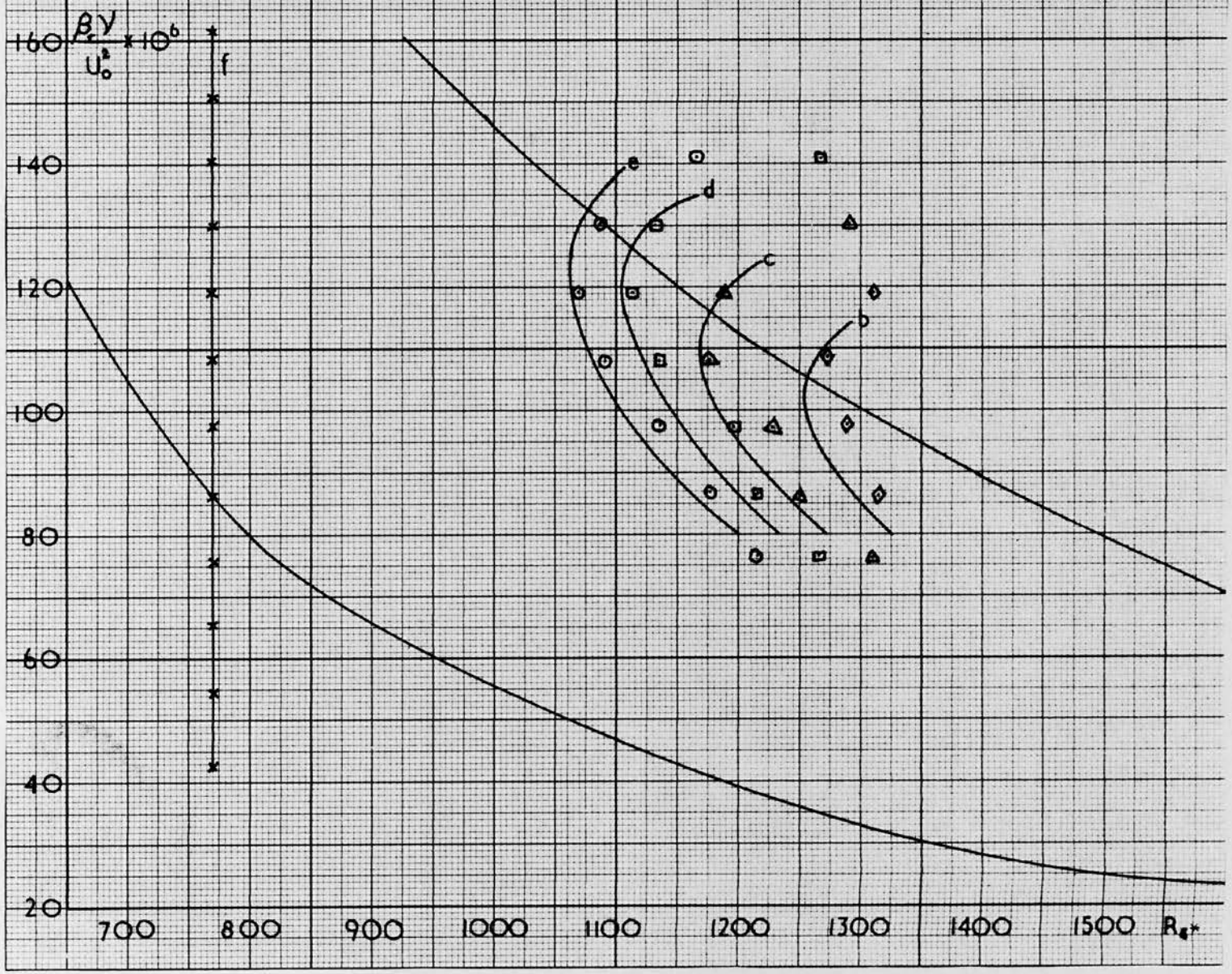
$\frac{\beta_c \gamma}{U_o^2} \times 10^6$
160
140
120
100
80
60
40
20
f
a
b
c
d
e
700
800
900
1000
1100
1200
1300
1400
1500
R_{δ^*}

Figure 46

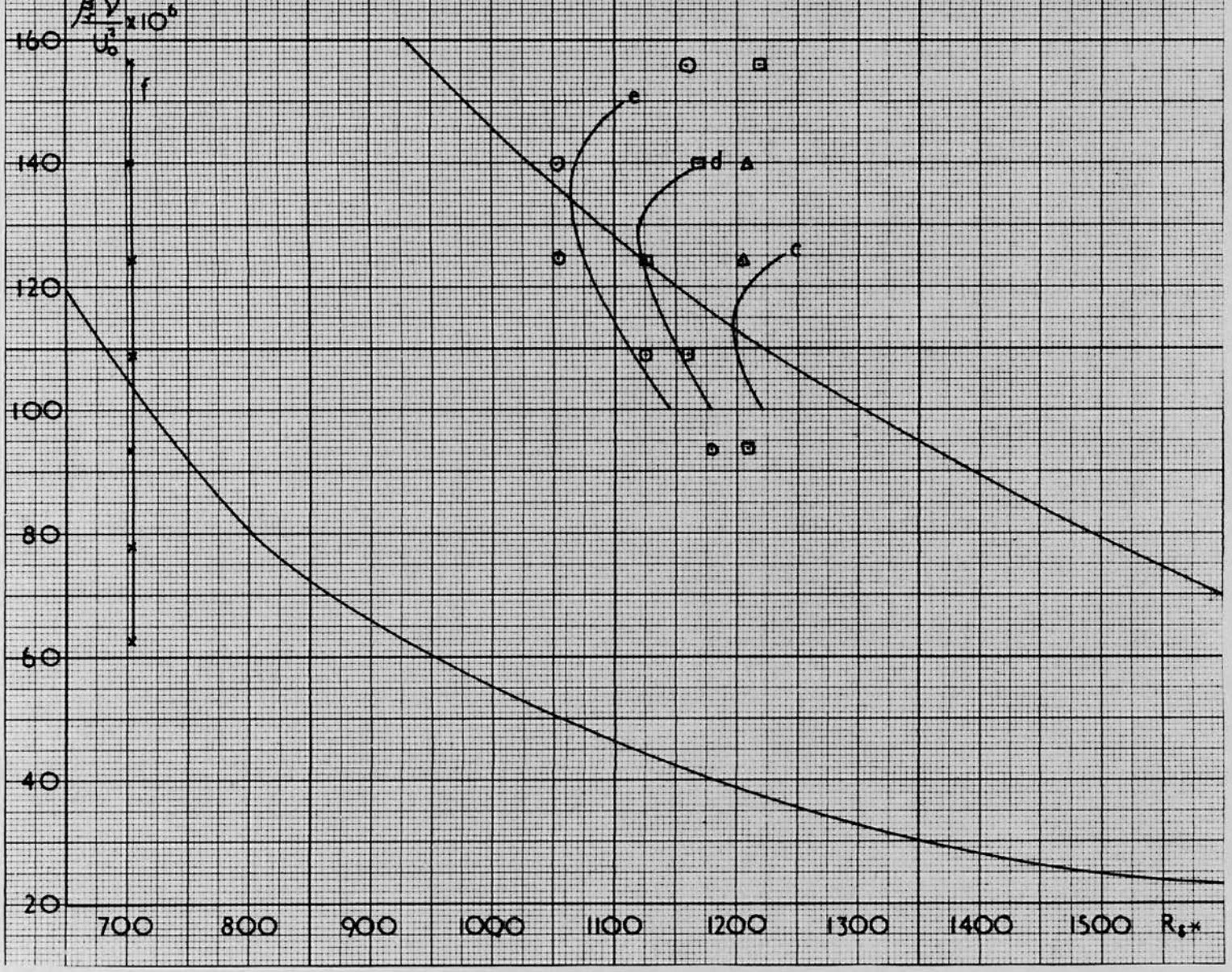
$\frac{\beta_x}{U_0^3} \times 10^6$
160
140
120
100
80
60
40
20
700
800
900
1000
1100
1200
1300
1400
1500
R_{δ^*}
f
e
d
c

Figure 47

each windspeed being 150, 120, 85 and 60 for windspeeds of 25, 30, 35 and 40 ft/sec. respectively. If these increases in Reynolds number are multiplied by U_o^2 then they become 94, 108, 104 and 96 x 10^3 respectively for each windspeed and it is seen that these are constant to an accuracy of ± 7%. It is thought that this variation could be easily accounted for between the calculations and the experimental results so it was concluded that the increase in Reynolds number required is proportional to $1/U_o^2$. The explanation for this may be that the breakdown process requires a certain amount of energy and therefore the greater the energy available the sooner breakdown will occur. The energy required must be supplied by the main flow and since the energy in the main flow will be proportional to U_o^2 the greater the windspeed the more energy will be available and the sooner breakdown will occur. The increase in Reynolds number between the point where $(\alpha\rho_\tau/U_o) \times R_{\delta^*} = 16$ and the point of actual breakdown will therefore be inversely proportional to U_o^2.

The following picture of the process of transition from laminar to turbulent flow in the boundary layer is now obtained. An injected disturbance travels down the boundary layer and grows according to the small disturbance

theory. If this amplified disturbance reaches a stage where the parameter $(\alpha\beta_r/U_o) \times R_{\delta^*}$ has a value of 16 then breakdown will eventually occur. The increase in Reynolds number required before breakdown actually occurs is dependent on the energy available in the free stream and since this will be proportional to the square of the free stream velocity, the required increase in Reynolds number will be inversely proportional to the square of the free stream velocity.

V. 5. Hot-wire measurements in the boundary layer

Using the total head and static pressure tubes to take pressure measurements in the boundary layer, only the point at which transition from laminar to turbulent flow occurs, can be detected; the method will give no information as to the actual process of transition, or the manner in which a disturbance grows as it travels down-stream from the ribbon. If, however, a hot-wire instrument is used, then the actual disturbance produced by the ribbon can be observed and so, once this disturbance has been produced, its progress can be traced down-stream until turbulence occurs. The distribution of the amplitude of the disturbance across the boundary layer can also be measured. In view of

the results obtained using pressure measurements it was thought that a more detailed picture of the transition process could be obtained if a hot-wire instrument was used. However, before attempting any investigation with the hot-wire, a general technique for using the hot-wire in the boundary layer was developed.

A hot-wire was manufactured and its distance from the flat plate, when the prongs of the probe were just touching the plate, was measured using the technique explained in section IV. 6. The hot-wire was then mounted on the traversing mechanism and calibrated as described in section IV. 7. The position of the hot-wire during calibration was such that it was well outside the boundary layer for all the wind-speeds used. After the hot-wire was calibrated the amplitude and frequency of the ribbon and also the free stream velocity of the air through the tunnel, were set at convenient values. (At this stage the second method of mounting the ribbon, as described in section III. 4., had been adopted and it was now positioned 1 foot from the leading edge.) The hot-wire was then traversed across the boundary layer at an x - position 2 inches down-stream of the ribbon. At intervals of 0.01 inches,

in the y - direction measurements were made of the wire resistance and the amplitude of the fluctuating voltage across the wire. The velocity at each y - position was then calculated, using the wire calibration and the values of wire resistance, and from these a boundary layer profile was drawn. The boundary layer thickness δ was then found and the value of y/δ calculated for each point. Finally the values u'/U_o were calculated, using the relationship given by equation (11), and plotted against the corresponding values of y/δ . In this way the distribution of the amplitude of the disturbance across the boundary layer was found for one x - position, one wind-speed and one set of ribbon conditions. The distribution obtained is shown in figure 48.

To obtain this distribution for a single set of conditions, the wire had to be calibrated, the wire resistance and the voltage fluctuations across it measured at each y - position, the velocity of the air calculated for each y - position and from this the value of δ found. The values of y/δ and u'/U_o could then be calculated for each position and a graph drawn. The whole operation involved a large amount of tedious arithmetic and was

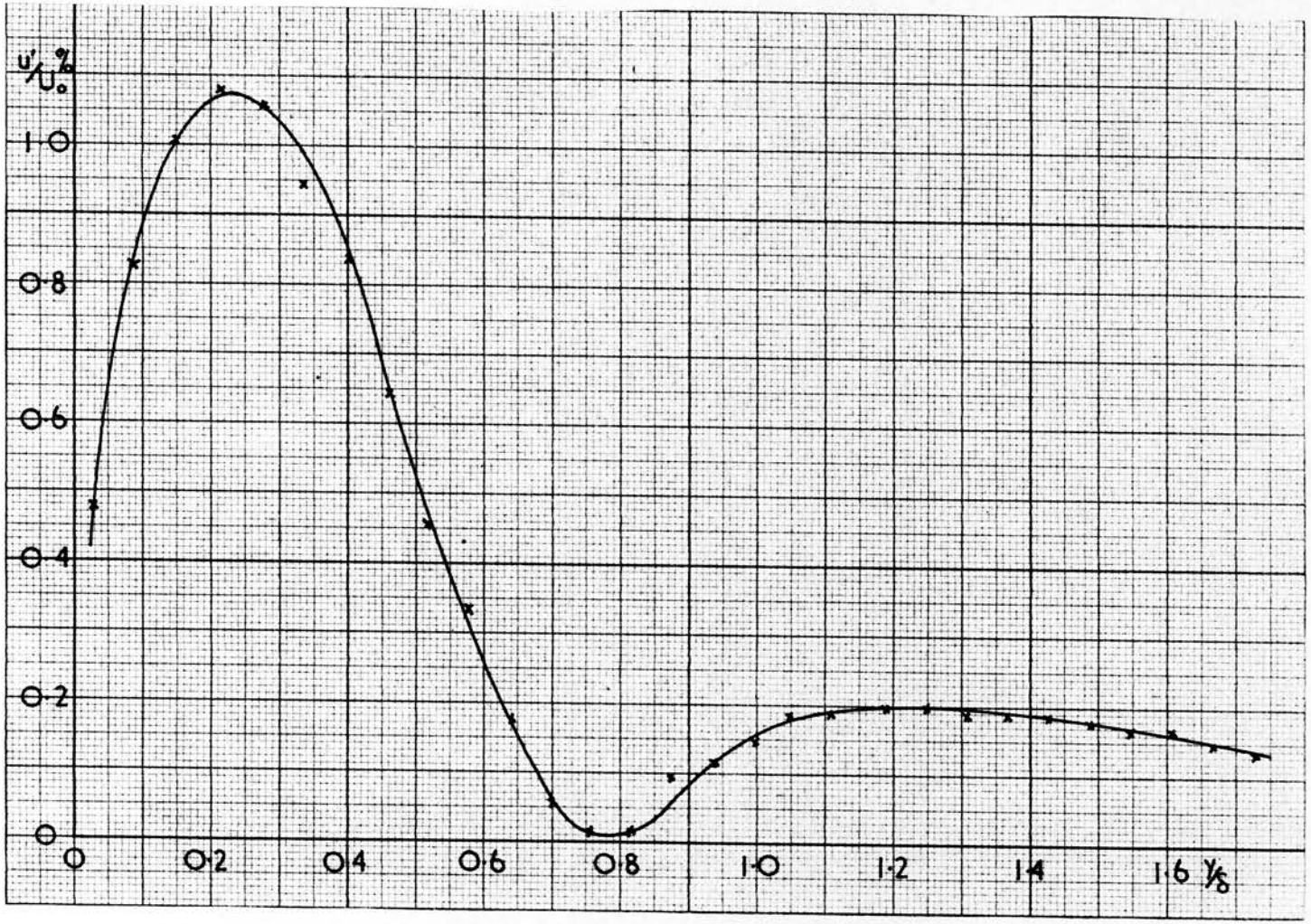

Figure 48

Initial measurement of distribution of disturbance amplitude.

therefore extremely time consuming. Since it was expected that a fairly large number of calculations of this type would have to be carried out, it was decided to make use of a computer to do the calculations and thus save a great deal of time and effort. Fortunately, permission was obtained to use the Ferranti 'Sirius' computer of the Heriot-Watt College for this purpose.

A programme for the computer was worked out for the calculation and this is given in the Appendix. Initially seven readings of wire resistance, corresponding to the seven wind-speeds used in the calibration, were fed to the computer and the best straight line obtained for the relationship between ρ and $U^{0.45}$. The values of y - position and resistance of the hot-wire were then fed in and U, the velocity of the air at each y value, obtained from the calibration. The value of the boundary layer thickness was then calculated from the relationship,

$$\delta = \frac{1}{0.341} \int_0^\infty (1 - U/U_\infty)dy$$

and y/δ found. Finally the values of the amplitude of the output signal across the hot-wire were fed to the computer and the values of u'/U_o calculated. Once the initial programme had been worked out it was a simple matter

to feed the data into the computer and obtain the distribution of the disturbance amplitude across the boundary layer.

Results for various wind-speeds and ribbon conditions were then easily obtained. Figure 49 shows the distribution of disturbance amplitude, across the boundary layer, for one frequency and various amplitudes of ribbon vibration, at one x - position. Figures 50 and 51 show contours, in the x, y plane, of equal amplitudes of the disturbance for a single amplitude and frequency of ribbon vibration. In figure 50 the amplitude was small enough not to have caused breakdown, but in figure 51 it is seen that the larger amplitude caused breakdown.

During the time that these measurements were being carried out it was noticed that under certain conditions, the output signal across the hot-wire contained an appreciable amount of second harmonic. Since Lin (22) had predicted that non-linear effects would result in generation of higher harmonics it was decided to examine the harmonic content of the wave in more detail. Lin predicted that this effect would be greatest in the vicinity of the critical layer, which is the position in the boundary layer where

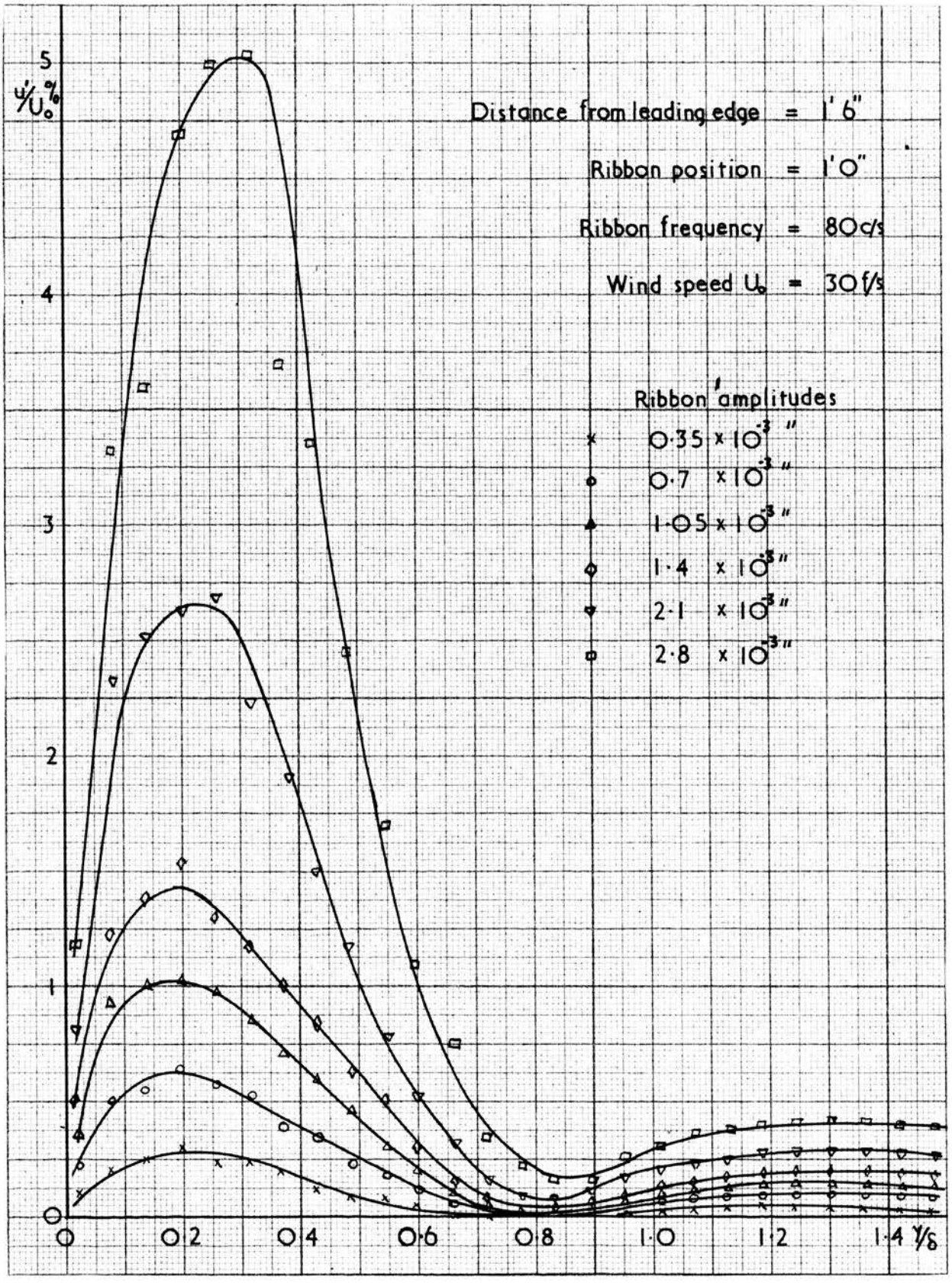

Figure 49

Distribution of disturbance amplitude for various ribbon amplitudes.

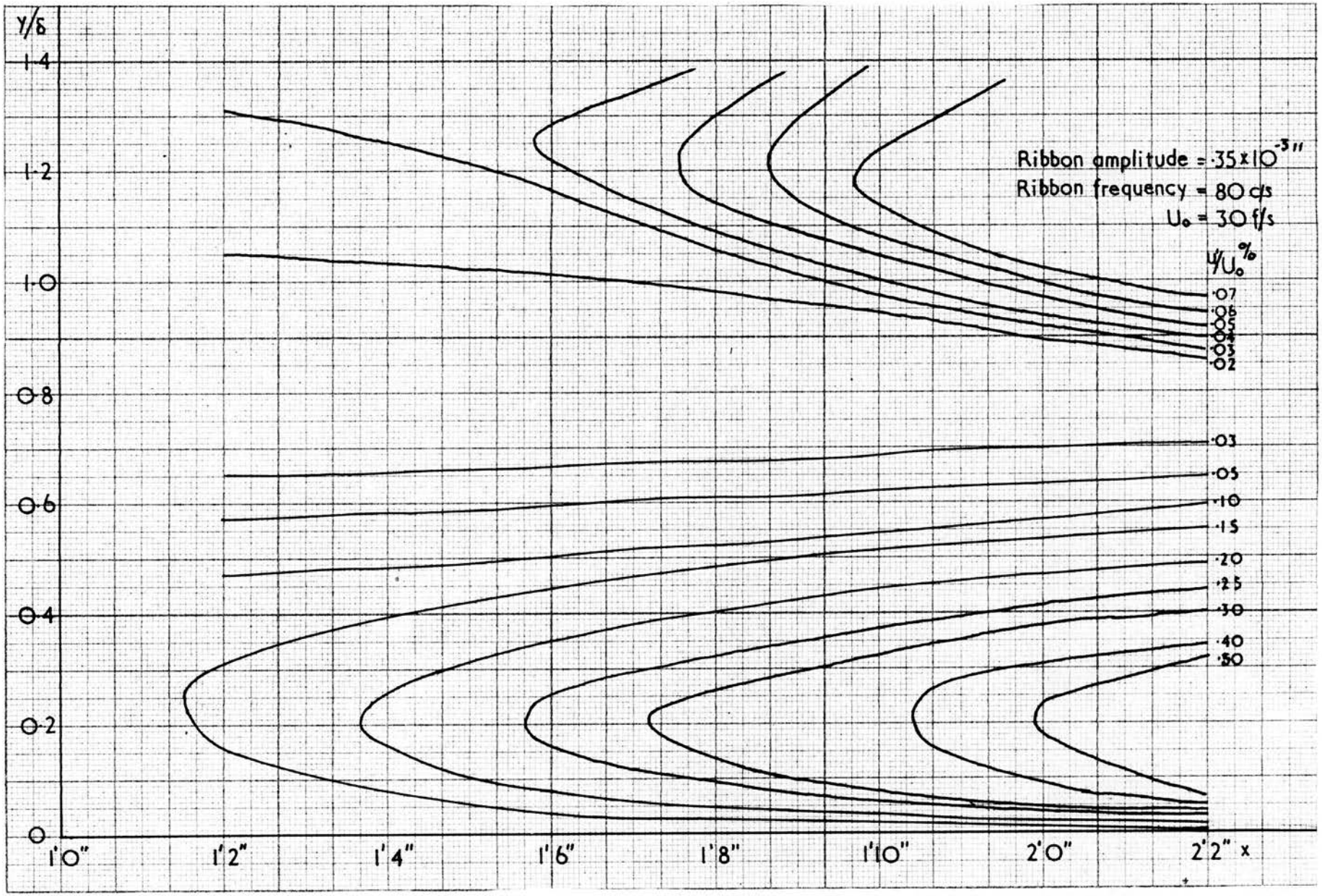

Figure 50

Contours of equal disturbance amplitude (small ribbon amplitude).

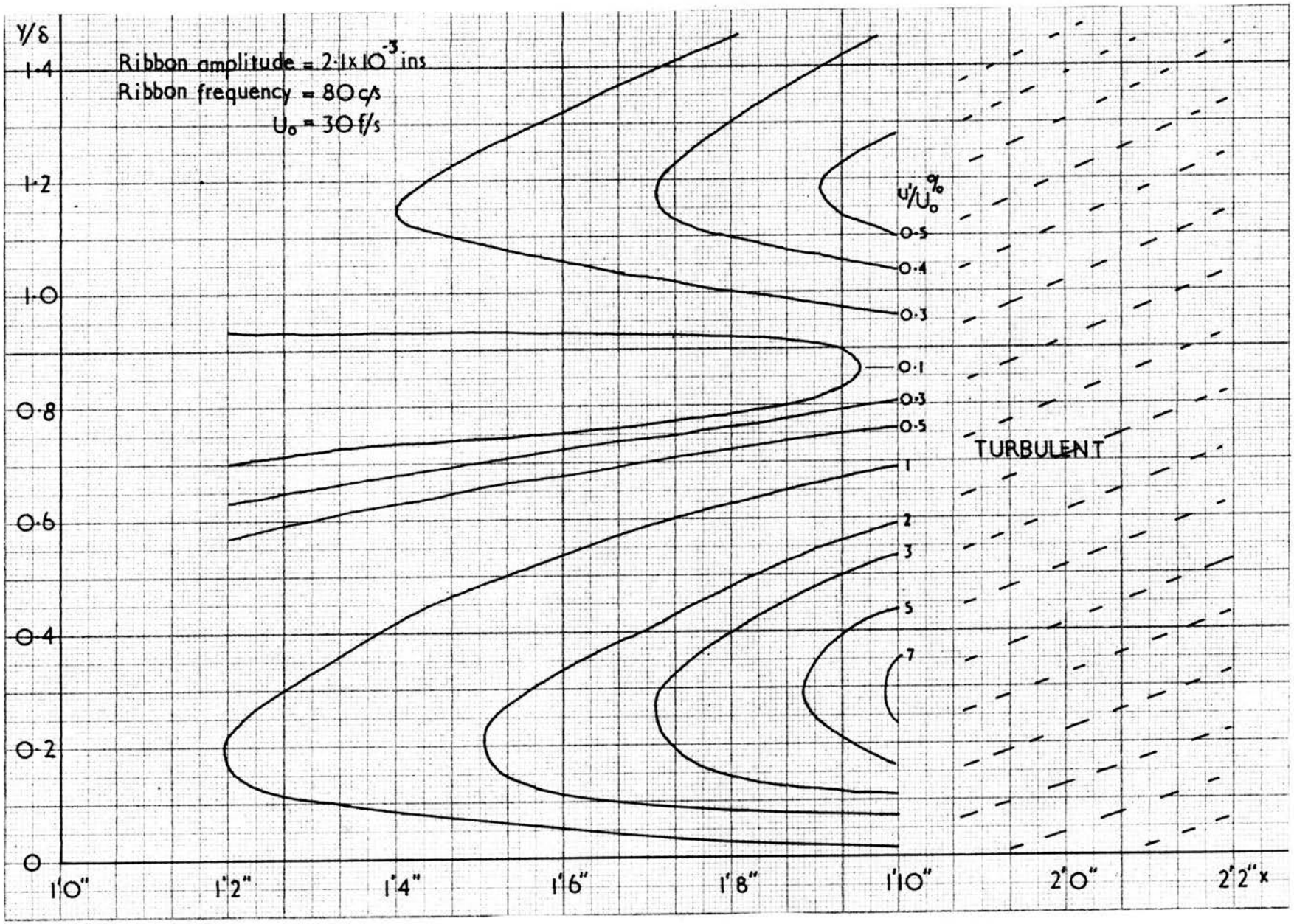

Figure 51

Contours of equal disturbance amplitude (large ribbon amplitude).

the disturbance velocity is equal to the local velocity of the air, and so examination of the harmonic content of the wave was confined to this region.

It had been observed previously, that the second harmonic content of the wave was most noticeable for a wind-speed of 25.5 feet/second and a ribbon frequency of 47 cycles/second, so it was with these conditions that the harmonic content of the wave was first examined. The hot-wire was placed in the boundary layer at an x - position 2 inches down-stream from the ribbon and at a y - position corresponding to a y/δ value of 0.2. The wire was then traversed down-stream, in the x - direction at this value of y/δ . This was easily achieved by traversing the wire down-stream so that its resistance remained unaltered and, since this means that the velocity of the air at the hot-wire remained constant, then it follows that the y/δ value must have also remained constant. The output from the hot-wire was displayed on an oscilloscope and photographs of the trace were taken at 2 inch intervals in the x - direction. Figure 52 shows the photographs obtained. A numerical Fourier analysis was carried out on the traces by dividing each cycle into twelve equal parts and representing the wave by

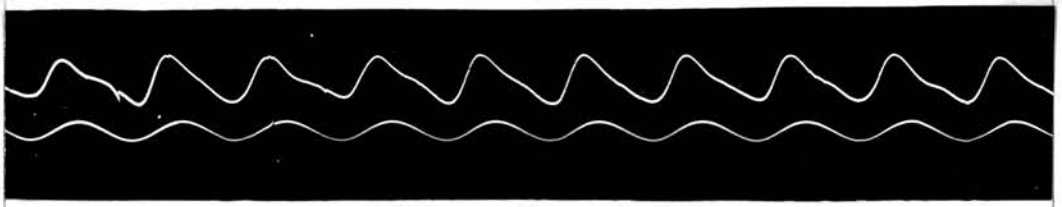

x = 1'2" gain = 10,000

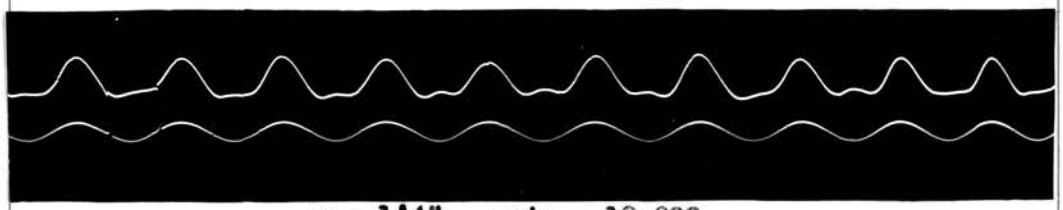

x = 1'4" gain = 10,000

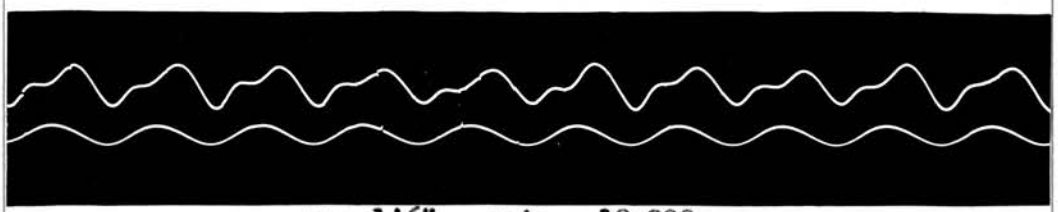

x = 1'6" gain = 10,000

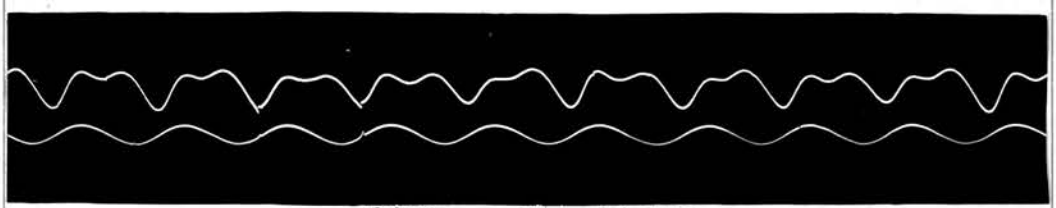

x = 1'8" gain = 10,000

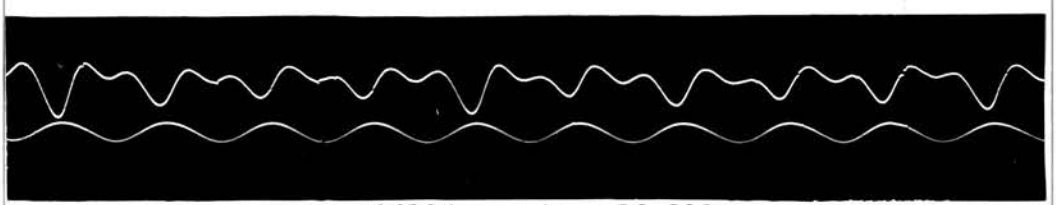

x = 1'10" gain = 10,000

FIGURE 52

Photographs of output from hot-wire for various x - positions
Uo = 25.5 ft/sec., ribbon frequency = 47 c/s, ribbon amplitude = 0.001 inches.
Lower trace is reference signal.

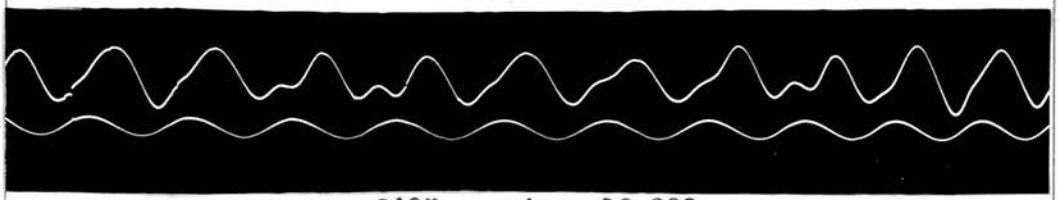

x = 2'0" gain = 10,000

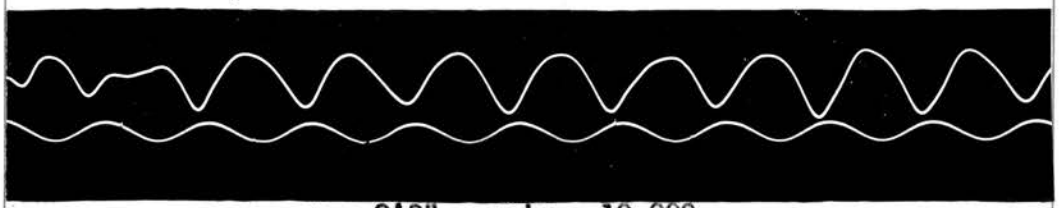

x = 2'2" gain = 10,000

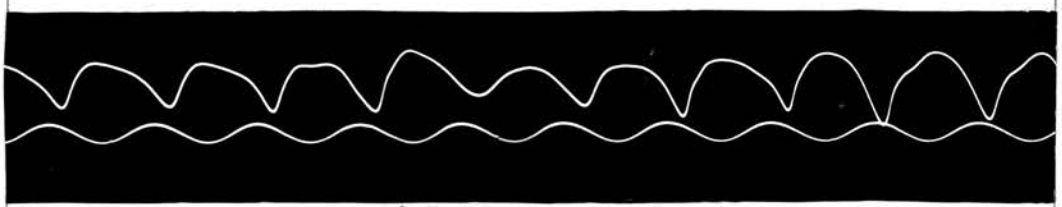

x = 2'4" gain = 4,000

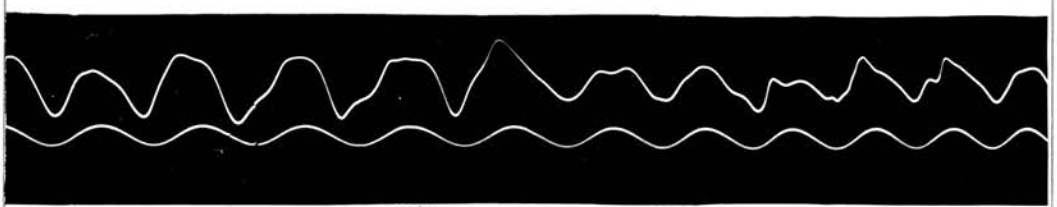

x = 2'6" gain = 2,000

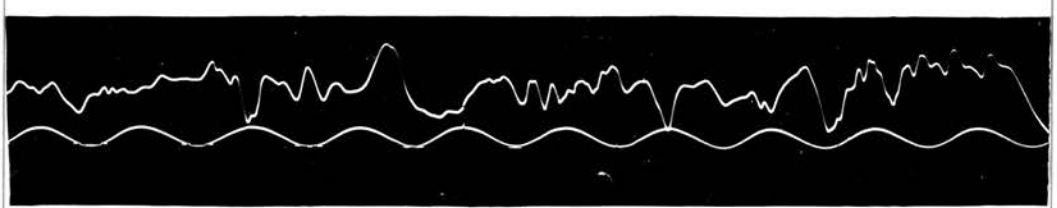

x = 2'8" gain = 2,000

FIGURE 52

the series,

$$a_0 + a_1\cos\theta + a_2\cos 2\theta + \text{----} + a_5\cos 5\theta + a_6\cos 6\theta$$
$$+ b_1\sin\theta + b_2\sin 2\theta + \text{----} + b_5\sin 5\theta$$

If u_0 to u_{11} are the ordinates at each of the twelve positions then the coefficients a_0 to a_6 and b_1 to b_5 can be calculated by the procedure shown in the Appendix. The ordinates were obtained by projecting the film on a screen and measuring the enlarged wave. A full analysis of the method is given by Whittaker and Robinson (37). The result of the analysis is given in figure 53.

Using the same values of wind-speed and frequency the experiment was repeated for two other ribbon amplitudes and the results of these are shown in figures 54 & 55.

V. 6. Discussion of results

Figures 48 to 51 show the initial hot-wire measurements of the distribution across the boundary layer of the amplitude of the disturbance under various conditions. For the smaller amplitudes these confirm the experimental results obtained by Schubauer and Skramstad and the theoretical calculations of Schlichting, shown in figure 56. The distribution shows the familiar 180° phase shift at a y/δ value between 0.7 and 0.8 and a peak amplitude at about

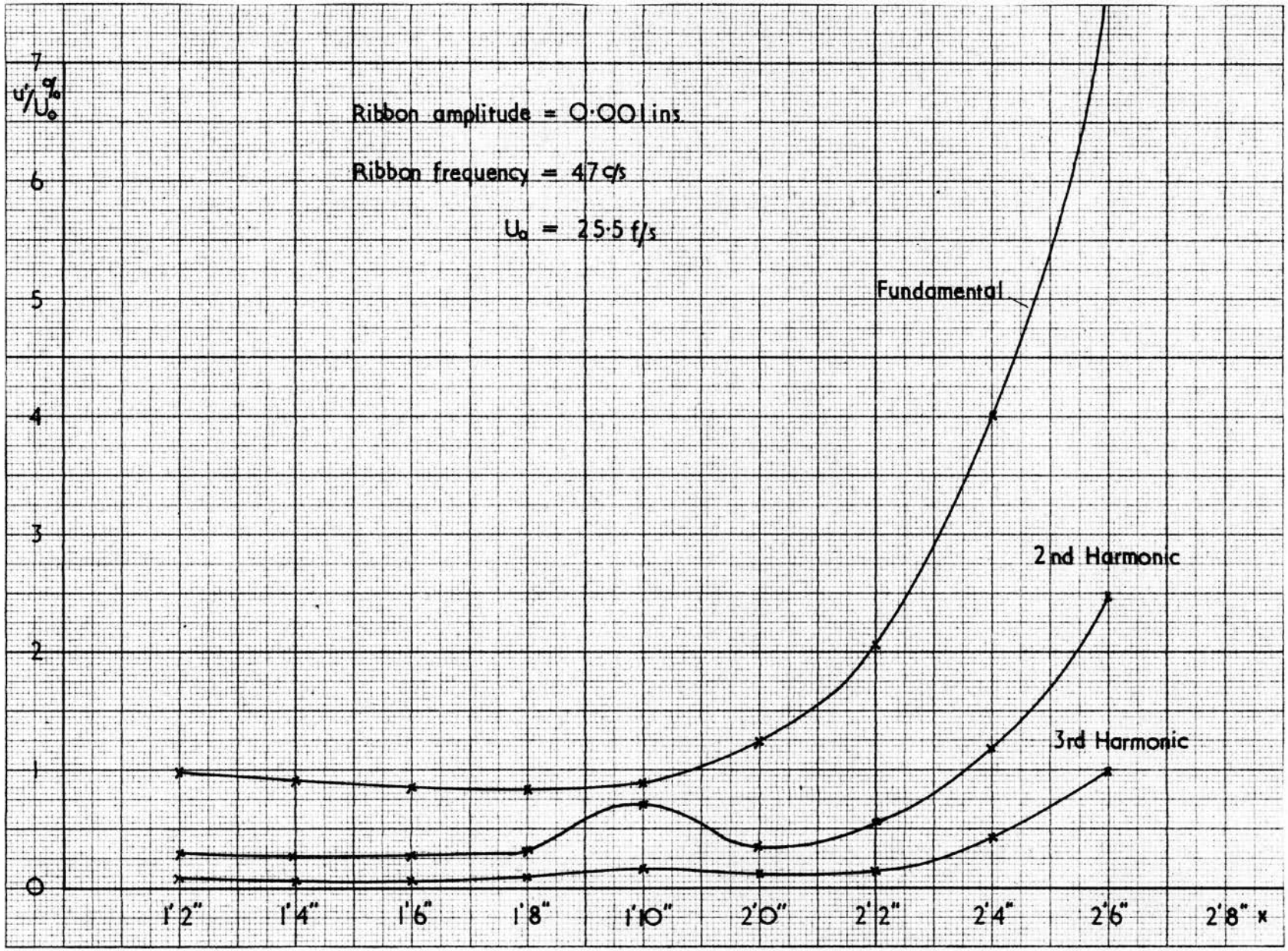

Figure 53

Analysis of harmonic content of wave.

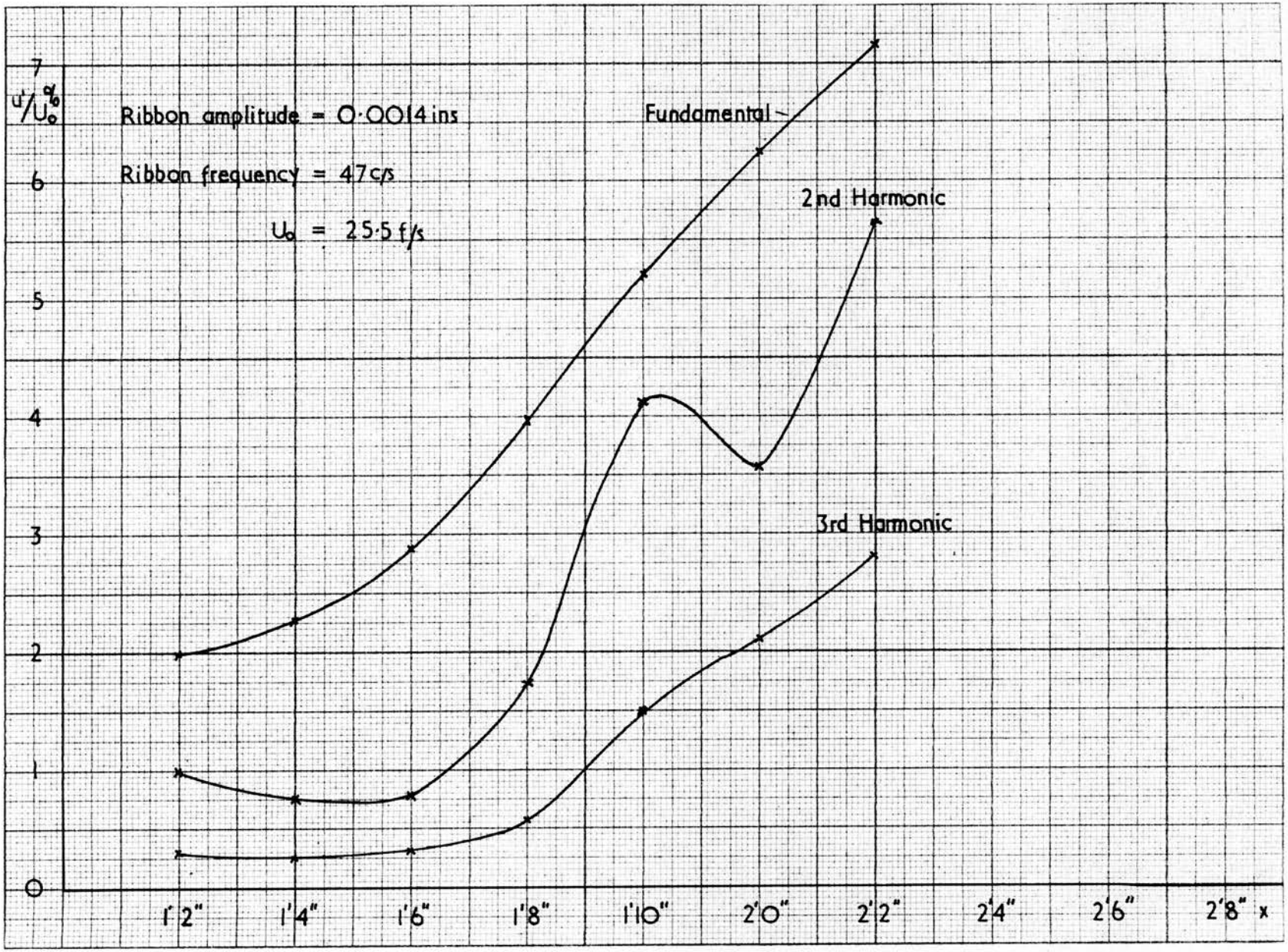

Figure 54

Analysis of harmonic content of wave.

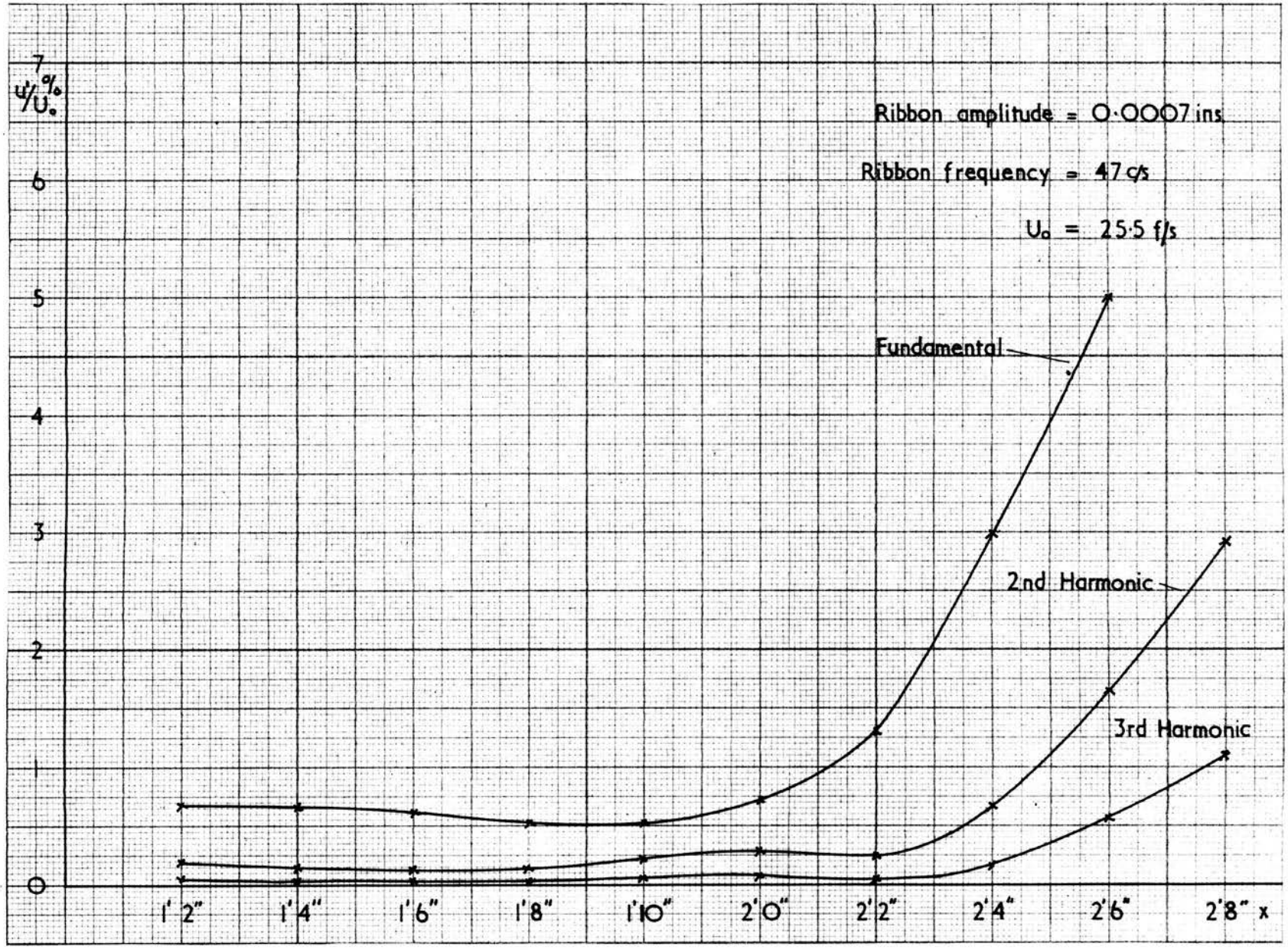

Figure 55

Analysis of harmonic content of wave.

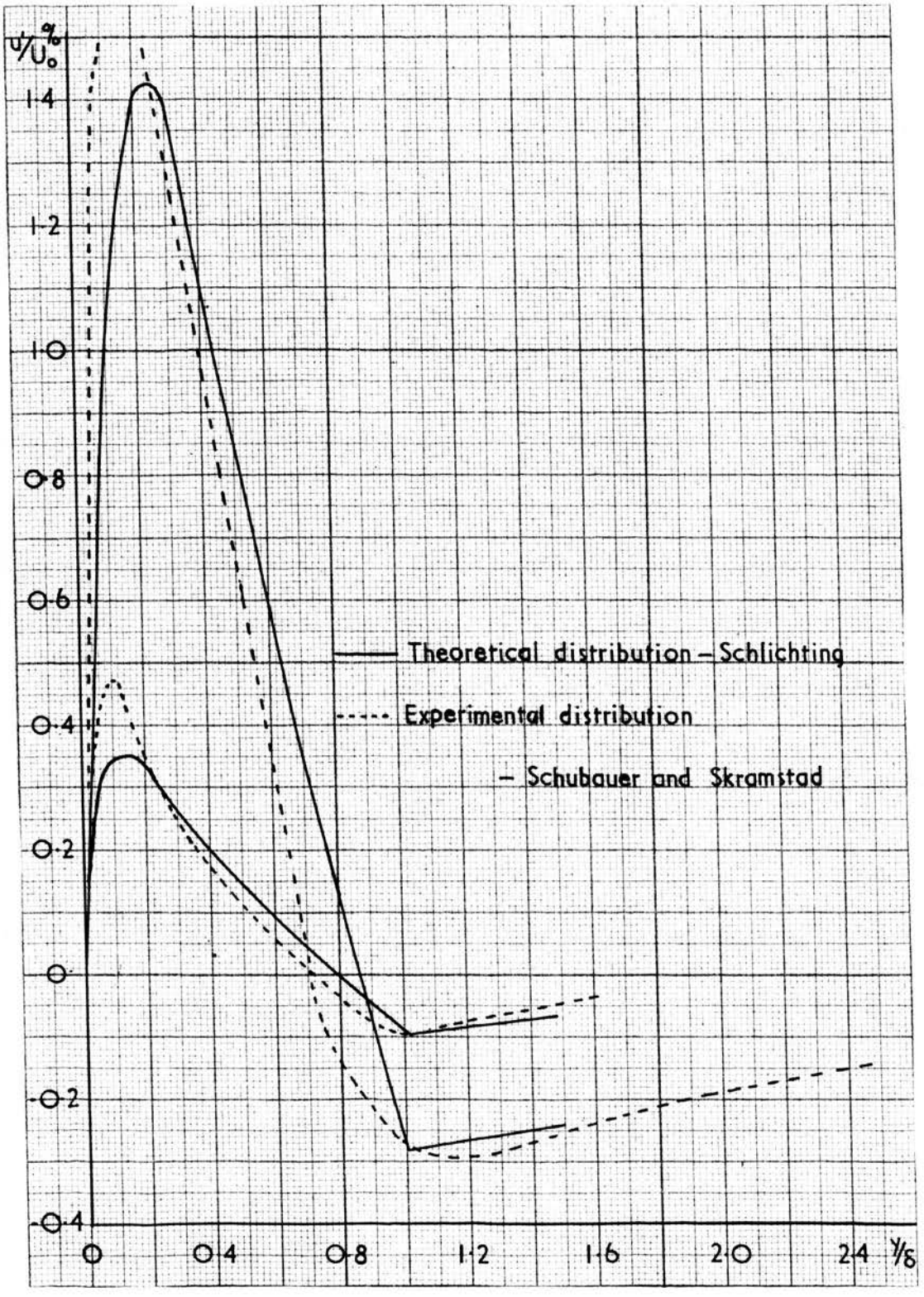

Figure 56

Experimental and theoretical distribution of disturbance amplitude.

0.2 y/δ . These values compare well with the curves of figure 56. As the amplitude of the ribbon is increased however, there is a rapid increase in the amplification of the disturbance which seems to take place mainly between the flat plate and the position of the 180° phase shift. This increase in amplification is greater at the outer side of the peak, resulting in outward movement of the peak to about 0.3 y/δ when the disturbance amplitude is 5% of the free-stream velocity. This shifting of the 'centre of gravity' of the intensity of the disturbance must be caused by the non-linear development of the disturbance; i.e. the amplitude of the disturbance has reached a value where it no longer conforms to the Tollmien-Schlichting theory of small disturbances. From the results it would appear that the non-linear effects produce uneven amplification across the boundary layer.

The results of the analysis of the harmonic content of the disturbance, as it proceeds down-stream in the x - direction, for three amplitudes of ribbon vibration, are shown graphically in figures 53, 54 and 55. The theoretical position of the neutral curve for the fundamental frequency is at 1 foot 6 inches, which is 4 inches down-

stream from the ribbon. It would therefore be expected, that the amplitude of the fundamental frequency would be damped initially and amplified after it crossed the neutral curve. For the two smaller amplitudes this appears to be true, but in the case of the largest amplitude the fundamental frequency is amplified immediately. This probably means that for the largest amplitude the initial disturbance produced by the ribbon was not small enough to be amplified according to the Tollmien-Schlichting theory and the non-linear effects came into operation immediately.

The pattern of the second harmonic content of the disturbance is similar for all three cases, rising quite rapidly, falling off and finally increasing rapidly again as breakdown is approached. A peculiar feature of the graphs is this falling off of the amplitude after the initial rise and the effect is very noticeable in the case of the two larger amplitudes. The photographs of figure 52 show the effect very clearly. It would appear that as the wave amplitude increases the amount of second harmonic present increases and after a certain stage some factor which reduces this amount becomes dominant; finally the breakdown process occurs and the amount of second harmonic present as would

be expected, again increases. The amount of third harmonic present is fairly small until turbulence begins to develop.

CHAPTER VI

Conclusion

A study has been made of the effects produced by a periodic disturbance which is artificially introduced into a laminar boundary layer on a flat plate with zero pressure gradient along the plate. The disturbance was introduced into the boundary layer by means of an oscillating ribbon, the amplitude and frequency of which was carefully controlled.

Before any investigation of the disturbance produced by the ribbon was carried out, a study of the static flow conditions over the plate was made and it was found that the boundary layer remained laminar along the centre of the plate, to a distance of 3 feet 6 inches from the leading edge. However, because of the turbulent wedges, originating at the top and bottom of the leading edge, the length of laminar boundary layer in the z - direction became progressively smaller as the distance from the leading edge was increased.

It had been noticed by several workers, that as the disturbance amplitude increased and transition to turbulent flow approached, a strong three-dimensional pattern became evident. It was shown by Klebanoff and Tidstrom that this three-dimensional pattern was associated with variations in boundary layer thickness in the z - direction. Examination of the boundary layer thickness in the z - direction confirmed that these variations were present, but owing to the initial three-dimensionality of the injected disturbance, any z - variation in the x - position of the onset of transition could not be detected. However, it is hoped that the modification to the method of mounting the ribbon made in the later stages of the work will allow the central portion of the ribbon to vibrate with a constant amplitude and thus make it possible to take measurements in the z - direction.

Using a surface pitot tube, measurements of the point at which transition from laminar to turbulent flow occurs were made for various conditions of wind-speed and ribbon amplitude and frequency. Although the injected disturbance cannot be regarded as infinitesimal at the point where it distorts the mean flow, it was decided to examine these

results to see if they could be related in any way to the predictions of the small disturbance theory. If the amplitude of the disturbance at the ribbon is known then by using the theoretical results of Shen, the amplitude of the disturbance at any other point can be calculated and this enables curves of some constant parameter to be drawn. After a considerable amount of manipulation it was discovered that a set of curves could be calculated which corresponded fairly well with the experimental points of breakdown. These calculated curves were found by initially obtaining curves of constant $(\alpha\beta_r/U_0) \times R_{\delta^*}$ and then shifting these curves by a fixed amount in the direction of increasing Reynolds number. The constant value of the parameter $(\alpha\beta_r/U_0) \times R_{\delta^*}$ was found to be 16 and the shift required was inversely proportional to U_0^2 .

It would thus appear that if a small disturbance is injected into the boundary layer it travels down-stream and is amplified or damped according to the Tollmien-Schlichting theory. If, however, it reaches a stage where the parameter $(\alpha\beta_r/U_0) \times R_{\delta^*}$ has a value of 16 then break-down will eventually occur. This means that up to the point where $(\alpha\beta_r/U_0) \times R_{\delta^*} = 16$ the small disturbance theory

will be valid but after this point non-linear terms become dominant and the break-down process begins. No conclusion can be made as to the actual mechanism involved in this process but the increase in Reynolds number between the beginning of non-linear development and breakdown is inversely proportional to the square of the free-stream velocity. This is probably not unreasonable since whatever the mechanism involved in the breakdown process, energy will be required and this could be supplied from the main flow.

Since it was required to study the development of the disturbance produced by the ribbon, it was necessary to make measurements of the actual disturbance and not only on the long term effects produced by it. These measurements were made using hot-wire apparatus and a technique was developed whereby hot-wires were manufactured from 0.0002 inch diameter tungsten wire. A system to enable the hot-wires to be accurately positioned in the boundary layer, was also developed. The distribution of the amplitude of the disturbance across the boundary layer was measured for various conditions. For the smaller amplitudes of disturbance, the distribution agreed with that predicted by the Tollmien-Schlichting theory for small disturbances

and, as would be expected, the distribution for the larger amplitudes, deviated somewhat from this due to non-linear effects which seemed to produced a shift of the 'centre of gravity' of the distribution, towards the outside of the boundary layer.

The harmonic content of the wave in the vicinity of the critical layer was measured using the hot-wire, with one wind-speed and one frequency of ribbon vibration and for three different ribbon amplitudes. It was found that, under the conditions chosen, the amount of second harmonic present in the disturbance initially increased, but at a certain position, just before breakdown, the amount decreased quite sharply and then finally increased again as breakdown occurred. Klebanoff et. al. (31) did measure the harmonic content of the disturbance and found that the amount was not significant until breakdown occured. During the present work it was noticed that the second harmonic content did not always appear well before breakdown and the measurements were made under conditions where the amount was most noticeable. It would appear that although there are several theories as to the process by which turbulence occurs, it cannot be said that any one

theory fully explains the process. It is possible that the truth may lie in a combination of the various theories and, depending on the conditions present in any particular case, one effect becomes dominant and is instrumental in causing turbulence.

It is suggested that the harmonic content of the disturbance should be measured for a wide range of conditions and perhaps the criterion for this effect to be dominant would emerge from the results. It is also suggested that since there is definitely some form of three-dimensional process involved, whereby energy is transferred from one z - position to another, then it is essential that facilities should be available so that an extensive three-dimensional examination of the flow can be made.

The present results and those of previous workers suggest the following picture of the process of transition from laminar to turbulent flow in a boundary layer. A Tollmien-Schlichting wave may be set up in the boundary layer and, as the wave travels down-stream, it is amplified or damped according to the linearised stability theory. So long as the wave remains small in intensity, however, it is eventually damped out and does not result

in the onset of turbulence. If the wave reaches a point where the parameter $(\alpha\beta_r/U_0)xR_{\delta^*}$ has a value of 16 non-linear development takes place. It is believed that once this point has been reached breakdown will eventually occur, so that it is possible to obtain breakdown in a region where the linearised theory predicts damping. The increase in Reynolds number between this point and the breakdown position is inversely proportional to the square of the wind-speed. In the region between non-linear development and breakdown, there are probably several processes operating and it may depend on the external conditions, such as wind-speed, frequency of the disturbance and the amount of free-stream turbulence, which one becomes dominant.

It is clear that a very thorough investigation of the non-linear development of the wave is required and even after this has been achieved, since the process of transition from laminar to turbulent flow is extremely complex, it may still be impossible to obtain an explanation which completely satisfies all aspects of the process.

APPENDIX

Computer Programme for Disturbance Amplitude Distribution

```
Jv1
TEXT
BOUNDARY LAYER TRAVERSE

v1=TAPE8
no=o
1)v(9+no)=v(1+no)-v8
v(1+no)=v(1+no)/v(9+no)
n1=5xno
n1=n1+15
vo=n1
vo=LOGvo
vo=o.45xvo
vo=EXPvo
v(9+no)=vo
no=no+1
+1,no≠7
no=o
v16=o
v17=o
v18=o
v19=o
2)v16=v16+v(9+no)
v17=v17+v(1+no)
v20=v(9+no)xv(9+no)
v21=v(1+no)xv(9+no)
v18=v18+v20
v19=v19+v21
no=no+1
+2,no≠7
v20=7xv18
v21=v16xv16
v20=v20-v21
v21=v17xv18
v22=v16xv19
v21=v21-v22
v22=7xv19
v23=v16xv17
v22=v22-v23
v21=v21/v20
v22=v22/v20
TEXT
INTERCEPT
PRINTv21,4043
TEXT
GRADIENT
PRINTv22,4044
Xvo=v8
v1=TAPE2
v23=TAPE*
Xn1=no
Xno=o
3)n2=no/2
v(103+n2)=v(23+no)-vo
v(23+no)=v(23+no)/v(103+n2)
v3=v(23+no)-v21
v3=LOGv3
v4=LOGv22
v3=v3-v4
v3=v3/0.45
v(103+n2)=EXPv3
+9,n2≠o
v200=v103
9)v5=v(23+no)-1
v5=v5xv5
v5=v5/0.45
v6=v(23+no)-v21
v5=v5/v6
```

```
v5=v5xv(103+n2)
v6=voxv1
v6=v6xv2
v(143+n2)=v5/v6
v(103+n2)=v(103+n2)/v200
PRINTv(23+no),3023
PRINTv(103+n2),4023
PRINTv(143+n2),4042
v(103+n2)=1-v(103+n2)
no=no+2
→3,n1≠no
v10=v(101+n2)-v(100+n2)
v10=v10-v104
v10=v10+v103
v10=v10/12
v103=v103/2
v(101+n2)=v(101+n2)/2
v7=o
n3=n2-1
no=o
4)v7=v7+v(103+no)
no=no+1
→4,no≠n3
v8=v24-v26
v7=v7-v10
v7=v7xv8
v(102+n2)=v(102+n2)/2
v8=v(101+n2)+v(102+n2)
n4=2xn2
v9=v(20+n4)
v8=v8xv9
v7=v7+v8
v7=v7/0.341
Xn1=2xn2
Xno=o
5)v(24+no)=v(24+no)/v7
PRINTv(24+no),3023
no=no+2
→5,no≠n1
Xvo=vo
Xv1=v1
PRINTv7,3003
6)v23=TAPE*
Xn1=no
Xno=o
7)v(23+no)=v(23+no)xv(143+no)
PRINTv(23+no),3004
no=no+1
→7,no≠n1
Xvo=vo
Xv1=v1
Xv2=v2
→6
(→o)
```

Procedure for Calculation of Harmonic Amplitudes.

$(u_0$ to $u_6)$ ....

$(u_{11}$ to $u_7)$ ....

Sums $(v_0$ to $v_6)$ ....

Diffs. $(w_1$ to $w_5)$ ....

$(v_0$ to $v_3)$ .... $(w_1$ to $w_3)$ ....

$(v_6$ to $v_4)$ .... $(w_5$ to $w_4)$ ....

Sums $(p_0$ to $p_3)$ .... Sums $(r_1$ to $r_3)$ ....

Diffs. $(q_0$ to $q_2)$ .... Diffs. $(s_1$ to $s_2)$ ....

$p_1=$	$p_2=$	$q_2=$	$r_1=$
$h_1=$	$h_2=$	$l_2=$	$m_1=$

($\frac{1}{2}$ line above)

(0.866 x line above)

$q_1=$	$r_2=$	$s_1=$	$s_2=$
$l_1=$	$m_2=$	$n_1=$	$n_2=$

	$p_0=$ ... $p_1=$ ... $p_2=$ ... $p_3=$ ...	$q_0=$ ... $l_1=$ ... $l_2=$ ...	$p_0=$ ... $h_1=$ ... $p_3=$ ... $h_2=$ ...	$p_0=$ ... $p_3=$ ... $h_1=$ ... $h_2=$ ...	$m_1=$ ... $m_2=$ ... $r_3=$ ...	$q_0=$ ... $q_2=$ ...	$n_1=$ ... $n_2=$ ...	$r_1=$ ... $r_3=$ ...
Sum of 1st Column.	....	....	....	....	....			
Sum of 2nd Column	....	....	....	....	....			
Sum	.....$=12a_0$	....$=6a_1$			....$=6b_1$		....$=6b_2$	
Diff.	.....$=12a_6$	....$=6a_5$	....$=6a_4$	....$=6a_2$	....$=6b_5$	....$=6a_3$	....$=6b_4$	....$=6b_3$

Result : $u = a_0+a_1 \cos\theta + a_2 \cos 2\theta + a_3 \cos 3\theta + a_4 \cos 4\theta + a_5 \cos 5\theta + a_6 \cos 6\theta$
$+b_1 \sin\theta + b_2 \sin 2\theta + b_3 \sin 3\theta + b_4 \sin 4\theta + b_5 \sin 5\theta$

Checks: $u_0=a_0+a_1+a_2+a_3+a_4+a_5+a_6$

$w_1=b_1+2b_3+b_5+1.732(b_2+b_4)$

REFERENCES

1. Reynolds, O: Phil. Trans. Roy. Soc. 174, 935, (1883)

2. Prandtl, L.: Proc. 3rd International Math. Congr. (Heidelberg), (1904)

3. Blasius, H.: Z. Math. u. Physik. 56, 1, (1908) also N.A.C.A. Tech. Memo. No. 1256.

4. Howarth, L.: Proc. Roy. Soc. A, 164, 547, (1938)

5. Nikuradse, J.: Monograph, Zentrale f. wiss Berichtaresen, Berlin, (1942)

6. Schubauer, G.B. and Skramstad, H.K.: Journal of Res. of Nat. Bureau of Standards 38 R.P. 1722. (1947)

7. Taylor, G.I. : Proc. Roy. Soc. A, 156, 301 (1936)

8. Lord Rayleigh: Proc. London Math. Soc. 19, 67, (1887)

9. Tietjens, O. : Z. a. Math. Mech. 5, 200, (1925)

10. Tollmien, W.: N.A.C.A. Tech. Memo. No. 609, (1931)

11. Tollmien, W.: N.A.C.A. Tech. Memo. No. 792, (1936)

12. Schlichting, H.: Z. a. Math. Mech. 13, 171, (1935)

13. Schlichting, H. : Z. a. Math. Mech. 15, 313, (1935)

14. Lin, C.C.: Quarterly Appl. Math. 3, 117, 218 and 227, (1945)

15. Schlichting, H.: Boundary layer Theory, Pergamon, London (1955)

16. Schlichting, H.: Math. Phys. Klasse, 182, (1933) see also : Boundary layer Theory, Schlichting.

17. Shen, S.F. : J. Aero. Sci. 21, 62, (1954)

18. Emmons, H.W. : J. Aero. Sci. 18, 490, (1951)

19. Schubauer, G.B. and Klebanoff, P.S. : Symposium of Boundary Layer Effects in Aerodynamics, N.P.L. (1955)

20. Meksyn, D. and Stuart, J.T. : Proc. Roy. Soc. A, 208, 517, (1951)

21. Stuart, J.T. : J. Fluid Mech. 4, 1, (1958)

22. Lin, C.C. : Proc. I.U.T.A.M. Symposium, Freiburg, (1957)

23. Gortler, H. : Z. a. Math. Mech. 20, 138 (1940)

24. Liepmann, A.W. : A.R.C. report No. 7302, (1943)

25. Gortler, H. and Witting, H. : Proc. I.U.T.A.M. Symp. Freiburg, (1957)

26. Benney, D.J. and Lin, C.C. : Phys. of Fluids. 3, 656, (1960)

27. Benney, D.J. : J. Fluid Mech. 10, 209, (1961)

28. Hama, F.R. Long, J.D. and Hegarty, J.C. : J. Appl. Phys. 28, 388, (1957)

29. Hama, F.R. : Pro. 1960 Heat Trans and Fluid Mech. Inst., Stanford University, California.

30. Klebanoff, P.S. and Tidstrom, K.D. : N.A.S.A. Tech. note No. D-195, (1959)

31. Klebanoff, P.S., Tidstrom, K.D. and Sargent, L. M. : J. Fluid Mech. 12, 1, (1962)

32. Schlichting, H. and Ulrich, A. : see Boundary Layer Theory, Schlichting.

33. Whitelegg, S.M. : Ph.D. Thesis, Edinburgh, (1961)

34. King, L.V. : Phil. Trans. A. 214, 373, (1914)

35. Collis, D.C. and Williams, M.J. : J. Fluid Mech. 6, 357, (1959)

36. Bradshaw, P. : N.P.L. Aero. 427, (1961)

37. Whittaker and Robinson. : The Calculus of Observations, Blackie, London. (1946)

ACKNOWLEDGMENTS

I should like to thank Dr. M.A.S. Ross for suggesting the topic of this thesis and for her continued help and encouragement during the work, and Professor W.H.J. Childs for providing the laboratory accommodation and workshop facilities and for encouraging the project in every way.

My thanks are also due to Mr. A. Balfour who helped with the initial programming of the computer and to Mr. R.C. Dougal who read the manuscript and corrected many errors.